Ultrasonic cleaning line walker for high voltage power line insulators

By

Toriq Ramos

Dissertation submitted in fulfilment of the requirements for the degree

MASTER OF ENG: Electrical Engineering

In the Faculty of Engineering

At Cape Peninsula University of Technology

Supervisor: Mr J. Wheeler

Co-Supervisor: Dr Raji

Cape Town

Date submitted: October 2018

Declaration

I, Toriq Ramos, declare that the contents of this dissertation/thesis represent my own unaided work, and that the dissertation/thesis has not previously been submitted for academic examination towards any qualification. Furthermore, it represents my own opinions and not necessarily those of the Cape Peninsula University of Technology.

TRamos

_____

Toriq Ramos

06/02/2020

_____

Date

Abstract

This study investigates the feasibility to clean the insulators on live high voltage power lines autonomously, using ultrasound. Faulty and contaminated insulators on high voltage power lines cause flashovers, which contribute to load shedding and expensive repairs. Turning off the power in order to perform maintenance or clean insulators is a concern as it disrupts nearby businesses and homes. Regular maintenance of equipment on High voltage transmission lines (HVTL) is required to avoid major faults, thus saving money, and minimizing the pressure on the grid. Advancements in the field of robotics have catered for a solution to this concern. The study is divided into two sections; cleaning insulators using ultrasound and a line walker to navigate the high voltage transmission lines.

The cleaning station was developed using a peculiar ultrasonic delivery method. The transducer is suspended 2 mm above the insulator and water is pumped into the gap between the two surfaces. The ultrasound is then applied to a small volume of water trapped by the face of the transducer using the phenomenon known as water surface tension or skin effect. A 12 V generator controlled by a Pulse Width Modulation (PWM) circuit delivers over 300 V peak to peak to the transducer via a push pull transformer. The station is equipped with a 28 kHz piezoelectric transducer governed by an admittance locking routine. The generator tracks the resonant frequency of the transducer to ensure maximum power is utilised for cleaning the contaminated area.. This peculiar delivery technique effectively cleans insulators contaminated with grease, boasts short cleaning times, and only requires a small quantity of water.

A four wheeled line walker was then designed in order to transport the cleaning station to the contaminated insulators. Each wheel propels the line walker forward at 0.1 m/s, and a uniquely shaped leg mechanism couples them to the chassis. The four legs are capable of independently removing the wheels from the line to avoid obstacles, and a 16-bit Atmega 2560 microcontroller monitors and controls all on-board devices and moving parts. Limit switches, an accelerometer and an ultrasonic distance sensor allow the robot to navigate around obstacles such as strain clamps, vibration dampers and indicating spheres. The line walker is capable of maintaining a balanced horizontal position while navigating the line. A scaled prototype of the line walking robot was manufactured and tested in a laboratory environment. The results prove that the robot can effectively navigate around obstacles while the system is run completely autonomously.

The study provides proof of concept and enough evidence to suggest that the ultrasonic cleaning line walker is a feasible project with great potential.

Acknowledgements

Table of Contents

Table of figures

List of tables

Abbreviation table

ARFT	Automatic Resonant frequancy tracking
Bandwidth	A measure of the width of a range of frequencies, measured in hertz.
Cavitation	The fast formation and collapse of air pockets in a flowing liquid in regions of very low pressure. .
Compression	The decrease in volume and increase in pressure.
Contaminants	Something that contaminates.
CPU	Central proccessing unit .
Decrement	A reduction or diminution.
Elasticity	The ability of an object or material to resume its normal shape after being stretched or compressed
Electrodes	A conductor, not necessarily metallic, through which a current enters or leaves a non-metallic medium.
Flux-gate technology	An established and proven electric current mearsurment technology.
HVTL	High voltage transmission line
Hydrophobic	Tending to repel or fail to mix with water.
Implode	Collapse or cause to collapse violently inwards
Insulator	Insulating material, often glass or porcelain, designed to electrically isolate a charged conductor.
Linear	Arranged in or extending along a straight or nearly straight line.

Oscillator   A circuit which based on its components outputs a current of alternating frequency.

Piezoelectric Effect   The phenomenon exhibited by some non-conducting crystals of becoming polarized when mechanically strained and of becoming mechanically strained when an electric charge is applied to the crystal.

PWM   Pulse width modulated

Rarefaction   The reduction in the density of a medium, such as water or gas.

Resonant Frequency   In audio or frequency applications, a resonant frequency is a natural frequency of vibration of the object. This is predetermined by the physical characteristics the object has.

Shock waves   A sudden change in pressure in a medium, commonly air caused by an object travelling faster than the speed of sound.

Surface tension   Elastic properties on the surface of a medium, commonly liquids. The force of this elastic property is pre-determined by the intermolecular bods of the medium.

Transducer   A device that changes energy from one form to another.

Ultrasound   Sound outside the range of human hearing, approximately 20 kHz and higher.

Chapter 1

Introduction

At present the demand for electricity in South Africa is on the rise. As a result of maintenance issues, the primary energy supplier, Eskom, finds it challenging to cope with the rising demand (Eskom, 2011). Damaged power lines and insulators contribute to blackouts and the recent load shedding experienced in this region. Regular maintenance of equipment would save money and minimise the pressure on the grid.

Build-up of dirt and foreign deposits on the insulators of high voltage transmission lines is caused by weathering, aging, pollution and other factors (Minnaar, et al., 2012). These pollutants cause several problems related to flash-over between insulators followed by power failures. Flash over causes serious damage to equiptment on the line which then result in less or no power to surrounding area's. Regular power outages due to maintanance issues are affecting everyone in South Africa and the short term solution is load shedding. This power management strategy has been implemented in countries such as Pakistan, India, Japan, Ghana (Min, 2015), Canada, Italy and Egypt in order to prevent a complete collapse of the power system. Power outages result in loss of productivity in the workplace which, in turn negatively affects the economy and the employees (Bialek, 2005).

Current insulator cleaning techniques are tedious and labour intensive making them very costly. Cleaning and inspection of high voltage lines is currently a manual process. This means training a group of technicians that would be required to work on these lines. These highly trained men and woman have to be airlifted onto the lines using specialised helicopters. They walk the lines and check for any issues along them (Beaty, 1998). There are two ways of doing this: the first option is for the lines to be switched off to allow the inspectors to navigate without the risk of electrocution. The second is for the inspector to wear a metal suit called a Faraday cage (Stix, 1988), which allows the voltage to flow around the inspector rather than through him/her. The cage then acts as a less resistive path for the electricity to flow through, keeping the inspector safe while working the live lines.

At present insulators are cleaned using two common techniques (Gonen, 2013). The more conventional method requires the line to be de-energised so that teams on foot may ground the conductors at each pole and wipe them by hand. This technique is slow, requires a lot of man power and also interrupts the power to nearby homes and businesses. The second technique makes use of specialised trucks and helicopters equipped with high pressure pumps operated by small teams of powerline technicians. The lines remain energised as water is pumped out of a nozzle (Gonen, 2013). The water jet cleans the insulator surface with brute force by forcefully tearing away any contaminants. This method is much faster than the conventional method but is very costly.

Ultrasound has been extensively used in the past for cleaning purposes. It works by propergating high frequency sound waves into a volume of water to create area's of compression and rarefaction. The pressure changes create cavitation vacuoles, which effectively cleans an object when it implodes. A peculiar technique of applying ultrasound directly to the surface of the insulator using water surface tension between the transducer and the insulator is to be investigated (Fuchs, 1995).

The ultrasonic cleaning line walker proposed, is a battery powered drone that autonomously navigates high voltage power lines. The drone carries an ultrasonic cleaning station which effectively cleans the insulators while the power lines remain energized.

1.1. Background

Regular inspection and maintenance of high voltage transmission lines is required to ensure that electricity is safely and reliably transported from power stations to consumers. Most of this work is currently being executed by specialised helicopters and power line technicians on foot. The line men on foot are often subjected to tough terrain and obstacles, making the task physically demanding and slow. The helicopter teams are faster but are expensive and more dangerous (Buhringer, et al., 2010). With the technology available in the twenty first century, a more economical solution must surely exist. The history of ultrasonic cleaners goes back to the 1930's but the majority of cleaning systems were only developed in the 1950's. Cleaning with ultrasound yields good results in a wide range of applications, even in areas

where no other cleaning methods prove to be effective. It was also found to be destructive when not used correctly, causing damage to some materials. (Lamm, 2003)

The principle on which the cleaning method operates is compression and rarefaction of sound waves in a medium. As the waves travel through the medium, it expands and collapses the particles. When the medium expands, bubbles known as cavitation vacuoles form and grow until they can no longer support their own weight and then they collapse. High energy shockwaves explode from these tiny bubbles which, in turn separate the grime from the object being cleaned (Lamm, 2003).

The cleaning industry makes use of ultrasonic cleaning excessively, because it is environmentally friendly, effective and a low cost option in comparison to the other cleaning methods which normally require some form of heavy chemical to clean objects effectively (Lamm, 2003). Cleanliness in general has become a vital part of many industries and, in some cases, mandatory in order to perform operations. This has sparked many innovations and investigations, challenging engineers to continuously explore new and improved solutions to clean. The use of ultrasound for cleaning purposes has proved to be extremely beneficial to the cleaning industry (Fuchs, 1995).

The objective of this study is to clean the insulators suspending the lines by using a line walker that moves along the wires of a HVTL. Factors such as crossing two adjacent lines and deploying the cleaning station will complicate the task, not to mention mitigating factors such as corroded lines and the various hardware fittings suspended by the HVTL.

The purpose of the robot in this study is to navigate the lines while carrying a payload to clean the insulators. During this research we can assume that the diameter of the HVTL is constant and the pylons that connect the lines have similar dimensions between them. At present, several studies have resulted in robotic prototypes that inspect and cross obstacles. To this author's knowledge, none have incorporated ultrasonic cleaning while navigating the lines. (Toussaint, et al., 2009)

1.2. Problem statement

Maintenance teams cannot get to all the insulators and transmission lines in South Africa, the ideal solution will be a line-walker that will use ultrasound to remove foreign deposits from glass insulators on high voltage transmission lines.

The success of the research will be determined when the following questions are answered.
Research Questions:

- Can a practical (compact and portable) cleaning method be realised using ultrasound for cleaning glass insulators on high voltage transmission lines?

- Can an effective (efficient) ultrasonic generator be developed?

- Can a robot be designed to navigate an individual line on suspension type HVTL pylons, and transport the cleaning station?

1.3. Delineation of research

This study investigates a peculiar technique of delivering ultrasound to HVTL glass insulators. A compact ultrasonic cleaning station is designed to be transported by a line walker operating autonomously on live suspension type line configurations.A prototype of the cleaner will be realised but due to time constraints,the mechanism which changes the area being cleaned on the insulator will not. A basic line walker will be built, and the two devices will be tested separately in a laboratory environment.This feasibility study is undertaken in order to determine proof of concept.

The insulating characteristic of the insulator being cleaned will be jeopardized during this novel cleaning process. This would require a solution to compensate for the insulation lost and will not be covered in this research. The research to follow will assume that the extra insulation required is obtained, and that the cleaning will be limited to only one glass insulator instead of the complete insulator string. Ethical matters such as contaminated water effecting the environment is a concern and therefore it will also be assumed that the dripping water used to clean will be collected and recycled to eliminate any environmental damage.

1.4. Thesis structure

The layout of the remainder of this study is as follows:

Chapter 2: In this Chapter, the focus will be on the environment of high voltage transmission lines, ultrasonic cleaners in totality and factors to consider when developing drones for suspension type HVTL's. The function of ultrasonic cleaners, the different types of cleaners, and control methods will be investigated. Existing line walker designs, the obstacles they need to overcome and their fundamental components will be analysed thereafter.

Chapter 3: This Chapter will explore how the system will be constructed as a whole. Further factors will be decided on such as: the limitations or requirements of the intended system, which power sources will be used, after which the line walker hardware will be selected.

Chapter 4: This Chapter will provide insight into the individual problems experienced in the project and will also show all associated measurements, calculations, designs and schematic diagrams.

Chapter 5: This Chapter will show and discuss the results of the project and whether or not this prototype is successful. It will also look at the possible limitations, positive and negative aspects of the project.

Chapter 6: In the final Chapter the main points of the thesis is summarised and any unexpected findings are discussed. Topics that require further research are pointed out and recommendations are made.

Chapter 2

Literature review

The following Chapter provides an understanding around the project in its entirety. Firstly, the environment in which the project will be operated in is investigated. Secondly, an in-depth analysis into ultrasonic cleaning is reviewed, and finally, the area of research in this literature review shifts to the robotic line walker.

2.1. Overhead and underground electric cables

In South Africa, overhead transmission cables are most predominantly utilised. This is firstly because maintenance is easier to perform, and secondly, less environmental damage is caused when compared to the underground alternative. Weather related incidents which result in power outages on underground lines are scarce but it is more difficult to identify failures and faulty equipment (Tri-State Generation and Transmission Association, 2009).

Repairs and maintenance on underground wiring tend to be more costly and time consuming than the overhead alternative. The underground cabling also requires additional equipment for installation such as cable pushers and trench rollers (Alonso & Greenwell, 2013).

In overhead systems the wires are spread out for safety reasons. This ensures that no arcing occurs between lines, and any heat generated is dissipated by the air around the cable. In underground installations, both these factors need to be managed in other ways (National Grid, 2015). Depending on the system, cooling from the surface may need to be implemented and a concrete envelope is usually used to separate the wires for safety reasons as shown in Figure 2-1 (Alonso & Greenwell, 2013).
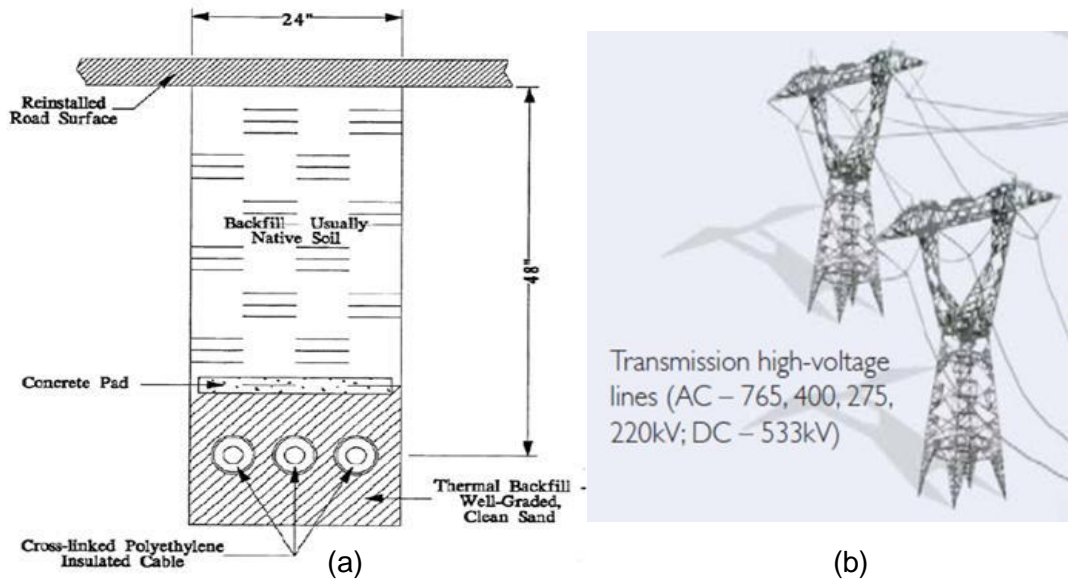
Figure 2-1: (a) An underground HVTL installation (Weiss, 2011).
(b) An overhead HVTL system (Eskom, 2009).

The overhead lines have several configurations, but all are based on two design types. Pylons are the support structures suspending the lines. The pylons are either configured to be suspension type (a) or tension type (b) as shown in Figure 2-2 .
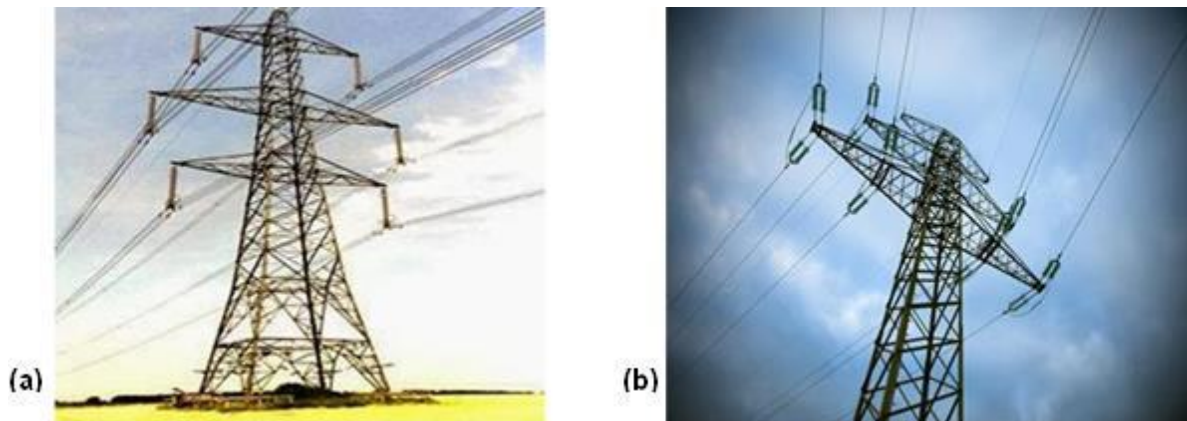
Figure 2-2: The two types of line configurations (mplgmg, 2017).

Overhead lines also have less environmental impact, as it only requires a concrete footing or foundation at each location where a tower is to be constructed, whereas the underground system requires a continuous concrete slab to house the wires. Overhead lines typically costs four to fourteeen times less due to materials and labour, further more when modifications and additions to the lines are required, it becomes much easier when using overhead lines (Tri-State Generation and Transmission Association, 2009).

Figure 2-3: A map of South Africa's transmission line network. (Eskom, 2009)

South Africa's high voltage transmission network has a total length of over 30 000 km operating at standard voltages of 132, 220, 275, 400 and 765 kV. The majority being overhead lines carrying voltages of 400 kV and 275 kV; these live lines are repaired and maintained by only a handful of specialised personnel (Eskom, 2009).

2.2. Electrical insulators

All electrical networks greatly depend on insulation to function. Electrical insulators are mandatory in an electrical system in order to prevent unwanted flow of electric current leaking to the earth. An electrical insulator provides an infinitely large resistive path through which no current is allowed to flow (Lancaster, 2012).

In a transmission and distribution system, the overhead conductors are supported by towers or poles. These structures are all fixed and grounded to earth. Consequently, there must be an insulator between the structure and the live conductors to avoid the flow of current leaking to earth via the supporting towers or poles (Lancaster, 2012).

2.2.1. Insulating Material

The materials used to design effective Insulators must adhere to the following criteria (Lancaster, 2012):

- The material must be mechanically strong enough to carry the weight and tension of the conductors,
- the material must have excessive dielectric strength in order for it to withstand the high voltages in the system,
- it must retain an extremely high resistance to prevent current from deviating,
- the insulating material must be pure and should not be porous,
- the material should not absorb gases or moisture, and
- the material's capabilities should not be affected by temperature fluctuations.

Four materials have been identified by the industry as having the requisite properties for a good insulator. These include porcelain, glass, soap stone and polymer.
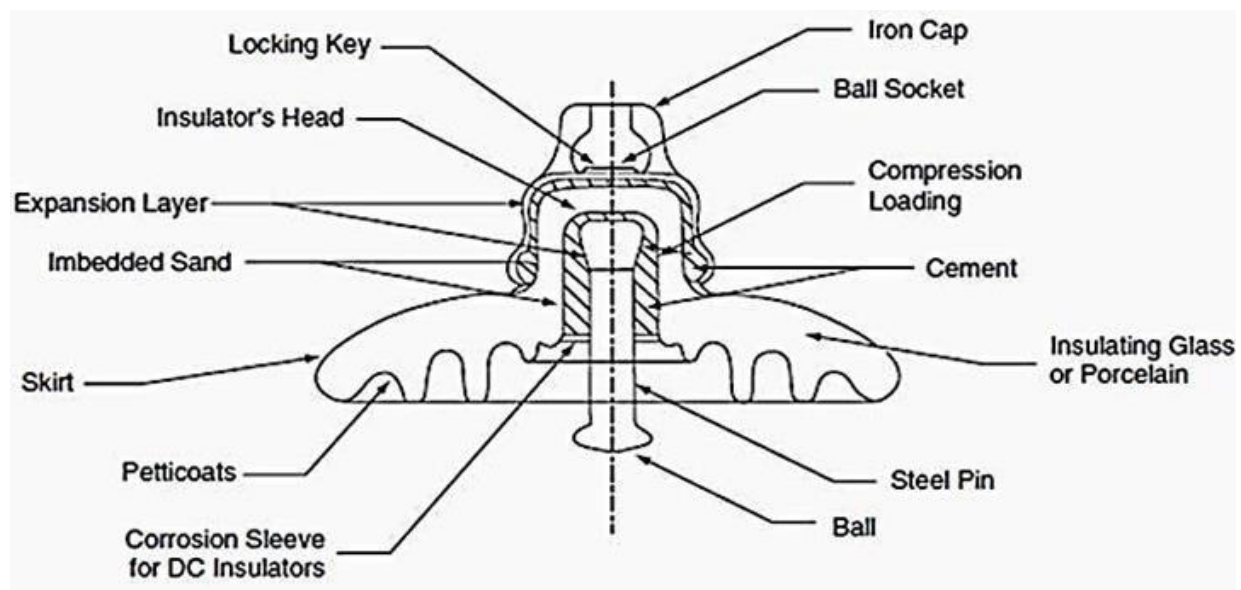
Figure 2-4: A detailed diagram of the traditional insulator. (Csanyi, 2012)

Formerly, insulators were traditionally manufactured with porcelain, glass or soapstone. These materials were used for their dielectric characteristics and their casting methods. They can still be seen performing at present due to their long life span. However, composite materials such as polymer are the new breed of insulating material for the 21st century (Ramos Hernanz, et al., 2006).

2.2.2. Porcelain Insulators

Porcelain (or aluminium silicate) insulators are the most common type. Porcelain is a subcategory of ceramics and should be free from pores and impurities in order for it to be utilised as an insulator (Ramos Hernanz, et al., 2006).

Figure 2-5: The porcelain insulator. (Lancaster, 2012)

Porcelain is essentially composed with a special clay called kaolin and is mixed with other minerals such as quartz, alumina and feldspar of the best quality. The insulators are baked to 1400 ºC and later varnished with a layer of silicate. These insulators are then boiled and their surfaces are glazed in order to prevent the adhesion of water, humidity and dust (Ramos Hernanz, et al., 2006). Table 2-1 shows the approximate strength of the material.

Table 2- 1: The properties of porcelain insulators (Lancaster, 2012).

PROPERTY	VALUE (APPROXIMATE)
Dielectric strength	60 kV / cm
Compressive strength	70,000 kg / cm^2
Tensile strength	500 kg / cm^2

The compressive strength of a porcelain insulator is good but it does not provide much tensile strength. An average dielectric strength of 60 kV / cm means that these insulator types are frequently found on lower voltage lines.

2.2.3. Glass Insulator

Glass is a material with good dielectric properties, this is why glass insulators are frequetly used across the globe. Figure 2-6 shows a typical glass insulator taken out of an insulator string.

Figure 2-6: The glass insulator (Lancaster, 2012).

Glass is formed with melting temperatures between 1300 ⁰C and 1400 ⁰C. A mixture with oxides of sodium, calcium, barium, aluminium and salicylic acid amongst others are used. The glass used for the insulators is created using a complicated technique of abrupt cooling via cold air during the fusion process, thus producing a calcium glass alkaline. Consequently, a tough glass is obtained, with a high mechanical resistance and good stability against temperature fluctuations. Table 2-2 shows the approximate strength of a glass insulator.

Table 2- 2: The properties of glass insulators (Lancaster, 2012).

PROPERTY	VALUE (APPROXIMATE)
Dielectric strength	140 kV / cm
Compressive strength	10,000 Kg / cm^2
Tensile strength	35,000 Kg / cm^2

Glass insulators have become popular in transmission and distribution systems, listed below are some advantages over the traditional porcelain substitute (Ramos Hernanz, et al., 2006).

Advantages of Glass Insulators (Lancaster, 2012)

- It has a superior dielectric strength and resistivity compared to porcelain,
- thermal expansion is less and tensile strength is greater than that of porcelain,
- it is transparent, therefore is not heated by sunlight, and impurities and air bubbles can be easily detected,
- glass has a long service life and its dielectric and mechanical properties are not affected by aging, and
- the cost of glass is much less than porcelain.

Disadvantages of Glass Insulators (Lancaster, 2012)

- Moisture condenses easily on to the glass, which is detrimental to the effectiveness of the insulator, and
- glass cannot be moulded into irregular shapes for use with higher voltages as strains in the glass can be caused by irregular cooling.

2.2.4. Polymer Insulator

In the past decade, polymer insulators have taken a firm grip on the insulator industry, in some cases to substitute the accepted porcelain and glass insulators and in others to improve the efficiency and feasibility. Researchers have attained many achievements in understanding the weaknesses of insulator designs and composite material properties. These composite/ polymer insulators have now been introduced to high voltage power transmission networks in Africa, Asia, Europe and many more countries (Ramos Hernanz, et al., 2006).
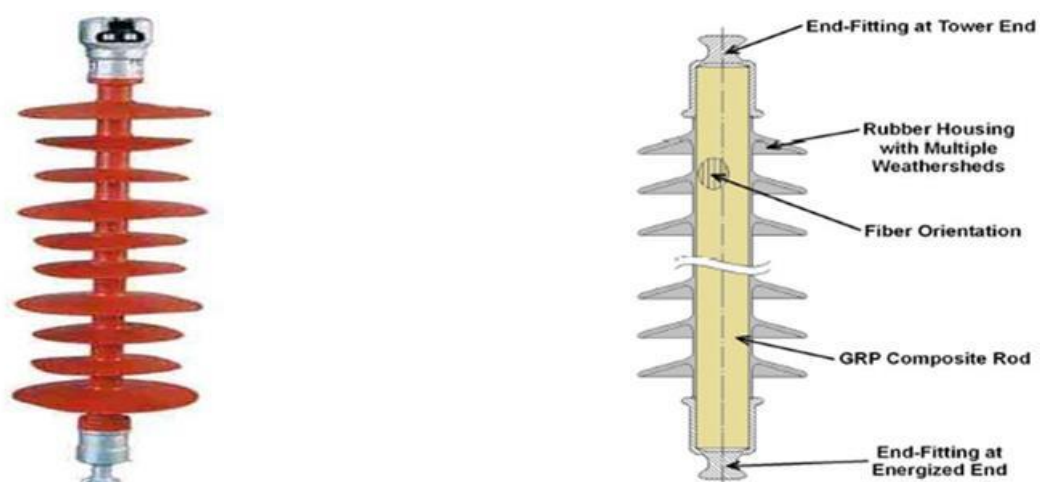
Figure 2-7: A polymer insulator (Lancaster, 2012), (Kumosa, et al., 2011)

Polymer insulators are comprised of two parts, the core is constructed with fibreglass reinforced epoxy resin, and the outer layer with silicone rubber. The rod-shaped core is shelterd by weather sheds, which protect the rod from environmental conditions. It is also called a composite insulator due to its two-part structure. The international use of composite insulators is due to some of the following advantages (Lancaster, 2012).

Advantages of Polymer Insulators

- Lightweight construction compared to the other types of insulator,
- retains a high tensile strength and good flexiblility,
- imposes less load on the supporting structure,
- performs better, particularly in polluted areas,
- it is hydrophobic in nature and thus requires less cleaning, and
- there are various insulator designs

Disadvantages of Polymer Insulators (Lancaster, 2012)

- Small material errors can render the device inefficient and lead to mechanical failure,
- these insulators can be affected adversely by high temperature conditions such as in the case of bushfires, where glass and porcelain would remain effective, and
- polymer insulators have failed in coastal areas with high salt levels in the atmosphere.

2.2.5. Electrical insulator breakdown

There are two phenomena which lead to electrical insulator breakdown and both are caused by excessive overvoltage in the system explained below (Kiessling, et al., 2014).

- A puncture arc is a failure of the insulating material which causes the conduction of electricity through the insulator. This condition sends an electric arc vigorously through the insulator. The heat resulting from this arc damages the insulator beyond repair. Puncture voltage is the potential difference across the insulator that causes a puncture arc.

- A flashover arc is the conduction of electricity through the air. This condition causes an arc along the outside of the insulator, essentially nullifying the use of the device. Insulators are manufactured to withstand this type of stress without damage. Flashover voltage is the potential difference that causes a flashover arc (Kiessling, et al., 2014).

High voltage insulators are designed with lower flashover than puncture voltages. It is for this reason that the insulators flashover before they puncture and become damaged. The insulator must prevent flashover for many possible operating conditions including; temperature, humidity, snow, rain, and air-borne contamination to the surface of the insulator. This is one of the reasons they are designed with such intricate shapes. In addition to resisting flashover and puncture arc, the insulator also has to withstand mechanical stresses against wind pressure, the weight of the conductor and ice deposits (Kiessling, et al., 2014).

2.2.6. Contamination of insulators

The sources of contamination to insulators are linked to the level of pollution and to the weather patterns in their respective installation regions. The steps in which contamination leading to flashover caused by pollution are (Kumar & Kumar, 2012) :

- The pollution settles on the surface of the insulator via the wind, gravity and the electric field. Polluted particles slowly build up, and a layer of contaminant is consequently developed,
- weather conditions then dampen the surface causing the contaminated (now conductive) area to be enlarged,
- when this layer dries, an increase of conductivity and leakage current occurs,
- heating this layer results in the formation of dry bands, through which partial arches appear,
- partial discharges are produced, creating an audible noise, and
- the flashover then occurs when the total discharge is produced through the contaminated layer.

Insulators are contaminated over time by pollutants from agricultural and industrial activity and salt from coastal moisture. Due to contamination, the insulators lose their

insulating properties, which results in power supply interruptions and failures. This is why they require regular cleaning to maintain their effectiveness.

Figure 2-8: Contaminated insulators due to industrial pollution (Kumar & Kumar, 2012).

The insulators are contaminated by several pollutants from a range of different sources. The type of contaminant found on a particular insulator, often depends on its the location. Table 2-3 depicts some of these pollutants.

Table 2- 3: The various forms of insulator pollutants (Ramos Hernanz, et al., 2006).

Contaminant	Source of pollution
Defecation	Bird droppings in areas where birds are mating or feeding
Salt	Seaside areas Salt mines and refinaries Enviroments where snow is melted with salt.
Cement	Cement processing plants Bulidung sites Stone rock and gravel quarries
Earth	Crop debris from agricultural areas
Coal	Coal mining Coal processing plants Coal power plants where coal is burned
Volcanic ash	Areas where volcanoes are active
Smog	Car exhaust emmissins Factory emmissions in industrial areas
Smoke	Forest conflagrations Burning Industrial waste Burning of agricutural waste
Fertilizers	Plant fertiliser around farming areas
Metallic	Mining and mineral handling processes
Chemical	Chemical process industries such as oil refineries.

When constructing a high voltage overhead transmission line, it is vital for the designer to take pollution into consideration and to choose the most adequate insulator for the respective installation zone. If this is done correctly, faults and

maintenance work can be greatly reduced, saving the company involved additional cost and time (Ramos Hernanz, et al., 2006).

2.2.7. Current methods of cleaning insulators

Highly polluted environments should have a good line maintenance plan and an equally good insulator selection. Maintenance includes cleaning and removing contaminants from the insulator, especially in areas where rainfall is low. This can be achieved while the system is energised (hot washing), or de-energised. The decision of which method is used depends on the terrain, adhesive properties of the pollutant, technical reasons, and whether the use of chemical solutions is required. The most prefered cleaning methods for insulators are (Ramos Hernanz, et al., 2006):

- Wash with water using different pressures,
- use dry compressed air,
- with specks of abrasive materials (fine sand, nutshells, fine lime dust, or shattered shell of corn),
- often, the wash is physically done by the hand of a lineman, and
- more recently the use of ultrasound.

It is mandatory that the technique selected does not harm or damage the insulator. Pollutants which do not rigidly adhere to the surface such as land, dust or salt can be removed most effectively and economically by washing with pressurised water or air. Washing with abrasive materials is usually done when the pollutant is highly adhesive such as cement or a contaminant caused by chemicals or petroleum.

Figure 2-9: linemen cleaning insulators by hand wiping. (Wang, et al., 2016)

Figure 2-10: (a) Hot washing using a specialised truck. (Pressure washers pro, 2013)
(b) Hot washing using a helicopter. (Red Eléctrica de España, 2008)

De-energising the lines so that teams on foot may wipe them by hand is time consuming, requires a lot of man power and also interrupts the power to nearby homes and businesses. The second technique makes use of specialised trucks and helicopters equipped with high pressure pumps and skilled teams of lineman to work on live conductors. This method is much faster but also more expensive. An ultrasonic technique might be a more efficient cleaning solution to this problem.

2.3. Ultrasonic cleaning delivery systems

Generally, ultrasonic cleaning systems employ the use of ultrasonic waves and a liquid solution. When both of these elements are present at the same time, ultrasonic cleaning can be achieved (Kim, et al., 1999). Many different approaches are used to implement ultrasonic cleaning. These approaches, amongst others include:

- Tank system,
- Brush system ,
- Horn system.

2.3.1. The tank system

This method makes use of a stainless steel tank, filled with a solution in which the object to be cleaned is submerged. The tanks are equipped with one or more transducers underneath the basin, and propagate longitudinal waves into the solution. The transducers are excited at high frequencies causing cavitation vacuoles to form in the solution. The tiny vacuoles then implode under the pressure changes, which culminates in the cleaning of the object (Fuchs, 1995).
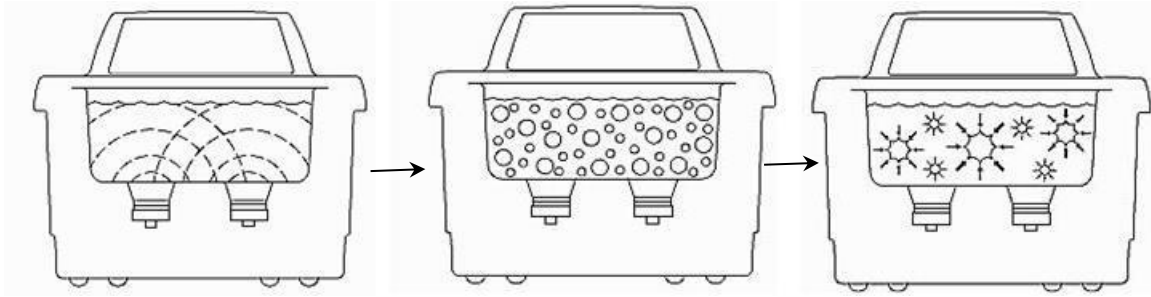
Figure 2-11: A small tank system, depicting the changes in the solution. (Branson Ultrasonics Corp., 2000)

The size of the tank is determined by application; the smaller tanks are used for cleaning jewellery and dentures, whereas bigger tanks the size of bath tubs will be utilised for cleaning gears, engine parts and other industrial purposes. The tanks can be bought off the shelf and are equipped with a control feature allowing the user to adjust the time and power intensity best suited for the application (Branson Ultrasonics Corp., 2000).

2.3.2. The brush system

Brush type ultrasonic cleaning technologies are most commonly found in the dental industry where it has revolutionised the standard of oral health and hygiene. Studies have proven the benefits of ultrasonic cleaning toothbrushes over conventional manual toothbrushes (Day & Martin, 1998). Ultrasonic toothbrushes remove dental biofilm using the principles of fluid dynamics. Dynamic shear forces combined with fluid pressure creates cavitation vacuoles, which clean the teeth as shown in Figure 2-12. The ultrasonic waves are applied to the base of brush and these waves travel along the bristles of the brush (Collins, 2009).
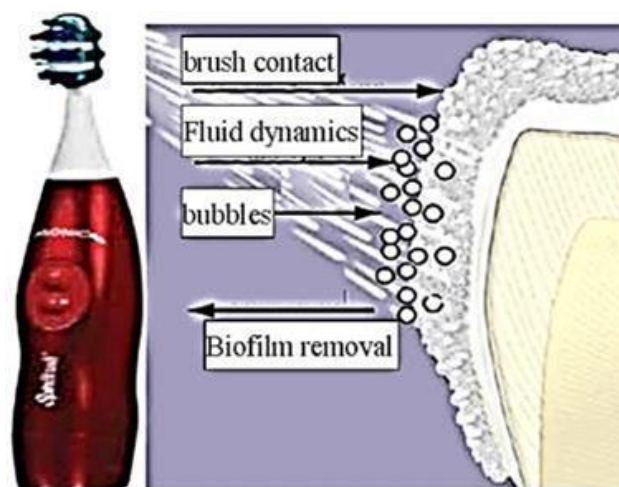
Figure 2-12: The brush method using the process of fluid dynamics (Collins, 2009).

The toothbrushes are battery powered and the bristles, which are used to deliver the ultrasound, are held 2 mm to 3 mm away from the teeth. The toothbrush is moved around the mouth, but the teeth are never actually scrubbed. These toothbrushes are very effective but significantly expensive when compared to manual toothbrushes (Collins, 2009).

2.3.3. The horn system

The horn system uses a jet of water, which is sprayed onto the contaminated surface. A pulsed water jet is vibrated at ultrasonic frequencies via an ultrasonic horn. A nozzle is used inside the horn to induce longitudinal waves thus applying both a solution and ultrasonic impulses on the contaminated object. Extremely high wave amplitudes are produced when utilising horn ultrasonic technology (Industrial Sonomechanics, 2015).
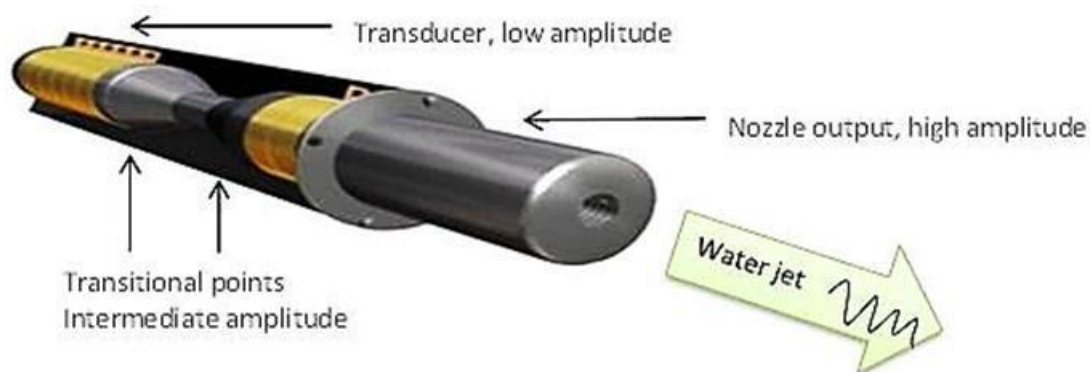
Figure 2-13: The ultrasonic horn assembly as redrawn from (Industrial Sonomechanics, 2015).

Continuous high pressured water jets are currently utilised in a considerable amount of applications, among them industrial cleaning and eradication of surface layers. The horn technique provides a superior cleaning performance in comparison to a continuous water jet at the same hydraulic parameters (Foldyna, et al., 2004).

2.4. Ultrasonic cleaning

The cleaning industry has shifted dramatically in the past two decades from the accepted chemical and mechanical methods to the use of ultrasound. Researchers have found solutions using ultrasound for most cleaning problems. In some cases the cleaning process becomes faster, cleaner and more cost effective (Kanegsberg & Kanegsberg, 2011).

Ultrasound is audio signals above the range humans are capable of hearing. The audio frequency for ultrasound is typically between 20 kHz and 1 MHz and humans typically have a range between 20 Hz – 18 kHz. In essence, Ultrasonics is the manipulation of sound waves. The tone one hears is dependent on the frequency of the wave (Kanegsberg & Kanegsberg, 2011).
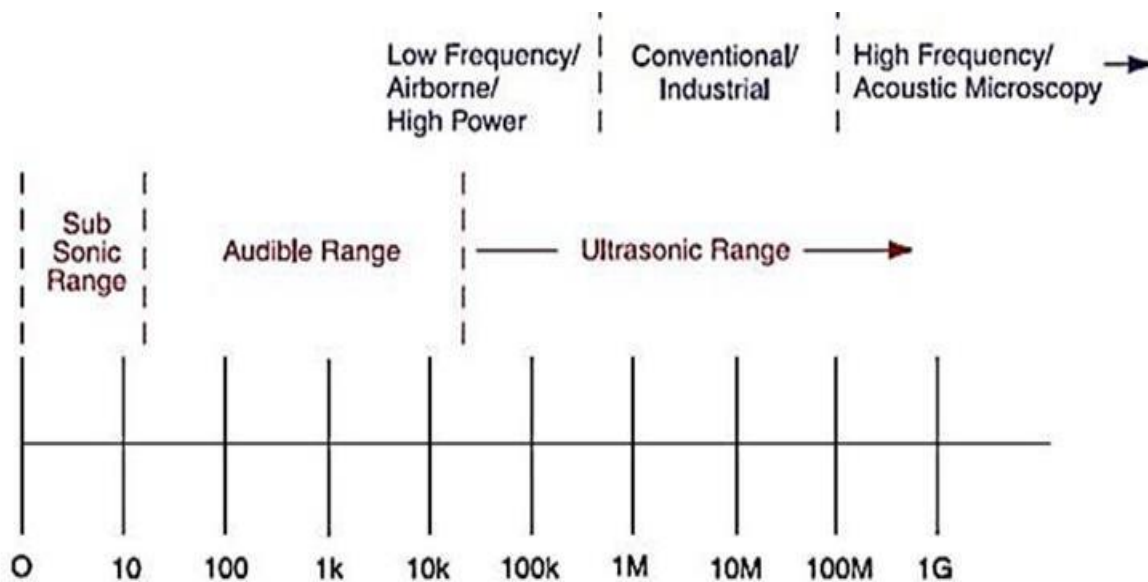
Figure 2-14: The acoustic spectrum of ultrasonic frequencies (Olympus NDT, 2011).

The tone of ultrasound is so high that humans are incapable of hearing it. Cleaning using ultrasound for industrial purposes typically takes place between the frequencies of 20 kHz & 50 kHz, whereas the smaller items cleaned in dental surgery's and jewellery stores vibrate at 50 kHz and above. Sound waves are the fundamental building blocks of ultrasound, and it is vital that they are understood if the concept of ultrasound is to be grasped (Kanegsberg & Kanegsberg, 2011).

2.4.1. Sound waves

A sound wave is generated by either a vibrating motion or a shock event. An audio speaker creating compression and rarefaction waves whilst displacing air with its cone is an example of a vibrating motion. A shock event creates a single compression wave which accelerates away from the source, a box falling flat on a solid floor is an example of a shock event occurring (Fuchs, 1995).
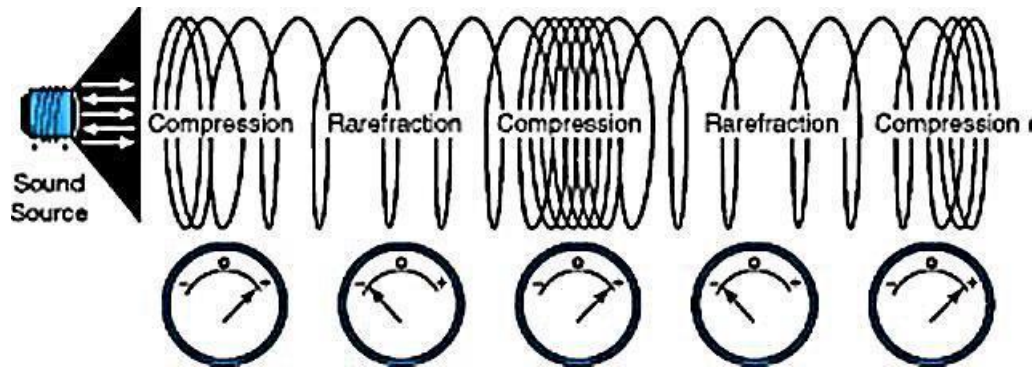
Figure 2-15: Sound waves being compressed and rarefied (Fuchs, 1995).

When sound travels through a medium it affects the individual molecules of that medium. The molecules are excited very similarly to that of a slinky. The pressure in the sound conducting medium where the area is under compression is found to be positive and the opposite is found at the area subjected to rarefaction (Fuchs, 1995).

2.4.2. Cavitation vacuoles

As the sound waves propagate through the medium, creating areas of compression and rarefaction, cavitation vacuoles (bubbles) are formed on the surface of the object. These bubbles expand and contract due to pressure changes until they implode vigorously at a temperature of 5000 degrees centigrade. The implosion also creates a plasma jet or shock wave which is the scrubbing force of ultrasound. This process of implosion is called cavitation (Fuchs, 1995).
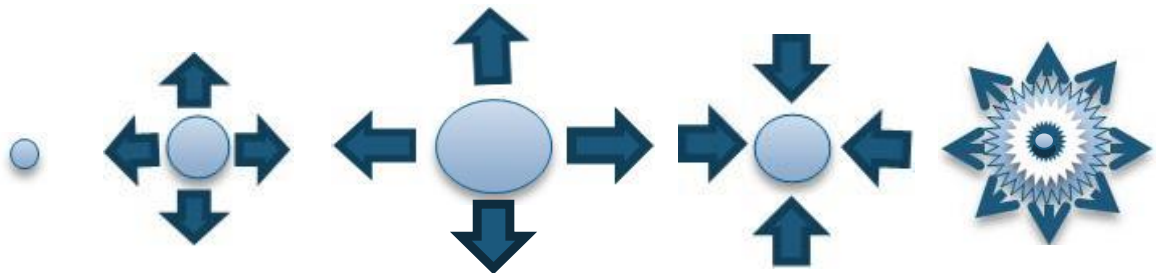
Figure 2-16: Cavitation bubbles as redrawn from (Fuchs, 1995).

Figure 2-16 shows how the bubble expands when negative pressure is experienced, before shrinking under the positive pressure and collapsing vigorously.

2.4.3. Cleaning topology

Ultrasonic cleaners are cleaning systems which use high frequency sound waves, generated by an ultrasonic generator, to agitate a solution or a medium around a contaminated object. Electrical energy is converted into ultrasonic sound waves by

means of transducers attached to the tank of the cleaning system. Cavitation causes the solution to rush into the vacuums left by the imploded bubbles, which provides a scouring action that flicks the contaminant particles away from the object, leaving its surface clean (Kim, et al., 1999).
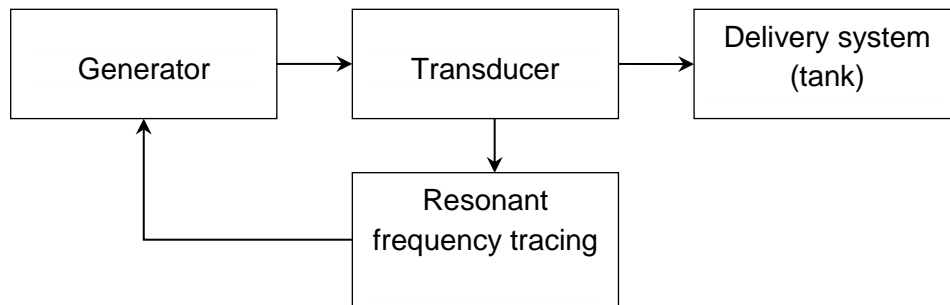
Figure 2-17: The topology of a typical ultrasonic cleaning system.

There are four main components integrated together in an ultrasonic cleaning system, shown in Figure 2-17. The cleaning efficiency and reliability relies squarely on the design and selection of these sub components. The responsibilities and function of these sub sections are explained below.

2.4.4. Transducers

Transducers are devices that convert electrical energy into mechanical energy and vice versa. The mechanical energy a transducer converts is in the form of sound waves above the range of the human spectrum, also known as ultrasound. Their material mass and elasticity are the two fundamental properties which allow these devices to propagate acoustic waves. A wear plate, backing and an active element are among the essential components of this device (Olympus NDT, 2011).
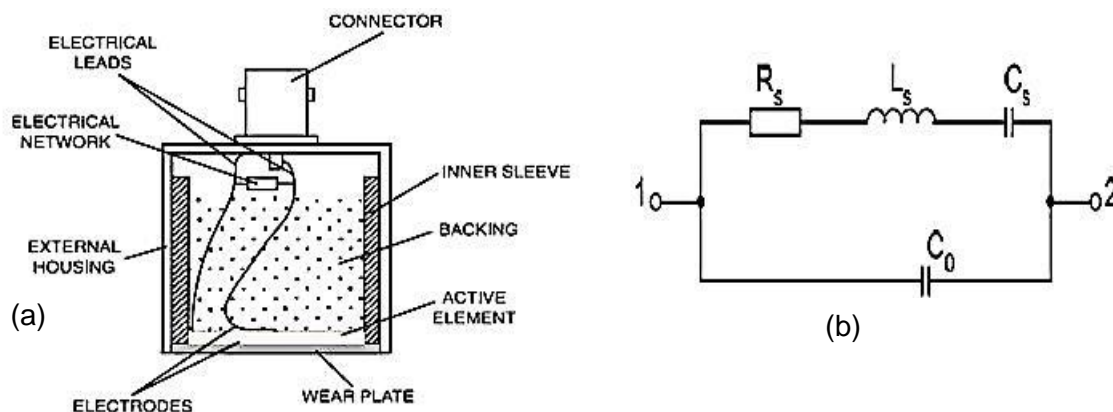
Figure 2-18: (a) The various components of a transducer (Olympus NDT, 2011).
(b) Butterworth –Van Dyke model (Svilainis & Motiejûnas, 2006).

The ultrasonic transducer in its main resonance frequency region is defined by using the Butterworth-Van Dyke (BVD) model. It describes the mechanical part (Rs, Ls, Cs) and the electrical part (C_O clamping capasitor) of the transducer (Svilainis & Motiejûnas, 2006).

2.4.4.1. Resonance in transducers

Resonance is the study of the frequency response of a particular circuit containing a combination of R, L and C elements. Resonant frequency of transducers can be defined as the frequency at which maximum vibration/ amplitude/ displacement occurs. When a transducer is driven in resonance the following is true (Sherman & Butler, 2007):

- The reactive components in the circuit are equal *(XL = XC),*
- impedance or admittance is purely resistive ($Z = R$),
- the input voltage is in phase with the current, and
- the current in the circuit is at maximum ($I = I\_max$)
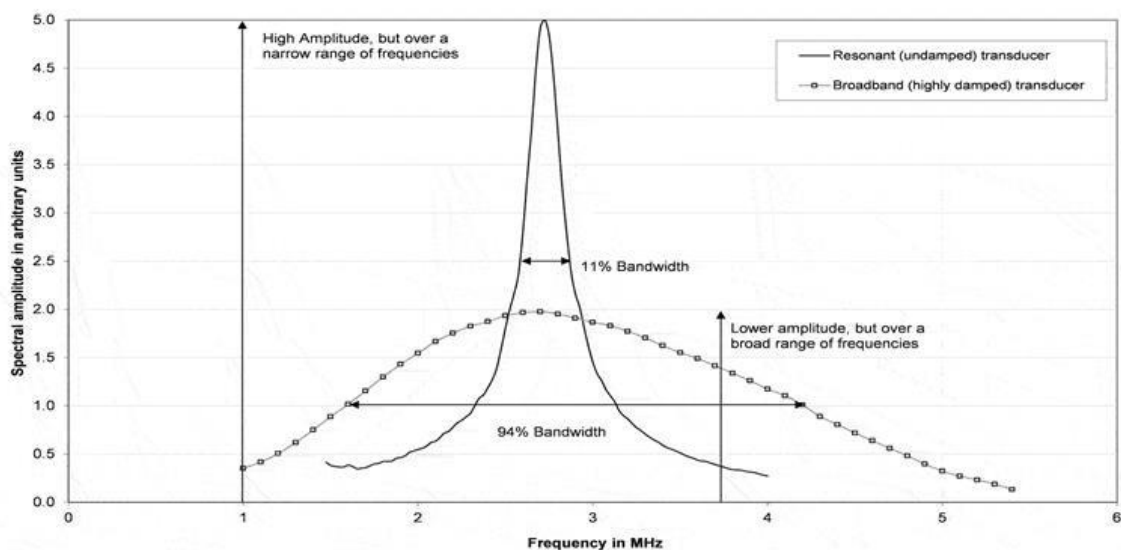
Figure 2-19: Frequency response curves of at resonant frequency (Precision Acoustics, 2015).

From Figure 2-19 one sees that the spectral amplitude of a transducer with a high quality factor is significantly reduced if the driving frequency deviates slightly from its resonant frequency. The transducer with a lower quality factor maintains its spectral amplitude even if the driving frequency changes moderately from the resonant frequency. The quality factor of a transducer is therefore a reflection on the width of the frequency range which causes vibration of a particular scale (Fuchs, 1995).

There are three transducer types used widely in the ultrasonic industry, each having a unique architecture and method of operation. Piezoelectric, magnetostrictive, and capacitive micro machined transducer's (CMUT) are evaluated and compared below.

2.4.4.2. Piezoelectric transducers

The prefix "piezo" is a Greek word meaning to squeeze also referring to pressure. Transducers comprised of piezoelectric material expand and contract when an electrical pulse is applied. Many piezoelectric materials are known to exist, among them are: single-crystal materials; piezo-ceramics; piezo-polymers; piezo-composites and piezo-films. The amount of movement the material shows is related to the voltage and the frequency applied to the transducer (Heywang, et al., 2008).
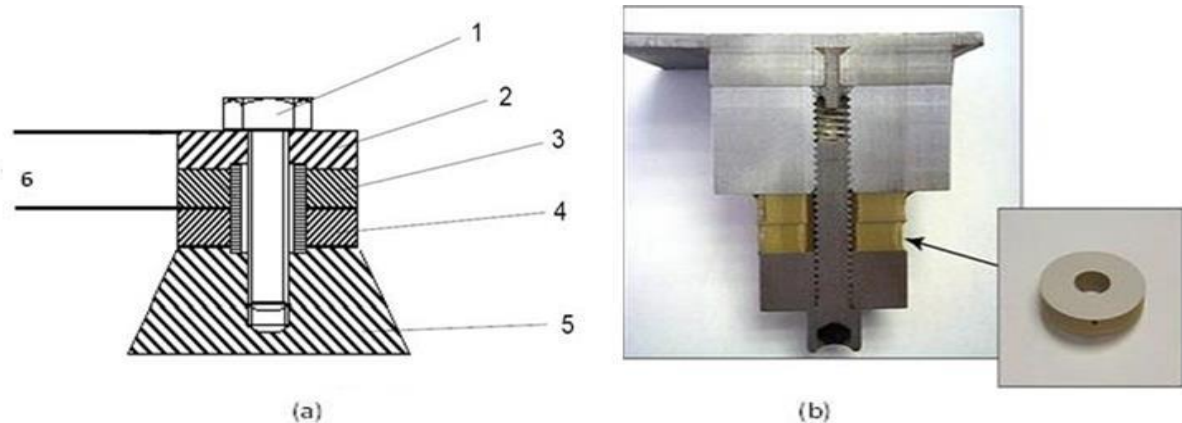
Figure 2-20: (a) A piezoelectric transducer diagram (Fabijanski & Lagoda, 2011).
(b) The physical transducer (Fuchs, 2012).

The heart of a piezoelectric transducer is a disc of piezoelectric ceramic material (3 and 4), typically Lead Zirconate Titanate (PZT), inserted between two electrodes (6) which provide the connection points for the electrical driving circuit. The ceramic assembly is wedged between two metal blocks (2 and 5), one aluminium block and a steel block with a bolt (1). When an alternating voltage is applied to the ceramic via the electrodes, the material expands and contracts resulting in to changes in its lattice structure. This rapid displacement pushes the aluminium block up which creates the sound waves used for ultrasonic purposes (Heywang, et al., 2008). There are five critical performance characteristics in piezoelectrics: the piezoelectric strain constant d, the piezoelectric voltage constant g, the electro mechanical coupling factor k, the mechanical quality factor QM, and the acoustic impedance Z (Uchino, 2003).

2.4.4.3. CMUTs

Capacitive micro machined ultrasonic transducers (CMUTs) are commonly used for medical purposes. They offer advantages such as compact form, higher sensitivity, higher resolution in imaging and therapy, wide bandwidth, ease of fabrication, and capability to integrate with electronics (Olabi & Grunwald, 2008).
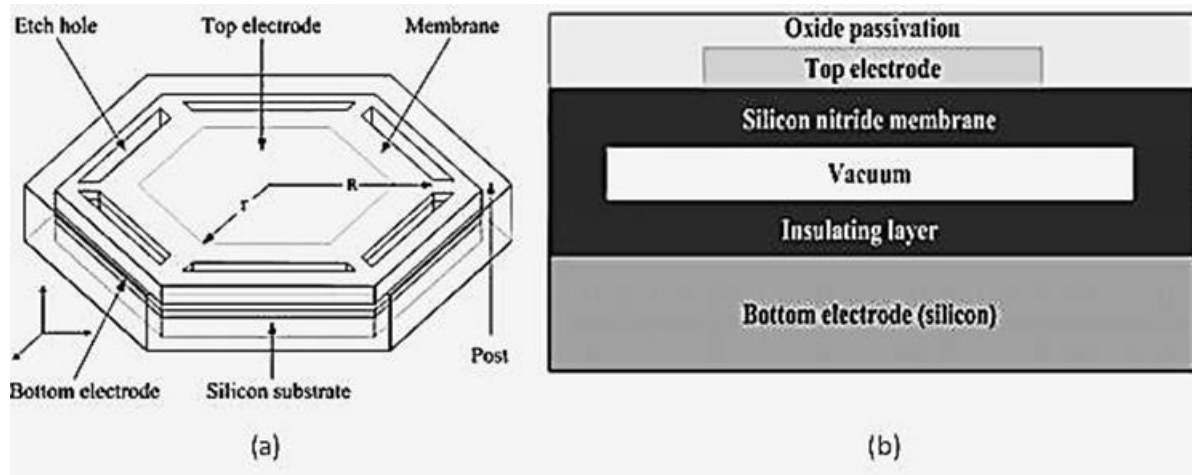
Figure 2-21: (a) A diagram of a CMUT transducer (Olabi & Grunwald, 2008).
(b) The schematic cross section of a CMUT cell (Oralkan, et al., 2002).

CMUTs are constructed on silicon and manufactured using silicon integrated circuit (IC) fabrication technology. A thin metalised membrane suspended on top of a cavity formed in a silicon substrate acts as a top electrode. Beneath the cavity separated by an insulating layer, a bottom electrode designed with silicone is found (Khuri-Yakub & Oralkan, 2011). The elements in CMUTs are actually an array of transducer elements each consisting of tiny capacitor cells connected in parallel.
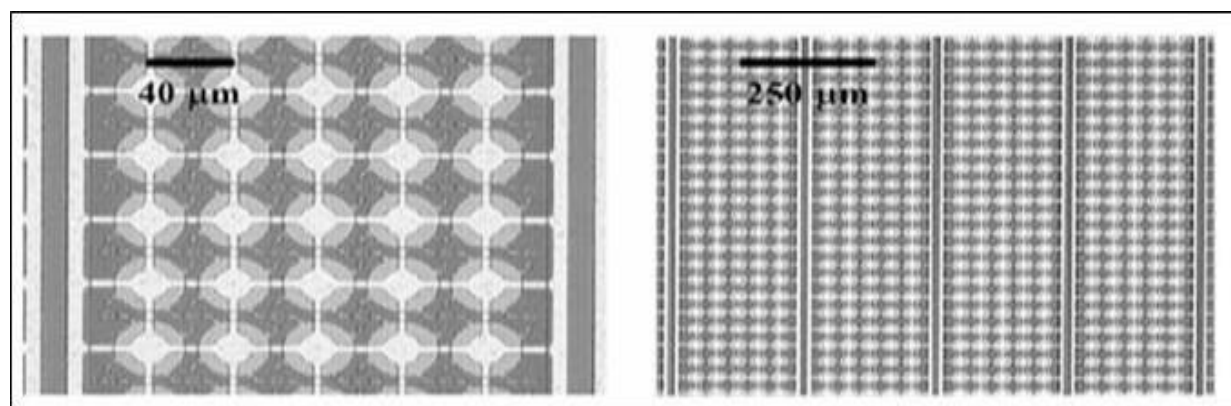
Figure 2-22: (a) A magnified view of a single 5-cell wide, array element.
(b) A portion of four elements of the CMUT array (Oralkan, et al., 2002).

During operation, an alternating voltage is applied between the metalised membrane and the substrate. During the positive cycle the top electrode is pulled down toward the substrate by the electrostatic force. The stiffness of the metalised membrane causes it to move back to its original position. When the negative cycle arrives, the opposite occurs and this creates ultrasound. They have a frequency range between 10 kHz to 50 MHz and when the biased membrane is subjected to ultrasound, a capacitance change generates a current output (Oralkan, et al., 2002).

2.4.4.4. Magnetostrictive transducers

These transducers are effectively electromagnets dating back to 1842. The term magnetostriction means to change the shape of materials by using the flux of an external magnetic field. This phenomenon is a reversible exchange of energy between a magnetic form and a mechanical form (Engdahl, 2000). The principle components of this device are a permanent magnet, wire coil, AC driving circuit, spring washer and a magnetostrictive core (rod) comprised of many nickel plates arranged in parallel or an alloy of Terfenol-D.
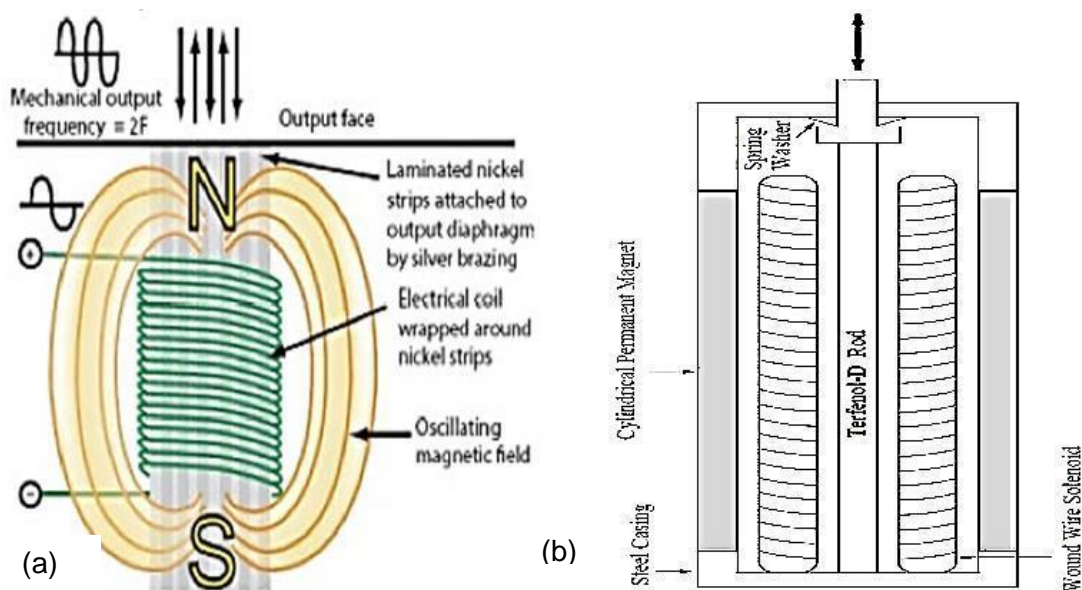
Figure 2-23: (a) A magnetostrictive transducer diagram (Mittal & Jaiswal, 2015).
(b) The magnetostrictive transducer cross sectional layout (Calkins, et al., 2000).

A current is induced into the coil of wire wrapped around the magnetostrictive material, creating a magnetic field. The field causes the core to contract or expand. The spring washer resists the movement and returns the the rod to position thereby introducing a sound wave. The core moves at the same rate as the driving AC

circuit. This technique requires two energy conversions, from electrical to magnetic, then from magnetic to mechanical (Calkins, et al., 2000).

2.4.5. Comparison between transducers

The following characteristics are important factors to consider when selecting a suitable transducer for a specific application.

2.4.5.1. Frequency Range

The ultrasonic frequency spectrum ranges from 20 kHz to 1 GHz. Magnetostrictive transducers typically operate below 30 kHz; this is because physical size constraints make them impractical for most applications of higher frequency (Cleaning Technologies Group, 2003). Piezoelectric transducers and CMUT's are more versatile as they have the ability to operate over almost any ultrasonic frequency whilst remaining small and compact in size (Oralkan, et al., 2002).

2.4.5.2. Audible Noise

Magnetostrictive transducer noise originates from three main sources: noise caused by magnetostrictive strain of the core, noise caused by interactions between the windings and the load current passing through it and the noise emitted by auxiliary equipment (Moses, et al., 2010). An adult human is capable of hearing sounds up to approximately 18 kHz which is the same frequency that magnetostrictive systems typically start operating. The first sub-harmonic is therefore within the human audible range. Consequently, magnetostrictive transducers may sound noisy to humans due to the large amount of energy released at the first sub-harmonic of the ultrasonic frequency (Cleaning Technologies Group, 2003).

Although piezoelectric transducers can start operating from 20 kHz, these transducers are designed to typically to start operating at 40 kHz, resulting in the first sub harmonic to resonate at 20 kHz. The first sub harmonic of these transducers is above the human audio range, and therefore cannot be heard (Cleaning Technologies Group, 2003). Their second harmonic, which does not contain as much energy as the first, can be heard at 10 kHz, but is consequently a lot less noisy. The CMUT is designed to be a low noise device for similar reasons (Gurun, et al., 2012).

2.4.5.3. Transducer reliability

Peizo and magnetostrictive transducers are highly reliable (Cleaning Technologies Group, 2003). CMUT technology is fairly new and has not yet proven to be as reliable as the peizo devices. Improvements in this area are being investigated and implemented in the newer designs (Huang, et al., 2005).

2.4.5.4. Generator Reliability

Piezoelectric and CMUT generators are more reliable due to the use of advanced semiconductors used in their production. Magnetostrictive designs use older technology which is more prone to failure due to high amperage and switching frequency (Cleaning Technologies Group, 2003).

2.4.5.5. Sweep frequency

Sweep frequency plays an invaluable role in the quality of the results which an ultrasonic cleaner can produce. CMUT and Piezoelectric transducers are capable of this feature, but magnetostrictive transducers are no (Khuri-Yakub & Oralkan, 2011).

2.4.5.6. Energy efficiency

Piezoelectric transducers and CMUT's are highly efficient devices because of there ability to directly convert electrical energy to mechanical energy. When power is applied to the piezoelectric active ceramic, it causes a change in shape which results into the formation of sound waves. Only 5% of the output energy is lossed in the ceramic caused by internal friction. This means that most of the energy (approximately 95%) applied to the transducer is utilised for cleaning (Cleaning Technologies Group, 2003).

Magnetostrictive transducers use a double conversion of energy, from electric to magnetic, and from magnetic to mechanical, and are thus usually less than 50% efficient due to this process. Their generators are also typically no more than 70% efficient. Therefore the comprehensive cleaning power is 30% - 40% efficient. Therefore piezoelectric transducers are by far a more efficient choice (Cleaning Technologies Group, 2003).

2.4.6. Ultrasonic generators

An ultrasonic generator is the device responsible for powering the transducers with the correct electrical parameters. The generator transforms the electricity from an input source with low frequency and amplitude, into a suitable form having high frequency and amplitude that would efficiently energise the transducers. The generator produces an electronic signal of high voltage in order to obtain these amplitudes, usually as an alternating current. The transducer has a intimate relationship with the generator as the latter is designed after the transducer is selected. One of the main reasons for this is because the frequency of the generator is determined by the response range of the selected transducer (Fuchs, 1995).

Figure 2-24: Signal transformation after the generator (Fuchs, 1995).

Each generator is designed with the capability of powering a specific number of transducers. Most transducers require a minimum amount of voltage to activate, which is typically 75% of the maximum operating voltage. Good quality generators have the ability to enhance the effectiveness of ultrasonic cleaning equipment. They have controls to vary the power and frequency transferred to the transducer and an additional feature which these generators may have is to control the degassing of a cleaning solution (Fuchs, 1995). The electronic structure of ultrasonic generators consists of three main components:
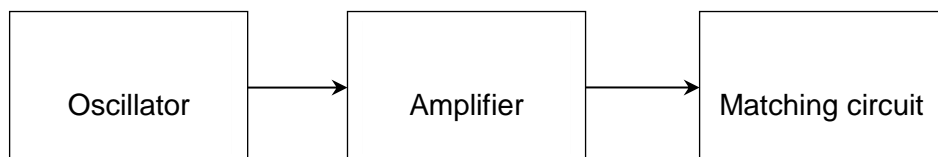
Figure 2-25: The block diagram of an ultrasonic generator. (Fuchs, 1995)

The reliability and functionality of an ultrasonic cleaning device relies predominantly on the quality of the ultrasonic generator and the transducers incorporated in its design.

2.4.6.1. Oscillators

An oscillator is an electronic circuit used to provide a system with an accurate timing reference. These circuits often incorporate 555 timers or a pulse width modulator, which generate a periodic output signal from a DC voltage as an input. The output voltages can be sine waves, square waves, triangular waves, or sawtooth waves depending on the type of oscillator (Floyd, 2012). These waves are then used as the input signal to the amplifier.
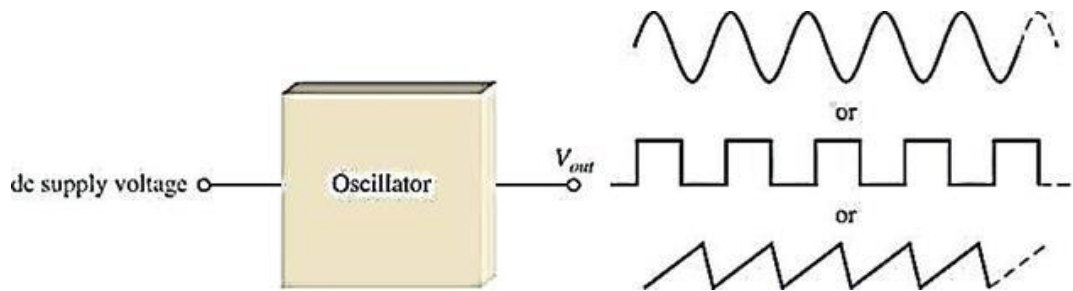
Figure 2-26: The oscillator concept showing the different output waves (Floyd, 2012).

The 555 timers such as the LM555 render fast rise and fall times, precision and stability (Fairchild Semiconductor Corporation, 2002). A PWM device such as the SG3425 on the other hand provides dual inverted outputs allowing for ease of connection to amplifier stages, better protection, higher input voltage, simple external circuitry and greater output power capabilities (Texas Instruments, 2003).

2.4.6.2. Amplifier

The amplifiers used in ultrasonic generators are either transformers, linear or switch mode amplifiers. They magnify the oscillator output signal to produce enough power to drive the transducer, their topologies differ greatly and are shown in Figure 2-27.

Linear amplifiers such as a class AB amplifier magnify their input signals by using the gain of a transistor. They have good efficiency, low distortion and remain linear over a wide bandwidth. This topology is common in applications which do not require very high output power such as distance measurement (Floyd, 2012).

Switch-mode amplifiers use transistors as switches which toggle on and off alternatively. They offer benefits of smaller size and less weight. The amplifier can be smaller and lighter because of compact circuits and smaller heat sinks. Compared to a linear power amplifier, a switching amplifier is more efficient because it operates at a lower temperature and draws less current (Berglund, et al., 2006).
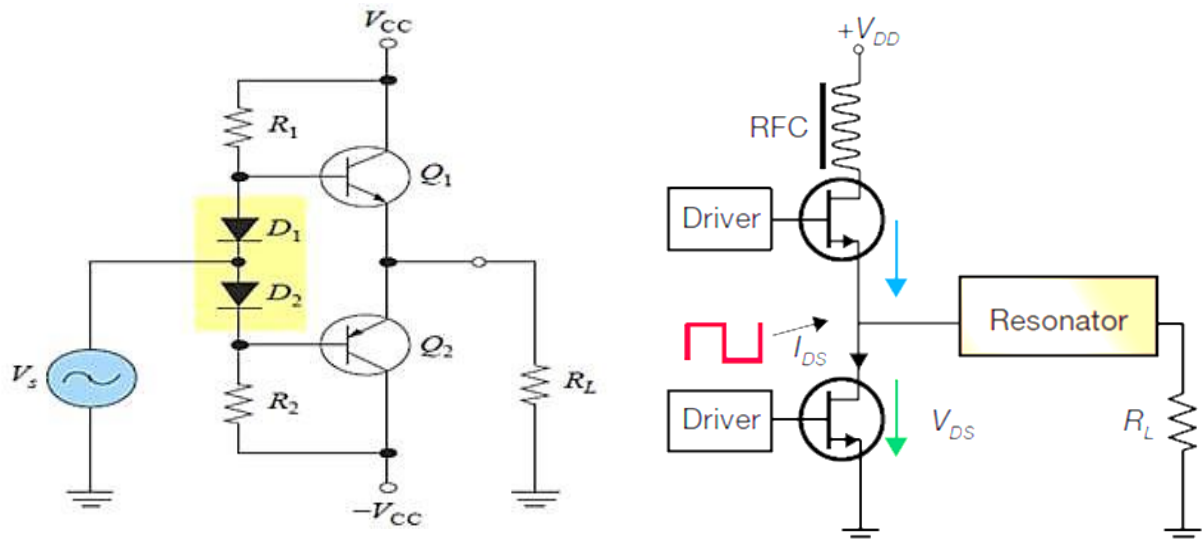
(a) Linear amplifier (Floyd, 2012).　　　(b) switch mode (Berglund, et al.,
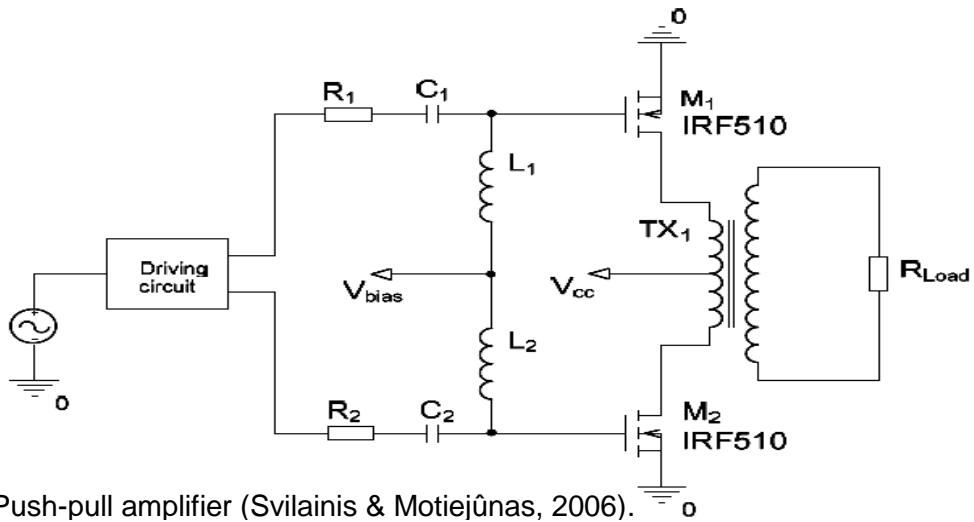
(c) Push-pull amplifier (Svilainis & Motiejûnas, 2006).

Figure 2-27: Amplifier topologies for ultrasonic applications.

Push-pull transformers function when a signal current is applied through a primary winding. The signal creates a magnetic field which induces a voltage across a secondary winding. When a load is connected to the secondary winding, it causes a magnitude of AC current to flow depending on the turn's ratio. These devices can be configured to step voltage and current up or down, provide DC isolation between circuits and yields efficient AC transmission. In ultrasonic applications specifically, transformers contribute towards impedance matching and noise suppression (Lefrak, 2015).

2.4.6.3. Matching circuit

Matching the genrator output impedance to the input impedance of the transducer is very important in ultrasonic systems. A matching circuit is required to maximize the power delivered to the transducer which would otherwise be wasted in the form of heat. Introducing an inductor in series or parallel is a frequently used method to acquiring a match. The purpose of this inductor is to compensate for the reactive component of the transducer (Garcia-Rodriguez, et al., 2010).
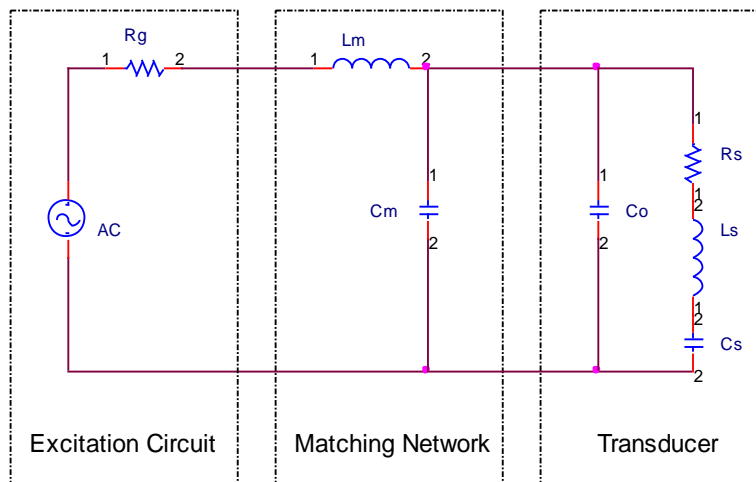
Figure 2-28: A low pass filter configuration (Garcia-Rodriguez, et al., 2010).
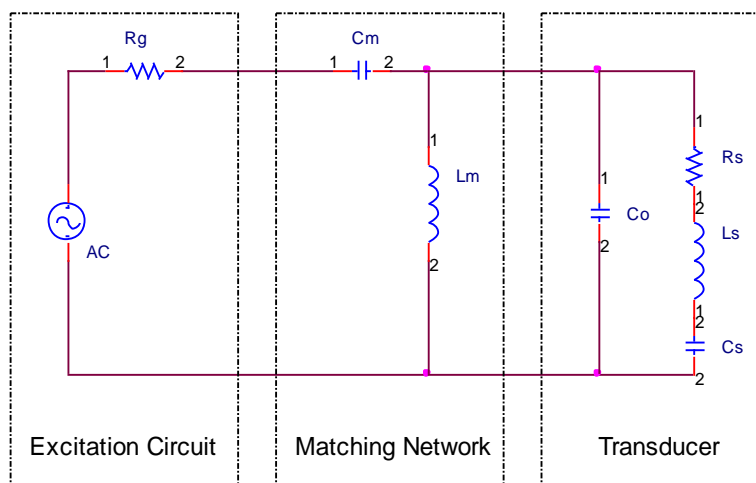
Figure 2-29: A high pass filter (Lou, 2012).

The configuration of a low-pass filter or high-pass filter can be utilised but the former is preferred in nonlinear systems to avoid false excitation due to harmonic interferences. Implementing these filters result in a more efficient ultrasonic system and maximises power, their equivalent electronic circuits are shown in Figure 2-28 and Figure 2-29 respectively (Garcia-Rodriguez, et al., 2010).

2.4.7. Power Intensity Control

This is a control feature which allows the operator to reduce the overall power being provided to the transducers. It causes a reduction in the power sent to the liquid, hence reducing the size of the cavitation bubbles and imploding force. This control gives the operator the ability to balance between maximum cleaning efficiency and minimum damage to the contaminated object. Cavitation threshold is the minimum amount of power required to achieve cleaning. This threshold is determined by the type of transducer and the solution used (Capelo-Martínez, 2009).

2.4.8. Operating frequencies

Each ultrasonic operating frequency possess unique characteristics. These characteristics determine which operating frequencies should be used depending on the cleaning application.Higher operating frequencies produce a gentle scrubbing action, and cleaning is more evenly distributed across the targeted surfaces. The lower frequencies produce a more aggressive cleaning action, but the targeted surfaces are not as evenly cleaned within the tank (Yaku, et al., 2009).

Different operating frequencies are required for optimal cleaning results. The object size and shape aswell as the type of contaminant will determine which frequency would be best suited for a specific application.

- 20 kHz - 40 kHz: this is the optimal frequency range for cleaning larger objects more effectively such as engine blocks and heavy metal objects, with greasy contaminants (Yaku, et al., 2009).

- 40 kHz - 70 kHz: This range is optimal to efficiently clean machine parts, amongst others. Hotspots of approximately 12.7 mm apart are common using this frequency range. Cavitation distribution is more even than at 25 kHz and this is the best range to remove small particles (Yaku, et al., 2009).

- 70 kHz – 1 MHz: Produces a gentler and more evenly distributed cleaning action. The blast radius of cavitation at these frequencies are not as large as that produced in lower frequencies. The contaminated areas are however evenly cleaned at all times. This range allows for extremely fine cleaning of semiconductor wafer disks and optics (Yaku, et al., 2009).

When selecting an ultrasonic frequency, the physical size of the part being cleaned has to be considered. Lower frequencies are typically used for large and heavy objects as their penetration into internal gas cavities are deeper. If a high frequency were used for this application, the exterior surface of the object would be cleaned, but the interior of the object would still be contaminated. This is why Multi-frequency ultrasonic cleaning systems which contain two or more ultrasonic frequencies in the same tank were developed. By merging two or more frequencies, the range of particle sizes cleaned effectively is greater than that of a single frequency system while maintaining an evenly distributed cleaning action. (Zenith Mfg & Chemical Corp., 2010).

2.4.9. Resonant frequency tracing techniques

Due to changes in the load and transducer, the resonating frequency of a transducer does not remain fixed. If the output of the generator does not match the resonating frequency of the transducer, the system efficiency will be reduced. Consequently, automatic resonance frequency tracing (ARFT) techniques are implemented to latch onto the resonant frequency and retain the optimum performance of the transducer (Dong, et al., 2012)

2.4.9.1. Phase-locked loop

This control method in effect follows the resonant frequency of the transducer by monitoring when the current and voltage are in phase. If a phase difference is present, the phase-locked loop will adjust the frequency until the current and voltage are again in phase (Claassen, 2005).
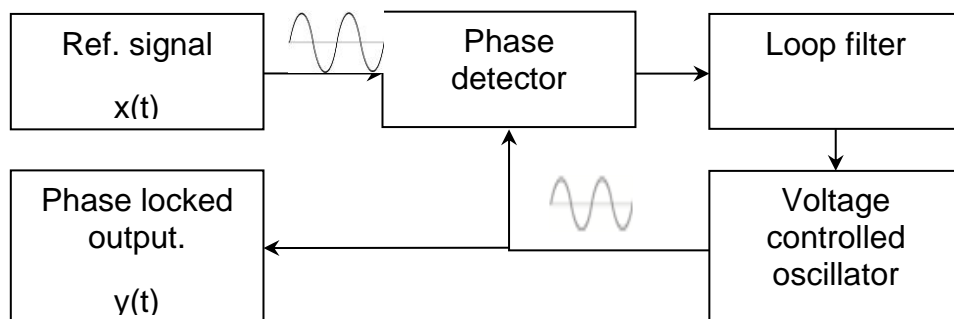
Figure 2-30: A block diagram of basic phase-locked loop technique (Terlemez, 2004).

Phase-locked loops are found in a wide range of applications in the areas such as wireless systems, digital circuits and communications. (Kolumban, 2012)
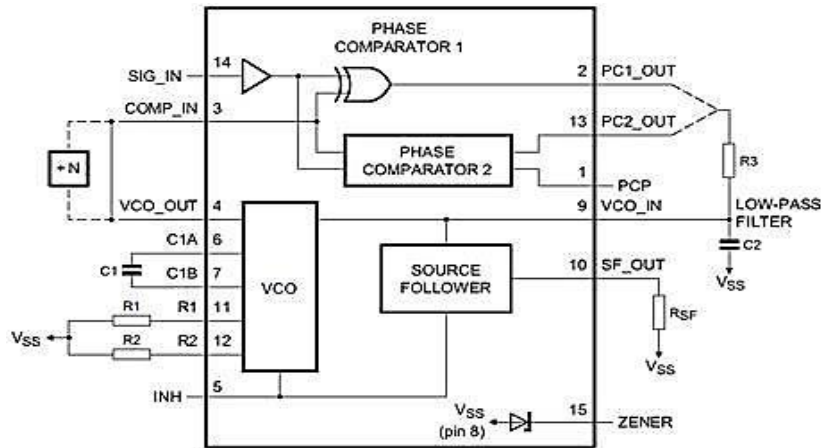
Figure 2-31: The functional diagram of a phase-locked loop IC (Nexperia, 2016).

2.4.9.2. Admittance locking

This tracing technique is also called the current locking method. Based on the fact that at resonance, maximum power and current flows to the transducer. A current sensor samples the current and feeds it into a peak detector which stores the peak current of each sample. A microcontroller then does the necessary manipulations and adjusts the frequency one increment at a time via the voltage controlled oscillator until maximum current is sent to the transducer (Mortimer, et al., 2001).

Admittance locking is a method based on the principle that maximum power transfer from the transducer to the load occurs when the transducer is operated at maximum admittance. This phenomenon occurs when the transducer is being operated at its series resonant frequency. This also implies that the voltage and the current driving the transducer are in phase (Payne, 2005).
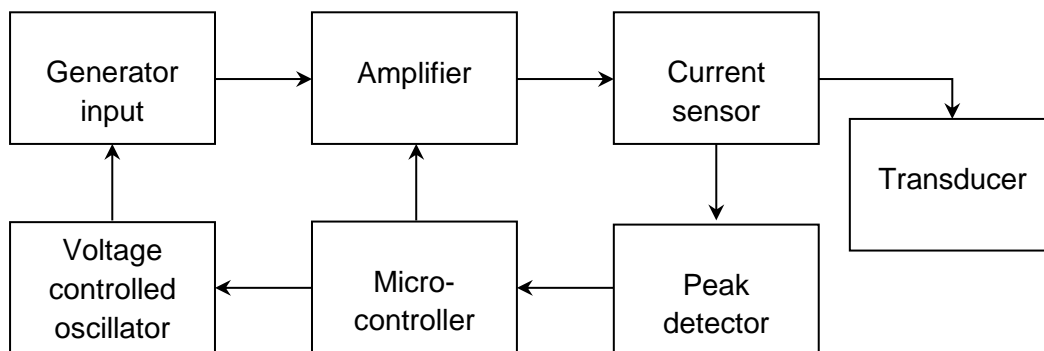
Figure 2-32: A block diagram of the admittance locking technique (Payne, 2005).

A current transducer such as the LEM depicted on Figure 2-33, is used to sample the current readings for the microcontroller. It operates by using the magnetic flux created by the primary current, Ip, to induce a balanced complementary flux into the

secondary windings. A hall device equipped with flux-gate technology,and two amplifiers are used to generate the highly precise secondary current, Is (LEM, 2011).
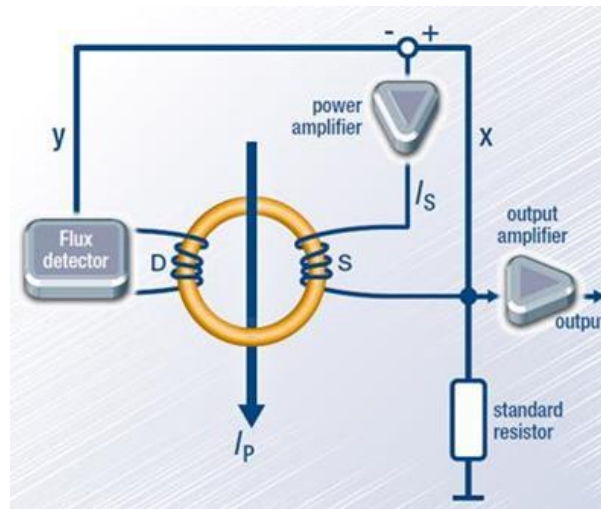
Figure 2-33: Current transducer operation (LEM, 2011).

The current transducer is used to sample current at each set point in order to perform the admittance locking technique. The LEM has some desirable features such as a broad frequency range, satisfying overall accuracy, quick response times, and eliminates the need for a peak detector.

2.4.9.3. The benefits of ultrasonic cleaning

Cleaning using ultrasound has many advantages over conventional methods. The waves created in ultrasound are evenly distributed in an ultrasonic tank and cause even implosions in a liquid medium. This means that the cleaning energy will be able to get to the awkward areas as well as the easier areas. A notable advantage is that ultrasound cleans uniformly no matter what the shape of the object (Fuchs, 1995).

The use of ultrasonic cleaners reduces and sometimes completely eliminates the need for strong and often expensive solvents, making this cleaning method a more environmentally-friendly option. Waste water from this cleaning method is often solvent-free or can be treated on site, eliminating the need for costly waste-water management systems. Where solvents are used, they are mostly mild chemicals and do not give off CFCs and other harmful substances, as many other industrial cleaning compounds do (Sivakumar, et al., 2009).

Ultrasonic cleaners are mostly compact devices and can be moved and operated with ease, contrary to conventional cleaning methods which require either bulky machinery, or elaborate manpower. This not only makes them user-friendly, but also eliminates costly transportation or training costs for employers. Ultrasonic cleaning further provides for a standardised and guaranteed result. Less damage to an object will occur as a result of human error or harsh cleaning chemicals. Due to the nature of ultrasonic cleaning, it can be used to clean extremely small fissures and holes where conventional methods would be inept (Shoh, 1975).

2.4.9.4. The limitations of ultrasonic cleaning

While higher frequencies provide smaller bubbles, resulting in a gentler implosion and therefore a gentler cleaning motion, these small bubbles are not always sufficient to remove all of the contaminant on the object's surface. Conversely, a lower frequency, resulting in a larger bubble and stronger implosion, can cause damage to the surface of objects, particularly to the surface of smooth objects (Lamm, 2003).

The number of cavitation bubbles increases proportionally to the temperature increase. This means that an ultrasonic cleaner may not be a viable option for the cleaning of temperature-sensitive objects. Due to the fact that water plays an important part in the ultrasonic cleaning process, items that may be damaged by liquids, such as electronic parts cannot be cleaned with ultrasound unless a proper drying process is implemented (Pedeflous, 2014).

2.5. Line walkers

Line walkers are drones which are suspended on the transmission lines in order to perform a specific task. Various types of line walkers have been developed to date, these machines reduce labour costs, improve efficiency and minimise the risk of injury to maintenance personnel. The transmission line robots developed to date are predominantly inspection types, utilising camera equipment to identify present faults and future problems. The latest designs incorporate light repair facilities related to broken strands, abrasion and corrosion either autonomously or remotely by an engineer on the ground (Toussaint, et al., 2009).

2.5.1. Transmission line robot technologies

Several methods of achieving locomotion and a few prototypes have been developed after much research and technological advancements. The existence of problems related to ability, autonomy and stability are among the main hurdles of these machines (Toussaint, et al., 2009).

2.5.1.1. Expliner

The Expliner inspection robot is developed by HiBot Corporation, one of the leaders in the field of robotics and Kansai Electric Power Corporation (KEPCO), the largest electric company in South Korea. The autonomous robot navigates along the transmission lines using pulleys. Their design uses a manipulator which moves its centre of mass (counter-weight and camera) in order to overcome obstacles such as strain clamps. This machine is one of the first to use two cables for its locomotion whilst conducting inspections (Debenest, et al., 2010).
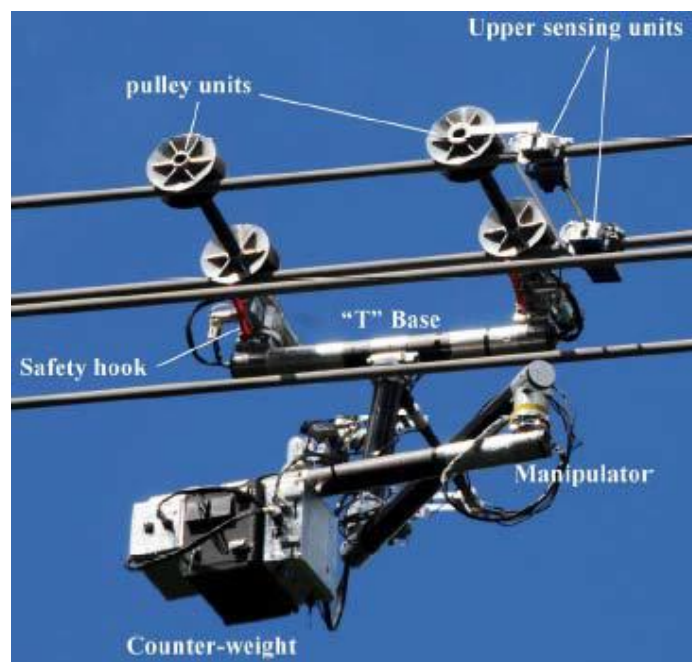
Figure 2-34: The main components of the Expliner robot (Debenest, et al., 2010).

The four wheels connected to a pulley system are responsible for propulsion, whilst the counter weight offers balance and stability when navigating the hot line. Safety hooks are locked in to ensure that the drone does not fall from the line, and several sensors provide data for analysis (Debenest, et al., 2010).

2.5.1.2. LineScout

The LineScout was developed at Hydro-Qu´ebec's research institute (IREQ). This pioneering robot has successfully been used in the field. It possess three pan-and-tilt cameras (PPTC) and a two-wheel platform capable of crossing obstacles up to 0.76 m in diameter within two minutes. Two grippers under the cable are used to securely grasp on either side of the obstacle (Pouliot & Montambault, 2008).

The propulsion wheels are then removed from the line, dropped down, and shifted across the obstacle.. This machine travels along a single energised conductor at a top speed of 1 m/s, and weighs 98 kg. The robot is shielded against radio-frequency and electromagnetic interferences (RFI/EMI) and can be operated in either teleoperation mode or autonomous mode (Pouliot & Montambault, 2008).

Figure 2-35: The LineScout crossing an insulator string (Pouliot & Montambault, 2009).

Recent upgrades to the LineScout include variuos sensors and maintenance tools. Among them are, an electric torque wrench, an electrical resistance measurement sensor and a tool to repair broken conductor strands (Pouliot & Montambault, 2009).

2.5.1.3. Chinese Academy of Science (CAS) robot

The Chinese Academy of Science (CAS) has developed an advanced dual-arm robot that travels along the overhead ground wires (OGW). The robot was is designed for live-line inspections using a video camera. The device has two wheels

which are each rigged with a clamp that can securely grasp the conductor to allow the mass (control unit) to be centred on either of the two arms (Zhu, et al., 2006).

This device uses two methods of crossing obstacles. One method, known as the "cankerworm method", centres the mass on the rear arm, lifts the front wheel, moves foward until the front has passed the obstacle after which it returns the front wheel back onto the conductor. The procedure is then repeated for the rear wheel. The second method moves close to the obstacle, stabilizes the robot by gripping the wire with the clamp on the front wheel, lifts and rotates the rear across to the other side of the obstacle, and repeats the procedure for the other arm (Zhu, et al., 2006).

Figure 2-36: The CAS robot crossing a vibration dampener (Zhu, et al., 2006).

This prototype is capible of reaching speeds up to 2 m/s, weighs 40 kg and the two arms are 240 mm apart. Its control algorithm is based on an advanced system that uses information from several on-board sensors to maneuver along the transmission lines autonomously (Zhu, et al., 2006).

2.5.1.4. Crab Crawler

The Crab Crawler is a Swiss designed line robot which navigates on the overhead ground wires (OGW) for the purpose of inspecting high-voltage power lines. This

drone uses six motorized rubber rollers, two of which are positioned horiontally, primarily to manage the weight. The remaining four rollers are vertically positioned for propulsion, and are used to overcome not only line hardware fittings, but mast (tower) tips as well. The design incorporates a spring system between the vertical rollers which are tapered in shape to increase stability (Buhringer, et al., 2010).

When an obstacle is sensed, the front rollers open and embrace the obstacle. The spring system in conjunction with the rollers then manoeuvre the robot back into a central position before latching on to the other side of the obstacle. The two horizontal wheels follow by traveling over the top of the obstacle. When the two rear vertical rollers approach the obstacle, the front pair has already passed and the sequence is repeated (Buhringer, et al., 2010).
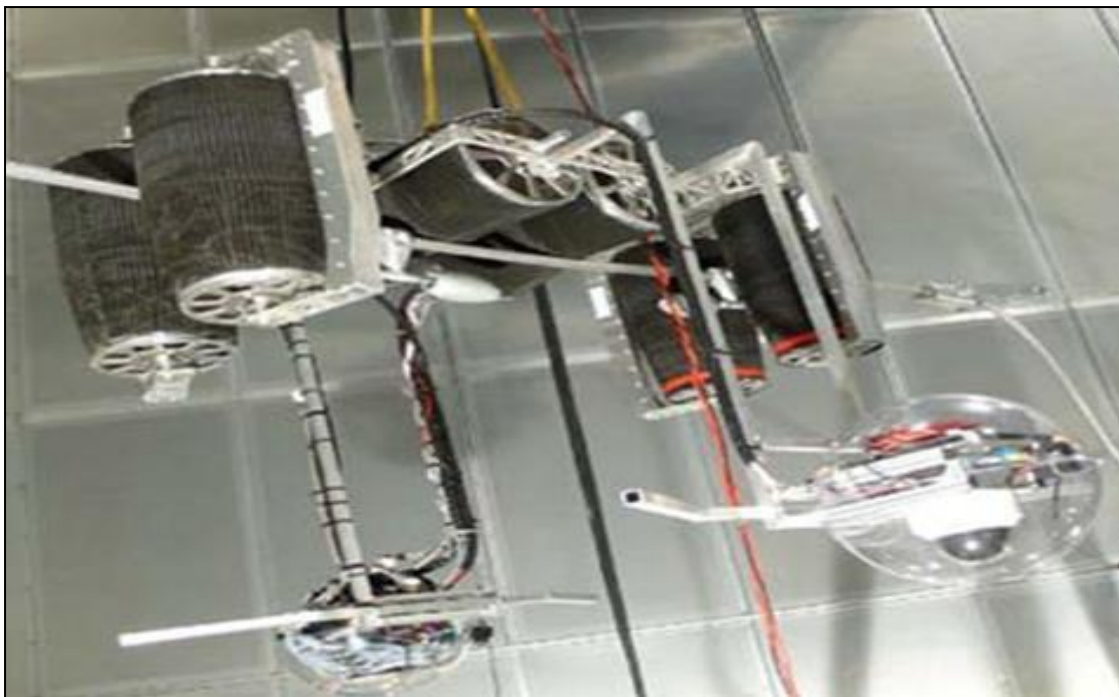
Figure 2-37: The Crab Crawler prototype (Buhringer, et al., 2010).

This prototype uses a dome camera for the inspection and is capable of some autonomous actions. The rollers produce a torque of 10 Nm through a gear belt reduction of 2:1 and this device only weighs 58 kg (Buhringer, et al., 2010).

2.5.1.5. AApe-C1

This robot is an intelligent insulator detector. It operates by measuring the resistance of the insulator under a live-line condition to determine if the insulator is faulty. A

synchronous belt coupled to a motor propels the robot supported by two brackets which wrap around the insulator string. Resistance is measured with two spring detection probes which make contact with the steel caps of the insulator strings (Hongguang, et al., 2010).
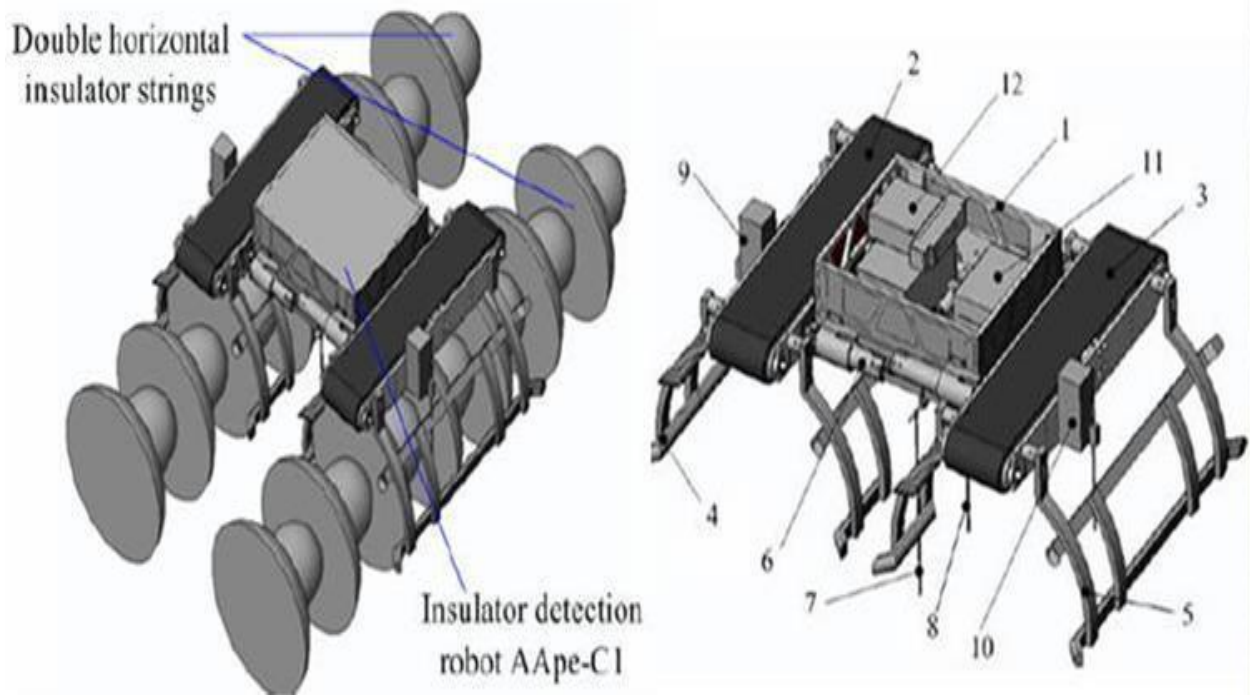
Figure 2-38: The AApe-C1 robot used to detect insulator faults (Hongguang, et al., 2010).

The insulator detection robot AApe-C1 is capable of autonomusly walking along double horizontal insulator strings while testing the insulator status one at a time. The device is protected against electromagnetic interference and proved reliable when tested in a field environment (Hongguang, et al., 2010).

2.5.1.6. Status of transmission line robots

Presently, some technologies have a much higher level of advancement than others. Several teams are investigating various challenges and many of their studies are only theoretical in nature.The possibility of these teams collaborating together could emerge, leading to promising developments (Toussaint, et al., 2009).
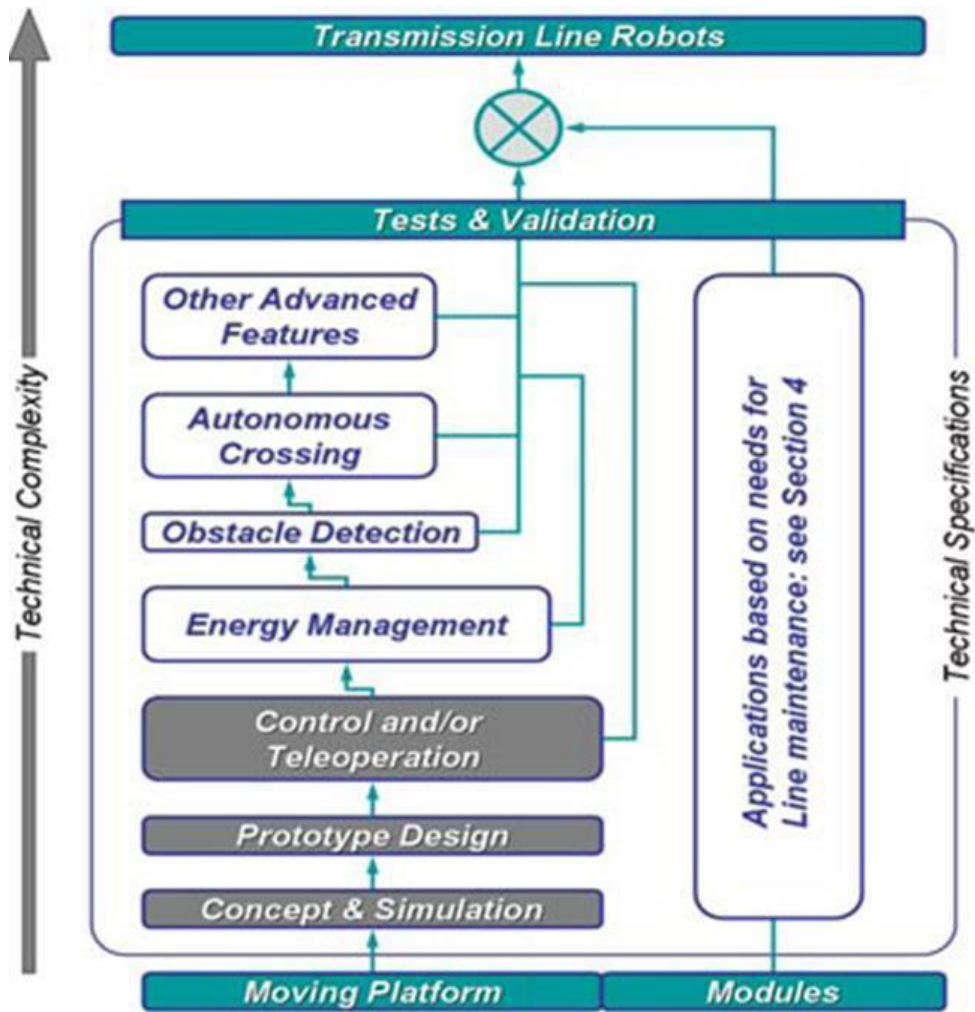
Figure 2-39: The state of line robot technology (Toussaint, et al., 2009).

Figure 2-39 depicts several levels of technological advancement that could result into mass production of transmission line robots. The shaded boxes also indicate research areas where results are plentiful and the white boxes indicating areas where there is much needed research required (Toussaint, et al., 2009).

2.5.2. Line walker's Operational environment

The environment of high voltage transmission lines is dangerous and complex (Beaty, 1998). Their complicated architecture, hardware fittings, high magnetic and electric fields make the locomotion of the suspended robot extremely challenging (Wei, et al., 2013). Figure 2-40 depicts the transmission line towers or pylons (1) supporting one conductor per phase (6) suspended by insulator strings (3), which can either be suspension (vertically positioned) or strain (horizontally positioned) type insulator strings. Other devices such as signalling spheres (7), clamps (4) and

- 43 -

vibration dampers (5) are common to the lines. More devices including spacers and spacer dampers (2) are used on bundle power lines (Pouliot & Montambault, 2008).
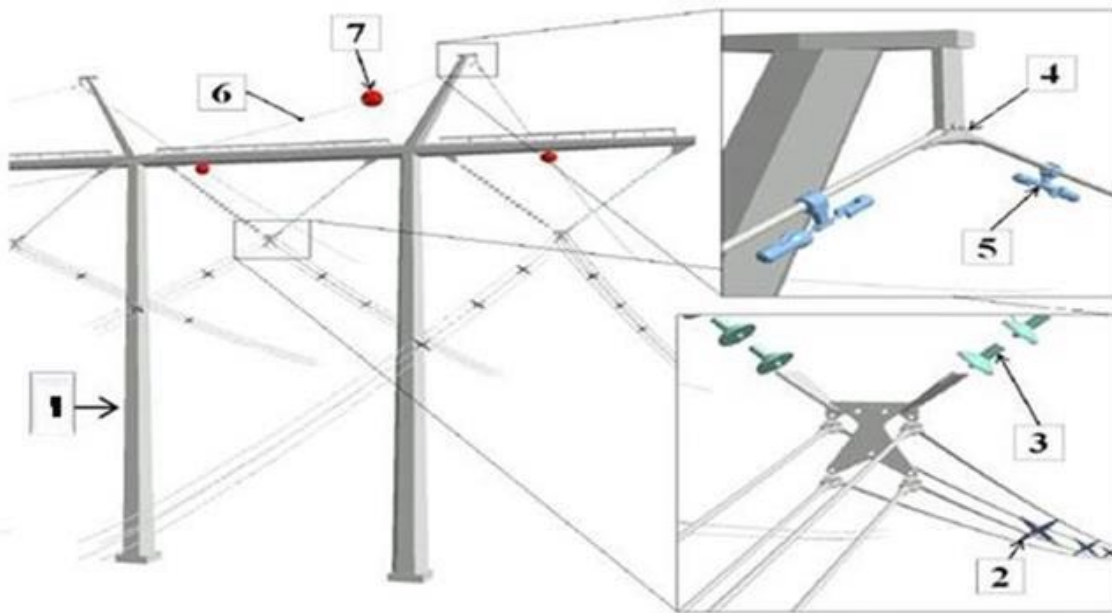
Figure 2-40: The architecture of transmission lines as redrawn from (Pouliot & Montambault, 2008).

There are several hardware fittings serving various purposes, which form part of the architecture of high voltage transmission lines. These devices can be seen as obstacles that the drone has to overcome and needs to be taken into consideration when designing a robot to be suspended by Aluminium conductor steel-reinforced (ACSR) cables. The most common obstacles are shown in Figure 2-41; from the left they are insulator strings, indicating spheres, vibration dampeners, spacers, repair sleeves and clamps (Wang, et al., 2010).

Figure 2-41: Several hardware fittings found on transmission lines (Wang, et al., 2010).

2.5.3. Line robot hardware

In this section the fundamental components and their alternative options of a basic line walker is discussed. The topology in Figure 2-42 describes the operation of a simple line walker and how they are linked (Toussaint, et al., 2009).
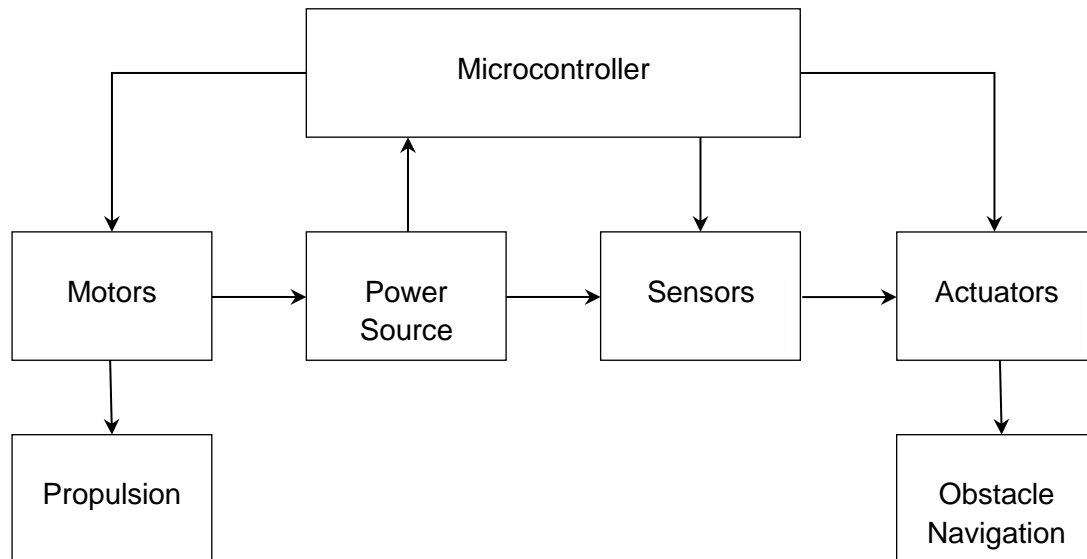
Figure 2-42: The line walker topology (Gonçalves & Carvalho, 2013).

2.5.3.1. Power source

The ability to harvest energy from the line which suspends the robot exists but adds a degree of complexity due to the high voltages and circuitry required to convert this energy. The advantage of tapping off the grid would be an excess supply of power but on the other hand, the occurrence of a power outage would cause the drone to shut down as well.

A rechargeable battery would be a simpler and more reliable option. Rechargeable batteries are manufactured with different sizes, shapes and capacities, ranging from small button cells to large megawatt systems. Batteries have several different combinations of electrolytes, electrode materials, weight, sizes and lifespans (Pinson & Bazant, 2013).

Figure 2-43 shows (a) Nickel cadmium (NiCad), (b) Lead–acid, (c) nickel metal hydride (NiMH), (d) lithium ion (Li-ion), and (e) lithium ion polymer (Li-ion polymer) battery types that can all be used as the power supply for these drones (Mantech Electronics, 2015).
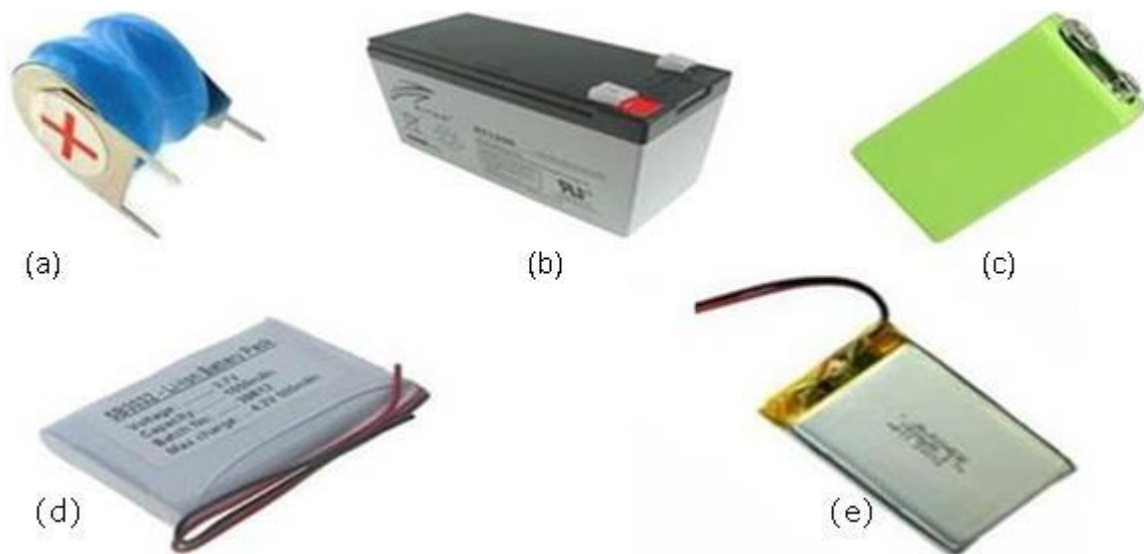
Figure 2-43: Various rechargeable batteries (Mantech Electronics, 2015).

The nickel cadmium and nickel metal hydride batteries are found to have small capacities, unlike the lead acid battery which would be a stable source but has a much heavier weight. The lithium ion and lithium ion polymer types are found to possess high capacities, are significantly lighter than lead acid batteries and can easily be connected together in banks to accommodate higher voltages. Capacity fade in Li-Ion and Li-Ion polymer batteries occur over thousands of cycles, and can be recharged by an renewable source such as solar or wind power. The former would be preferred on a line walker due to space constraints and weight reduction purposes (Pinson & Bazant, 2013).

2.5.3.2. Microcontroller

Every line robot has a one or more microcontrollers which can be considered to be the brains of the system. A microcontroller is a tiny computer on a single integrated circuit containing a processor core, some memory and programmable input / output peripherals. These semiconductor devices link together and control all the individual line walking components and event timing. Several types of controllers are developed by various companies.Their complex architecture is broken down into several categories noted below (Singh, 2008).
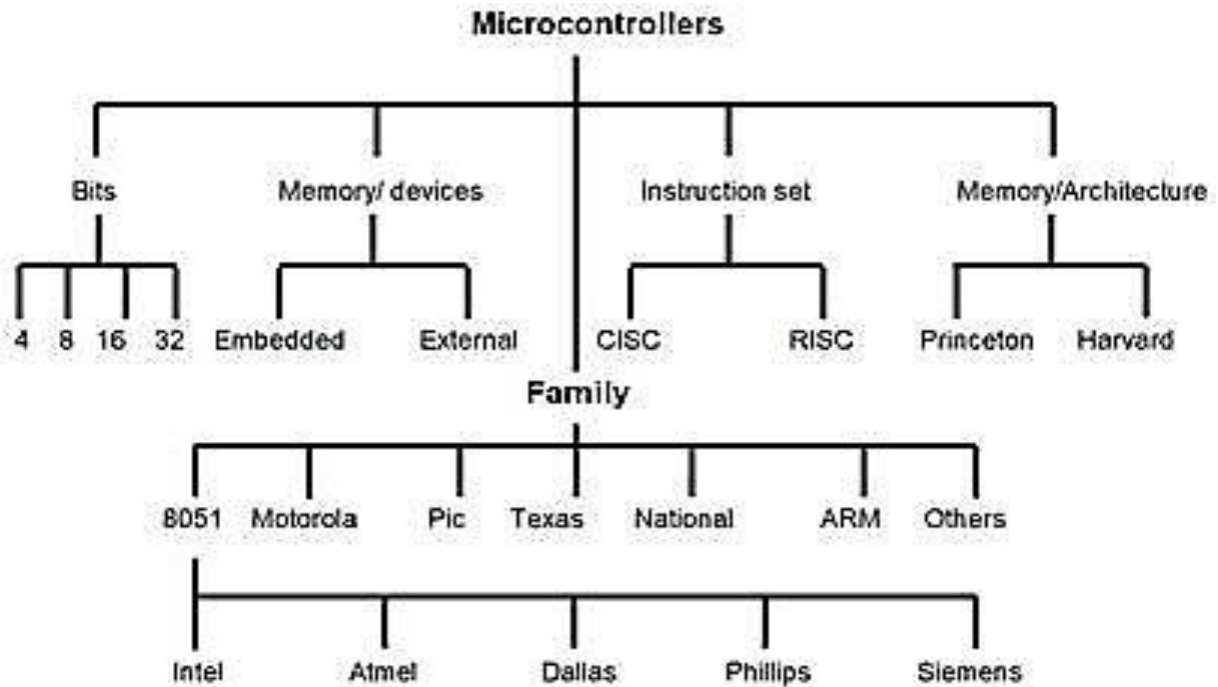
Figure 2-44: Different types of microcontrollers (Singh, 2008).

Microchip (PIC) and Atmel Corporation (Atmega) are amongst the leading companies in the industry. They manufacture devices which are powerful, fast and programmed via many platforms such as Arduino and visual basic. These platforms allow for ease of communication and offer programming support (Huang, 2013).

2.5.3.3. Propulsion motors

A Line Walker is propelled along the line by either AC or DC motors, the former being the Heavier of the two. These motors are capable of handling heavy loads through gearing systems. The motors in Figure 2-45 have several sizes, shapes, speeds, and operating voltages. They all convert electrical power into a mechanical movement through the forces produced by magnetic fields (Hughes, 2005).

DC (brushed) motor   Brushless DC motor   DC stepper motor

Figure 2-45: Several types of propulsion motors (Mantech Electronics, 2015).

The DC motors are the simplest and cheapest solution for propelling the line walkers. They are capable of changing their direction and are easy to control. These motors usually make use of a driving circuit to manage their power requirements. These circuits also allow for better speed control and offer a degree of protection against excessive voltages (Hughes, 2005).

2.5.3.4. Actuators

The robotic legs which suspend the robot are controlled by actuators. On one end the leg connects to the wheels and on the other to the chassis of the robot. They function by converting electric current, hydraulic fluid pressure, or pneumatic pressure into energy or power, often in the form of mechanical movement (Janocha, 2004).
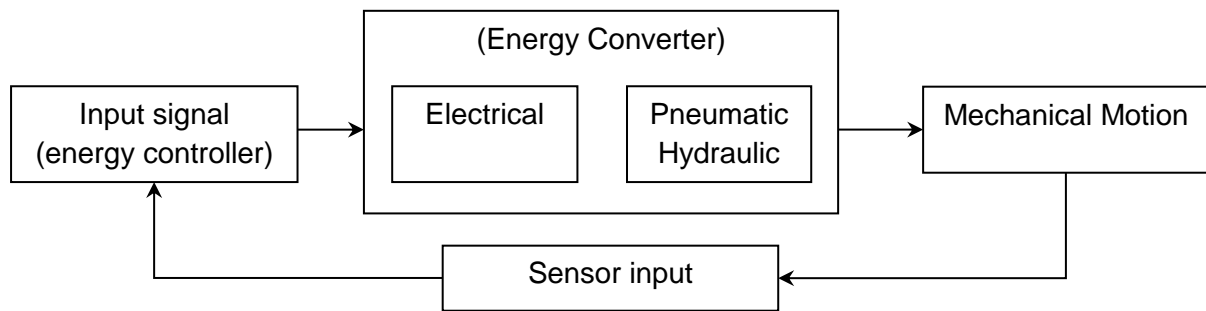
Figure 2-46: Actuator function block diagram (Janocha, 2004).

These devices achieve high torque and displacement accuracy through control circuits requiring very low electrical power. Communication to and from these mechatronic devices is simple as they often have logic level outputs making them microcontroller compatible (Janocha, 2004).

Hydraulic   Electric   Pneumatic

Figure 2-47: Types of actuators (Hoeribiger, 2015) (Mantech Electronics, 2015) (Langro, 2011).

The hydraulic systems can deliver high power and forces but are prone to problems such as leakage of the hydraulic fluid and contamination of fluid. The pneumatic

systems are large, loud and require compressed air to operate whereas electrical servo motors are small, silent, more efficient and simple to code. (Design World, 2008)

2.5.3.5. Proximity sensors

The line walkers need to be able to detect when obstacles are in their path. Various types of sensors are responsible for detecting obstacles using physical contact, light and sound. Limit switches, infrared, and ultrasonic distance sensors are among the most frequently used for this application. These sensors notify the robot if there are any obstacles ahead so the wheels can be moved out of the way.

The ultrasonic and infrared sensors send a high frequency pulse out and measures the time it takes for the signal to bounce off an object and return It, then calculates the distance between the sensor and the object using the speed of sound in air. The mechanical limit switch functions by pivoting a lever through physical contact. (Sinclair, 2001)

Ultrasonic sensor   limit switch   Infra -red

Figure 2-48: Various types of proximity sensors (Mantech Electronics, 2015).

The infrared sensors may prove to be unreliable during the day as the natural sunlight has the ability to saturate the sensor input. The mechanical limit switch is a good option for simplicity reasons, but can only detect obstacles in very close proximity. The ultrasonic sensor offers detection from a distance and requires minimal programming to operate.

2.5.3.6. Position sensors

These devices are responsible for balancing the robots on the line. They monitor the position and orientation of the robot and tranfer the data collected to the controller. This allows for correction when the robot is unbalanced due to wind or other circumstances. Robotic systems use many different sensory devices to determine the position and orientation of an object. The two favourable types are the gyroscope

and the accelerometer sensor. They serve a similar purpose, but provide different forms of measurement:

- Gyroscope

The Earth's gravity is used to determine the orientation or changes in rotational velocity in a gyroscope device (Sinclair, 2001). A vibrating wheel gyroscope functions by mounting a freely-rotating disk known as a rotor, onto a spinning axis in the centre of a larger wheel. Rotation causes the axis to turn, and the central gravitational pull causes the rotor to remain stationary, indicating which way is down (McGrath & Scanaill, 2013).

- Accelerometers

Non-gravitational acceleration is measured by an accelerometer and is useful in determining changes in velocity and changes in position. These devices can also measure tilt and shock but not rotation. An accelerometer is designed to respond to the vibrations occurring during movement. It uses tiny crystals that are excited when vibrations occur. From this excitation, a voltage is generated as a reading of any acceleration (McGrath & Scanaill, 2013).

(a)   (b)

Figure 2-49: (a) Gyroscope and (b) Accelerometer sensor (Mantech Electronics, 2015).

The fundamental purpose of a position sensor on a line robotis to determine whether the weight of the robot is balanced equally. It does this by monitoring and comparing the current position to a predetermined referenced position. Both devices are capable of performing this task but an accelerometer sensor is considerably less expensive.

2.5.3.7. Mechanics

Most of the line walkers researched has 2 or 3 mechanical legs fixed to a chassis. The robots have several approaches to navigating and locking the wheels on to the line. The mechanics of the line walkers are made from the most light weight materials in order to reduce power consumption. Aluminium, carbon fibre and plastic are viable options due to their low density to high strenght ratio's as well as the low risk of corrosion. The chassis of these robots are designed to be robust and durable.

2.5.3.8. Wheels

Shaped for the line, the wheels guide the robot and should spin freely to make the motors operate as efficiently as possible. Wheels can be fashioned out of a wide range of materials and usually incorporate some form of rubber for gripping. Aluminium, steel alloys, plastic and carbon fibre materials are often used to produce wheels depending on their application.

2.6.   Literature review Conclusion

The literature review chapter provides a good indication of the vast scale of this project. An overview of all the building blocks, their limitation's and advantages are highlighted and discussed. A close look at the HVTL environment gains one insight into the various operating equipment used on these lines, this equipment governs the design of the line walker. A broad understanding into ultrasonic cleaning is achieved and is required to build an effective and successful solution. The delivery methods and ultrasonic frequencies are investigated and have the biggest impact on the transducer selection. The robotic line walkers discussed show that the field of robotics is growing. These advanced machines are using complex systems and algorithms, which will require to be simplified for this application in order to remain feasible.

Chapter 3

Design Specifications

This Chapter lists the topology and hardware options best suited for the ultrasonic cleaning line walker. The limitations and requirements of the project will be determined and a peculiar cleaning technique is introduced.

3.1 Topology

The proposed system will clean the insulators on the live overhead transmission lines (OHTL's) using the concept of ultrasonic cleaning. A transducer driven by a light weight ultrasonic generator will deliver the ultrasound. This equipment will be transported by an autonomous line walker which moves along the line and stops at dirty insulators to deploy the cleaner. The diagram in Figure 3-1 depicts the major components of the project and shows how they connect / operate together.
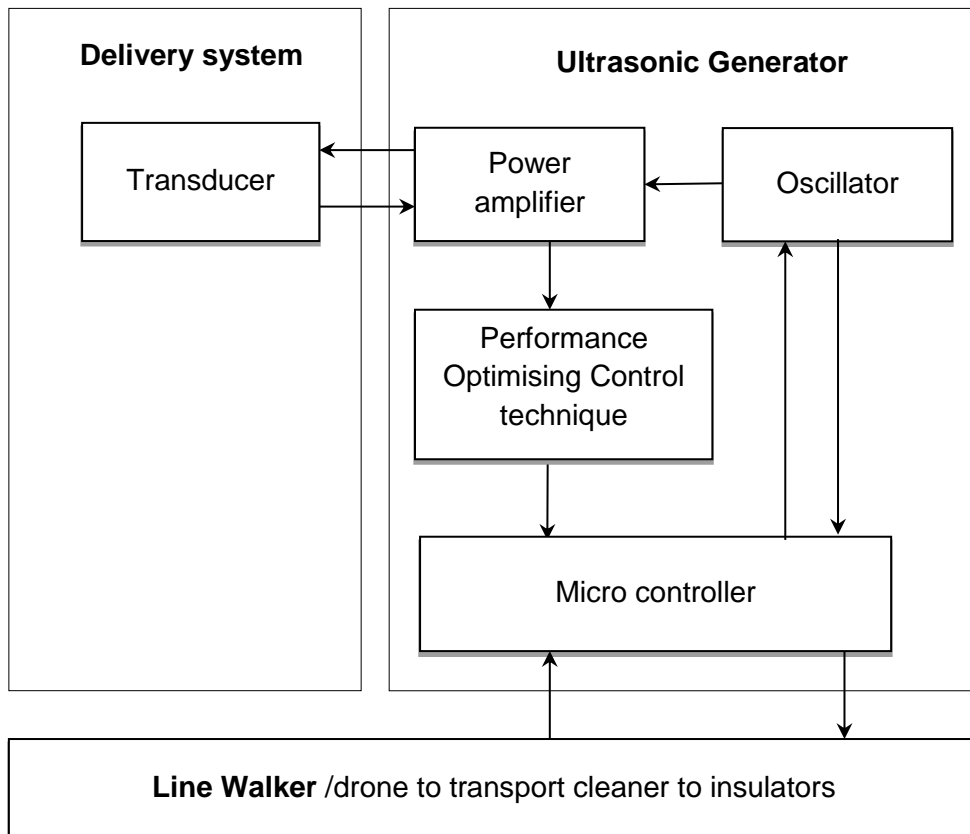
Figure 3-1: The Ultrasonic cleaning line walker block diagram

3.2 Delivery system

The delivery system must be compact, portable and efficient. Therefore the conventional bath system (which would require a pump, a filtration system and frequent solution change intervals) will not be practical. A peculiar technique of applying the ultrasound directly to the contaminated object will be used.

Similar to the brush method, the system will work by lowering the transducer just above the insulator and pumping a small amount of water through the face of the transducer. Cavitation will be achieved when the ultrasonic waves penetrate the water trapped between the transducer and the insulator, allowing cleaning to take place. This method eliminates the need for bulky equipment and would also minimize cleaning time as the ultrasonic energy is dispersed into a small amount of water instead of a large volume in a tank.

3.2.1. Transducer

The piezoelectric transducer is selected to clean the insulators, due to factors such as wide frequency range, reliability, availability, good efficiency and the ability to do a frequency sweep. The transducer used in this study has a resonant driving frequency of 28 kHz chosen because cleaning of heavy contaminants such as grease takes place at approximately 20 kHz - 40 kHz.

3.3 Ultrasonic generator

A PWM device is an ideal oscillator in this application. It provides the ability to manipulate frequency and duty cycle with minimal external circuitry. As the transducer is predominantly capacitive, a matching inductor will have to be designed to ensure that the transducer operates at resonance. The inductor will form part of a low pass filter which will contribute to better efficiency. This matching circuit configuration is chosen for its high output impedance and minimizes false excitation.

3.3.1. Automatic tracing technique

Digital admittance locking is chosen as the tracing technique to track the resonant frequency. This is done by decreasing the set point by one, then measuring the current. If the present current value is more than the previous current value, then the frequency is decreased another set point. If, however the present current value is less than the previous value, the frequency is increased by one set point and a new current value is measured. By tracking the points of maximum current, the sytem will be effectively locked on to the resonant frequancy.

3.4 Line walker hardware

This ultrasonic cleaning line walking prototype is controlled by an Atmega 2560 microcontroller; it is a powerful device, contains many I/O's and is compatible with the flexible and user friendly Arduino platform. Simple DC motors propel this robot with high torque properties, and digital servo motors are the more efficient choice of actuators chosen to manipulate the position of the robotic legs. A microprocessor inside the servo recieves the Atmega signals and processes them into very high frequency voltage pulses to the servo motor. The result is a servo that has a much faster response, smaller deadband, superior holding power and smoother acceleration. Two types of proximity sensors are used to detect obstacles. They are

limit switches and an ultrasonic distance sensor, the former for its reliability and the latter for the distance they can cover. The position sensor chosen is the less expensive accelerometer, which monitors the tilting movements to prevent the robot from being unbalanced.

The chassis of this prototype is fashioned out of fiberglass and aluminium as they are light weight, robust materials and plastic wheels is used to avoid arching whilst maximizing insulation. The robot size is determined by the distance between each leg, as this parameter is restricted by the size of the largest obstacle on the line. The diameter of the 132 kV line is 22 mm and therefore the wheels have a gap of 27 mm, to accommodate for ease of mounting whilst ensuring that the robot does not slip off.

3.4.1. Power Source

A good power source capable of delivering a stable voltage to the ultrasonic generator and line walker hardware is required. The solution is a 12 V lithium ion polymer battery pack which has large charging capacities, many life cycles, is light weight, small in size and locally available. It also reduces the risk of damage caused by voltage spikes that may occur if power is harvested from the line.

3.5 Requirements and limitations

A list of the specifications governing the requirements and limitations of this project is shown in Table 3-1. They are broken down into three categories: the generator; the High voltage transmission line environment; and the robotic platform.

Table 3-1: Specifications of the ultrasonic cleaning line walker

Specification	Value
Ultrasonic Cleaning generator	
Frequency range	20 kHz – 40 khz
Power source	12 VDC
Efficiency	> 65 %
Cleaning time	< 10 minutes
Ambient operating temperature	0 °C – 40 °C
Length x breath x Height	0.1 m x 0.1 m x 0.1 m
HVTL components and environment	
Conductor diameter	12 mm – 20 mm
Maximum obstacle length	0.22 m
Maximum conductor temperature	95.0 °C
Number of conductors	1
Maximum slope in span	25°
Ambient operating temperature	0 °C – 40 °C
Line walker robot	
Weight	< 60 kg
Length x breath x Height	1.40 m x 0.4 m 0.75 m
Traction force	500 N
Linear speed	0.1 m/s
Battery life	1.0 – 5.0 hours

Chapter 4
Design methodology

This Chapter walks through the design process and covers the three main stages of the project. The delivery system that would do the cleaning on the insulator is explained, thereafter the generator that would drive the transducer is analysed and finally the development of the line walker will be discussed in detail.

4.1 Delivery system

Initially a 28 kHz transducer was connected to an impedance analyser (Hewlett Packard 4192A LF) to determine the exact resonant frequency of the unloaded transducer. The process was recorded in a laboratory environment and the following data was captured:
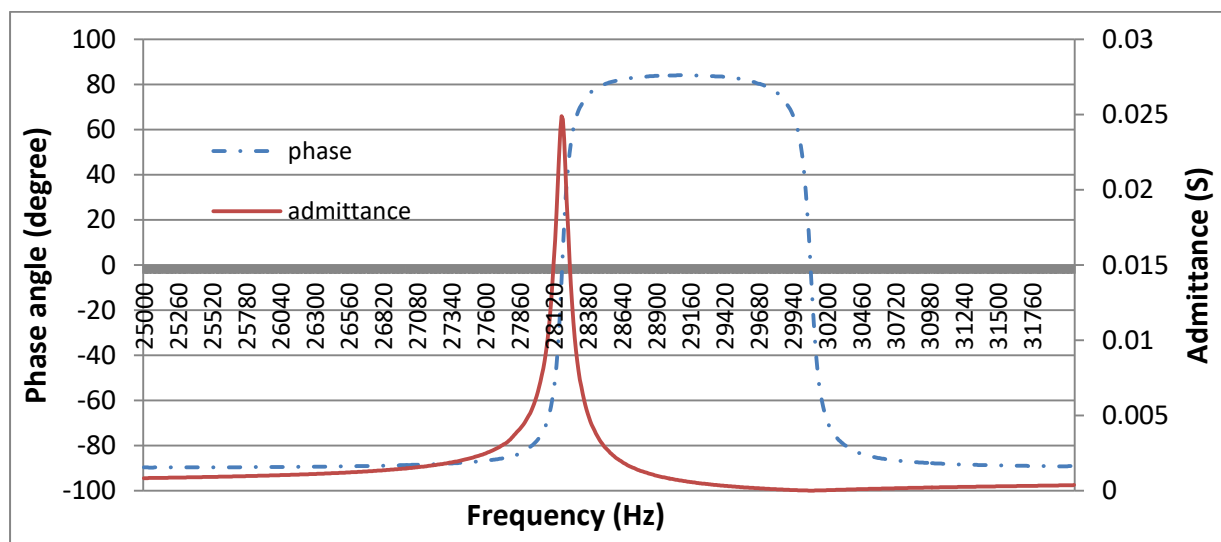
Figure 4-1: Frequency response curves of the piezoelectric transducer at resonance.

From the Figure 4-1 It is deduced that the actual resonant peak of the unloaded transducer is at 28.22 kHz. The phase angle between the voltage and the current has a magnitude of -90˚ to 90˚. The angle is positive only between 28 kHz and 30 kHz, indicating that this transducer has a narrow bandwidth. The generator will therefore require a sensitive and accurate control technique in order to operate the transducer at optimum efficiency.An experiment was then set up by placing a few drops of water in a 2 mm gap between the transducer face and a contaminated glass sheet.A crest amplifier and a signal generator were then used to drive the transducer in resonance to prove that this peculiar technique would work.

The signal amplitude was then increased until the concept proved to work upon visual inspection. An oscilloscope was finally used to measure current and voltage to the transducer. The voltage amounted to 60 Vrms whilst the current trended around 20 mA resulting in a power output of only 1.2 W.

By using this peculiar cleaning technique of applying ultrasound directly to an object, it is possible to design a compact portable device. This delivery method is subject to fewer limitations due to size, and broadens the range of application possibilities.

Figure 4-2: The peculiar cleaning technique.

A hole was drilled into the side of the transducer towards its face that would allow the delivery of water to the contaminated surface. 6 mm fish tank tubing was placed into the hole to transport the water from a reserve to the dirty surface.

Figure 4-3: The hole drilled through the transducer.

Delivering the water to the face of the transducer maximizes the effects that this peculiar technique can offer. Then, by using the principle of surface tension, the water is held between the face of the transducer and the object being cleaned and ultrasound is then applied directly to the object.
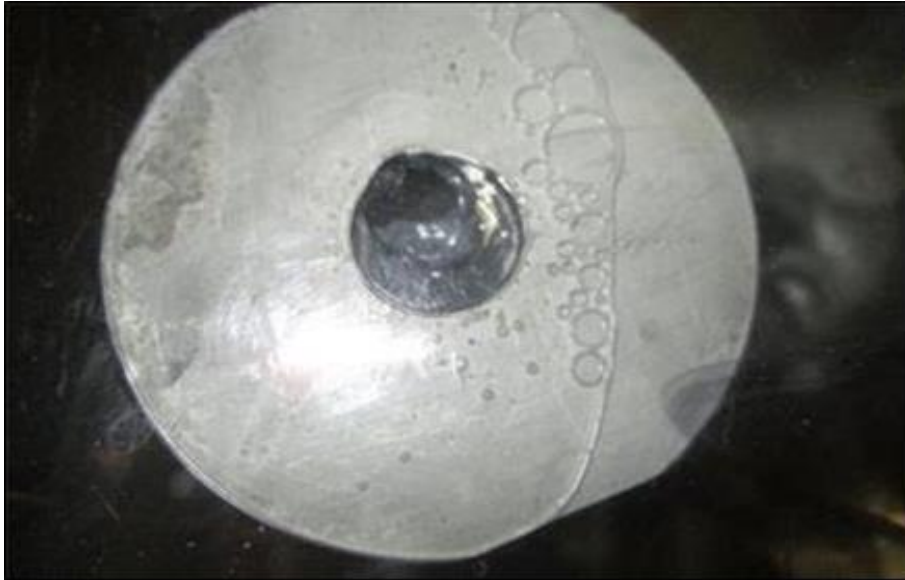
Figure 4-4: Surface tension of water between transducer and glass sheet.

A 12 V centrifugal DC water pump was connected such that it draws water from a reserve and delivers it to the face of the transducer. By applying a frequent rinsing cycle, one is able to flush away the contaminant from the glass.

4.2 The Generator

The ultrasonic generator is responsible for producing high voltage sinusoidal signals which are used to drive the transducer at its resonant frequency. The following section features the major design components and topology used to manufacture a portable ultrasonic generator.

4.2.1. Oscillator

An oscillator was designed to operate between 25 kHz to 31 kHz, as this would cover the bandwidth for a good output signal. The oscillator was built using a SG3524 PWM integrated circuit. This chip would allow the duty cycle and frequency to be adjusted with ease. The circuit and components in Figure 4-5 are based off the refrence design in the Texas Instruments SG3524 datasheet. Rt and Ct were

selected by using the oscillator frequency vs timing resistance graph, along with the formula provided in the same datasheet . (Texas Instruments, 2003)
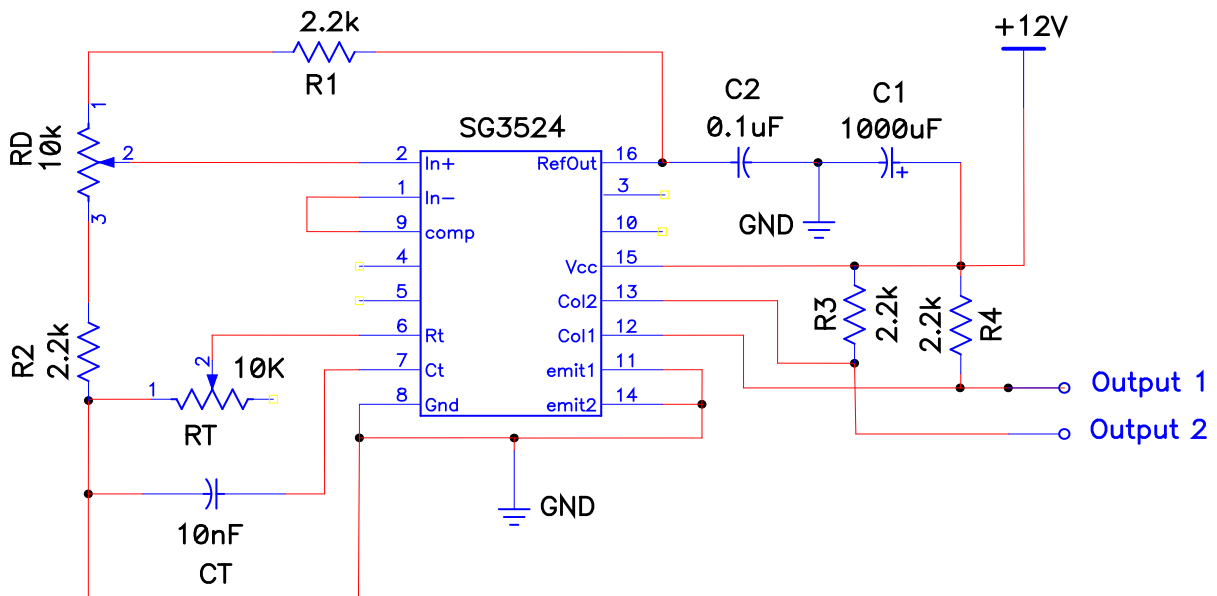
Figure 4-5: The oscillator circuit diagram

The SG3524 IC has great power ratings and is the PWM device used as the oscillator in this generator. Dual alternating outputs provided by this PWM device, simplifies interfacing with push-pull amplifiers. After the circuit in Figure 4-5 was build, an oscilloscope was used to measure the two square wave output voltages. Figure 4-6 shows the two square waves inversely proportional to another and modulated to a frequency of 28.5 kHz.
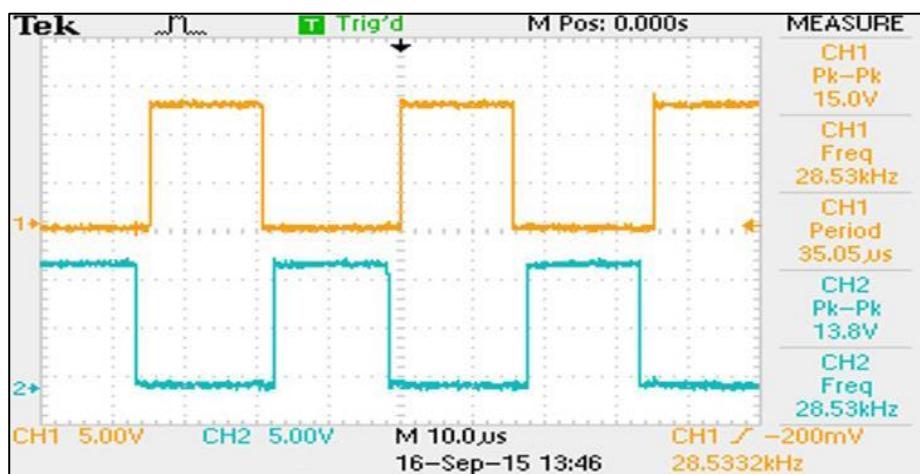
Figure 4-6: The actual driver output stage obtained via an oscilloscope.

RD in Figure 4-5 was tuned to set the duty cycle to 45 %, and the frequency is set using the capacitive and resistive combination of CT and RT. The capacitor selected for CT has a value a 1 nF and Rt was tuned to 45,5 kΩ to produce a frequency of 28.5 kHz

This power unit is favoured for its size, availability, efficiency and high gain ratios. The PWM signals obtained from the SG3524 IC safely drive the power mosfets located in the DC - AC inverter circuit of the ultrasonic amplifier to follow.

4.2.2. Amplifier

A combination of the Class D switch mode amplifier and the push pull transformer is used as the power unit for this generator. The 5 V peak to peak output signal from the oscillator is fed into a dual power mosfet driver IC (ICL7667). This pre amplification stage increases the signal amplitude to 15 V peak to peak before the push pull transformer amplifies the signals to the transducer. This transformer required a driver circuit which was configured in the direct mosfet gate drive formation. Two IRFP460 mosfets's were selected as the power transistors for the circuit because of their high voltage rating and ability to accommodate for large voltage spikes.
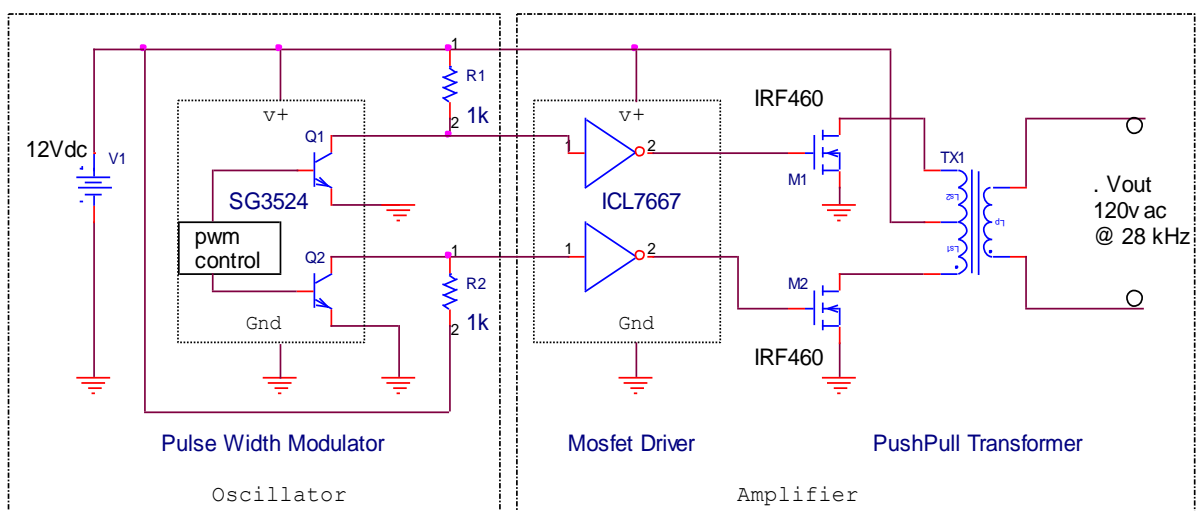
Figure 4-7: The generator circuit with the push-pull transformer.

The transformer was designed using transformer design software found in (Mohan, et al., 2003), Table 4-1 illustrates the specifications used to design the transformer, accompanied by the physical transformer in Figure 4-8.

Table 4-1: Transformer design

Core type	ETD-core
Core #	ETD29
Material	N27
Ta (°C)	24
Ts (°C)	42
Frequency	28 kHz
Vprim rms	15 V
Vsec rms	150 V
Iprim rms	0.7 A
Nprim	13
Acu prim (mm²)	0.41
Nsec	130
Acu sec (mm²)	0.04
Pout	21 W
Efficiency	95.7 %

Figure 4-8: The transformer windings wrapped around the ETD29 core.

The transformer was hand wound and tested in the CIR lab at the CPUT Cape Town campus. Once completed, the Butterworth Van Dyke technique was used to calculate and model the electrical equivalent circuit parameters.

4.2.3. Butterworth-Van Dyke model calculations

The methodology behind the matching circuit calculations is based on (Queirós, et al., 2005) where experts have proven similarities between measured and calculated results. By making use of equation 4 to 7 from (Queirós, et al., 2005) and the data accumulated by the response curve of the unloaded transducer in Figure 4-1, the following Butterworth-Van Dykemodel was calculated.

$$C_O = \sqrt{\frac{(Z_{\omega s})^2(\omega_p^2 - \omega_s^2) + \sqrt{(2\omega_p^2. \, Z_{\omega s}.Z_{\omega p})^2 + \, Z_{\omega s}{}^4(\omega_P^2 - \omega_s^2)^2}}{2(\omega_p^2. \, Z_{\omega s}.Z_{\omega p})^2}} \qquad \ldots\ldots\ldots(1)$$

$$R_1 = \sqrt{\frac{(Z_{\omega s})^2}{(1 - (C_{O.} \, \omega s \, .Z_{\omega s})^2)}} \qquad \ldots\ldots\ldots\ldots\ldots(2)$$

$$C_1 = C_O\left[\left(\frac{\omega_P}{\omega_s}\right)^2 - 1\right] \qquad \ldots\ldots\ldots\ldots\ldots\ldots(3)$$

$$L_1 = \frac{1}{C_1.\omega_s^2} \qquad \ldots\ldots\ldots\ldots\ldots\ldots.(4)$$

The following data is taken from Figure 4-1:

$$\omega_s = 28.180 \; kHz$$

$$\omega_p = 30.080 \; kHz$$

$$\therefore Z_{\omega s} = 40.16 \; \Omega$$

$$\therefore Z_{\omega p} = 54.64 \; k\Omega$$

These values are then substituted into equations (1) to (4) and produce the following results:

$C_O = 22.44 \; nF$............	from	(1)
$R_1 = 40.17 \; \Omega$.............	from	(2)
$C_1 = 3,12 \; nF$.............	from	(3)
$L_1 = 402 \; mH$.............	from	(4)

Following the methodology proposed by (Queirós, et al., 2005), the optimization toolbox in MATLAB was then used to optimize the calculated parameters shown in Figure 4-9.
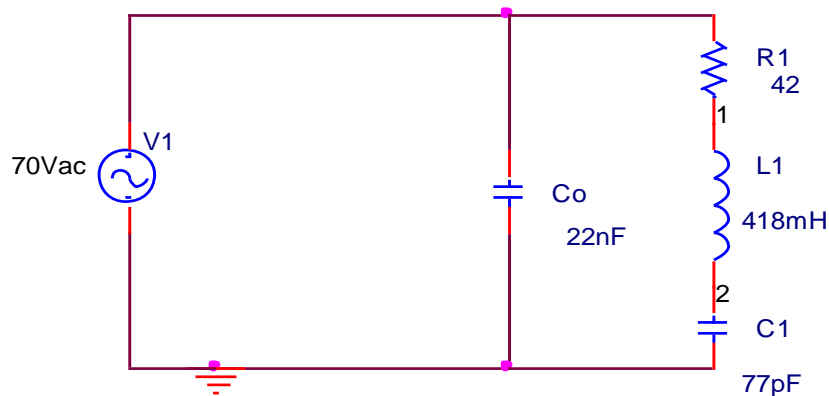
Figure 4-9: The BVD equivalent circuit of the transducer.

The calculated Butterworth-Van Dyke results were then simulated in Pspice Orcad Capture lite edition.

The Hewlett Packard 4192A LF impedance analyser can deliver a maximum output voltage of 35 V peak, and this is the reason why the ac source in Figure 4-9 has been set to 70 Vac. A transient analysis AC sweep was executed via the simulator which produced a resonant peak very similar to the actual reading taken by the impedance analyser shown in Figure 4-10.
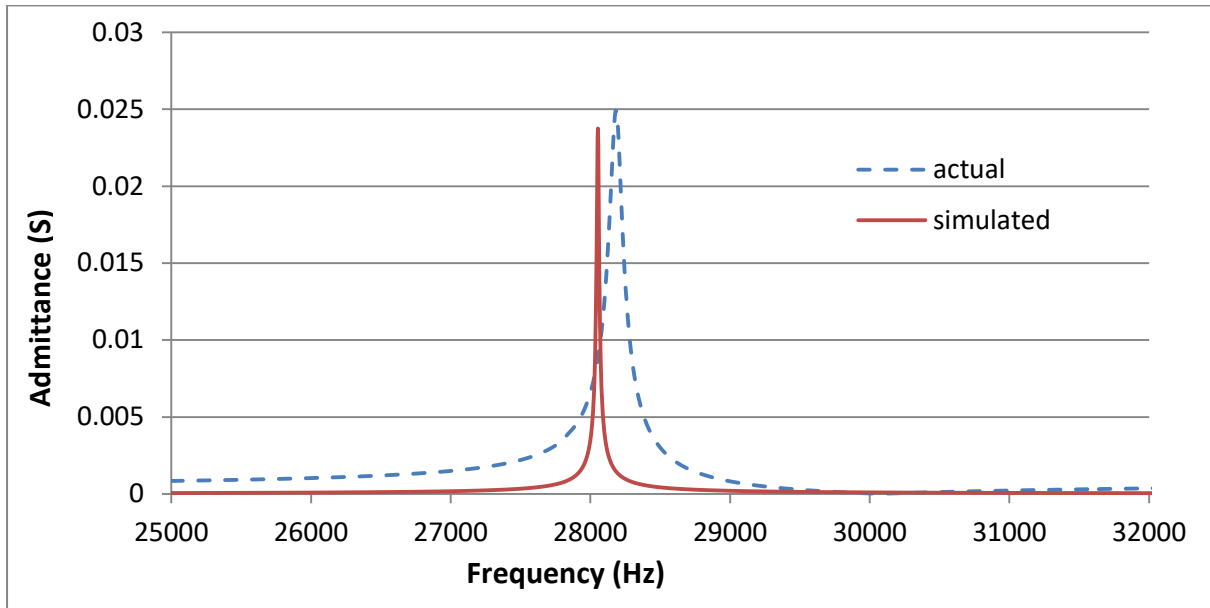
Figure 4-10: The admittance curves of the actual vs. the simulated results.

The frequency of the generator was then set to 28 kHz and the duty cycle to 45 %. The system was the powered up and an oscilloscope was used to read the mosfet gate signals, along with the output voltage across the transducer.
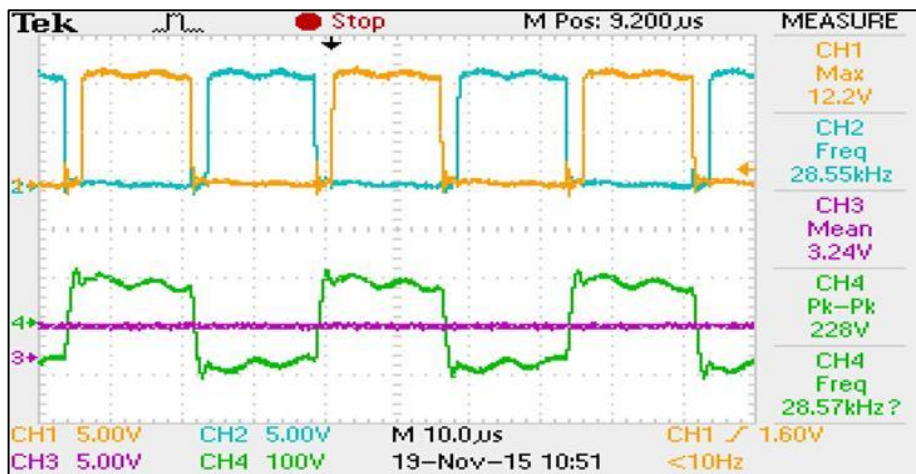
Figure 4-11: The voltage across the transducer measured by an oscilloscope.

In Figure 4-11, the gate signal's on channel 1 and 2 (top) are steady and tuned to 28.5 kHz, while channel 3, the transducer peak to peak output voltage (bottom) is measured at 228 V. The reactive components of the transducer cause harmonic distortion (ripples on wave), these distortions can also be heard and result in a loss in efficiency. The need for fine tuning this resonant circuit is apparent and will be discussed next.

- 64 -

4.2.4. Matching network design

A low pass filter was constructed to maximise power transfer, while simultaneously increasing the bandwidth and system efficiency. The impedance matching network was calculated using the methodology proposed by (Garcia-Rodriguez, et al., 2010). The circuit incorporates a matching inductor and capacitor that has to compensate for the predominantly capacitive transducer. By using equation (4) from (Garcia-Rodriguez, et al., 2010) the following matching circuit was calculated:

Where $Rg = 25\ \Omega$; $\omega = 2\pi f$; $Rs = 42\ \Omega$; $f = 28\ kHz$

$$l_m = \frac{R_g}{\omega}\sqrt{\frac{R_s}{R_g} - 1} = 42\ \mu H$$

$$C_m = \frac{1}{\omega . R_s}\sqrt{\frac{R_s}{R_g} - 1} - C_0 = 400\ pF$$
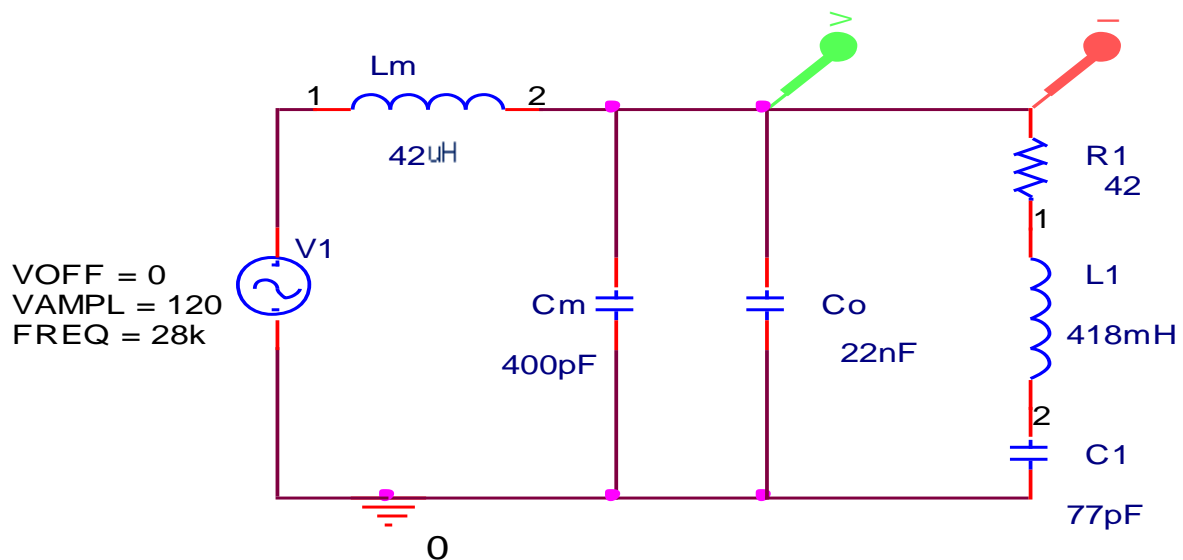
Figure 4-12: The calculated impedance matching network.

The matching network was then added to the generator circuit and simulated in Pspice Orcad capture lite to see if the ouput signal would be improved. The graph in Figure 4-13 shows the output voltage across the transducer over a period of 400 μs.The shape of the graph resembles a ringing sine wave and the ripples at the peaks indicate that the transducer is resonating.
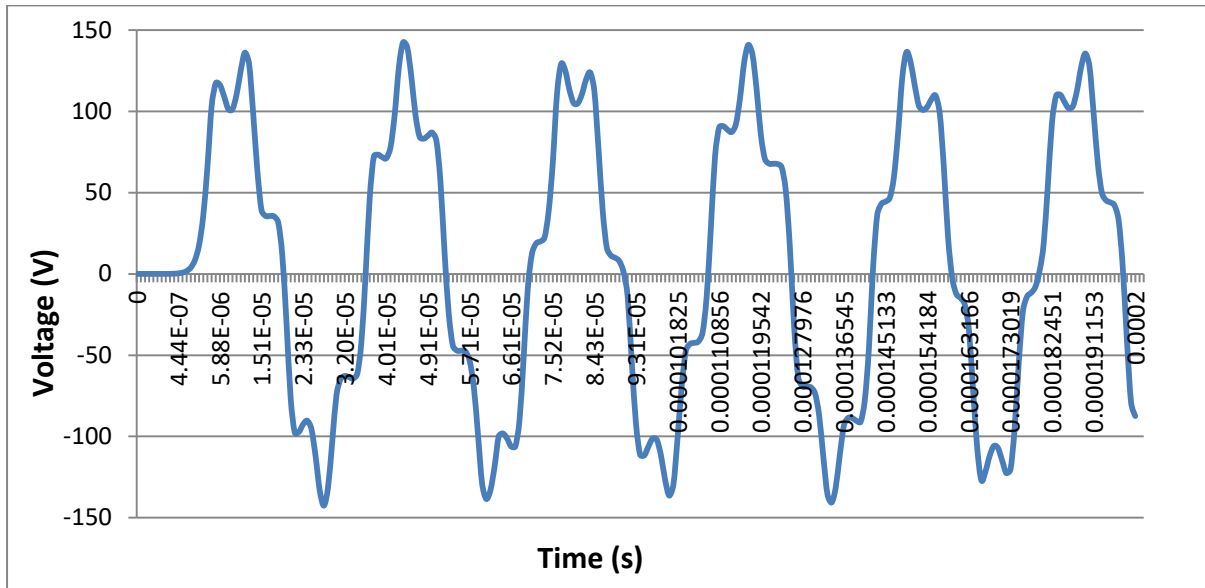
Figure 4-13: The simulated transducer output voltage with matching network incorporated.

An inductor of 42 µH was then designed and a 400 pF capacitor added in parallel to the transducer to fine tune the resonant circuit. Table 4-2 illustrates the design specifications of the inductor accompanied by the physical inductor in Figure 4-14.

Table 4-2: Inductor design.

Core type	ETD-core
Core #	ETD29
Material	N41
Ta (°C)	25
Ts (°C)	42
Frequency	28kHz
Inductance	42uH
N	9
Acu (mm²)	2.24
Irms (A)	6
Air gap (mm)	0.17
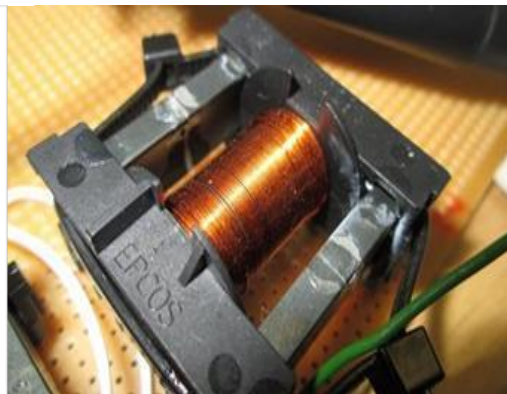
Figure 4-14: The matching inductor.

Once the matching network was populated, measurements of the output current and voltage were taken. The result is a much more symmetrically shaped sine wave shown in Figure 4-15. The square wave inputs are driven at 45 % duty cycle while the output current can be seen in phase with the voltage.
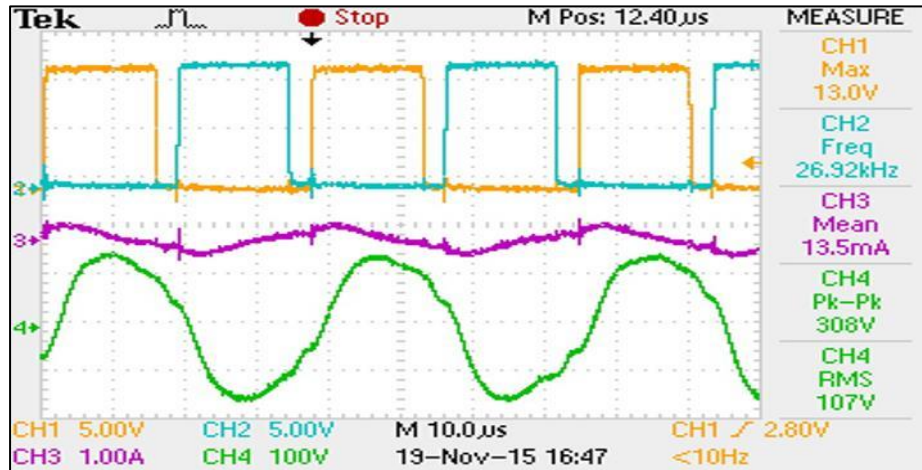
Figure 4-15: The generator output current and voltage.

The current was recorded as 13.5 mA at 308 V peak to peak. Figure 4-15 was exported from the digital oscilloscope, herewith it can be deduced that the transducer is resonating while transmitting a peak output power of 4.158 W.

4.2.5. Microcontroller

The microcontroller chosen to control the cleaning of the insulators in this project is an Arduino Atmega 2560. This choice was motivated by the fast analog to digital conversion speeds and a user-friendly environment. The microcontroller is used as a master controller which introduces our automatic tracing technique of admittance locking.

The function of the microcontroller is to:

- Read the current converted by the LEM and express it as a voltage,
- accept commands from the user by means of 4 push buttons,
- control the transducer frequency by setting the digital potentiometer,
- manage the transducer output power by manipulating the duty cycle, and
- to set the frequency range of the ultrasonic generator.
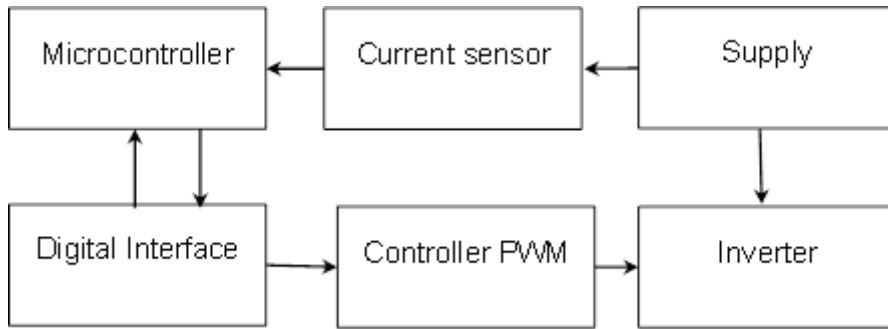
Figure 4-16: The global control block diagram for the microcontroller.

4.2.6. Digital interface

The purpose of the digital interface is to allow the user to manually configure, and the microcontroller to automatically configure the PWM output signal. The interface is comprised of two 50 kΩ digital potentiometers and four push buttons. The buttons communicate with the microcontroller when the user would like the frequency or duty cycle to be altered.

The two analog potentiometers in Figure 4-5 (RD and RT), are replaced with the digital potentiometers which manipulate the oscillator circuit to change the output signal as requested. It achieves this via the RC combination on Pins 2 and 4 of the SG2534 PWM IC which controls the frequency and duty cycle respectively. The microcontroller requires four input peripherals to monitor the activity of the buttons, and a total of six output peripherals to control the digital potentiometers shown in Figure 4-17.
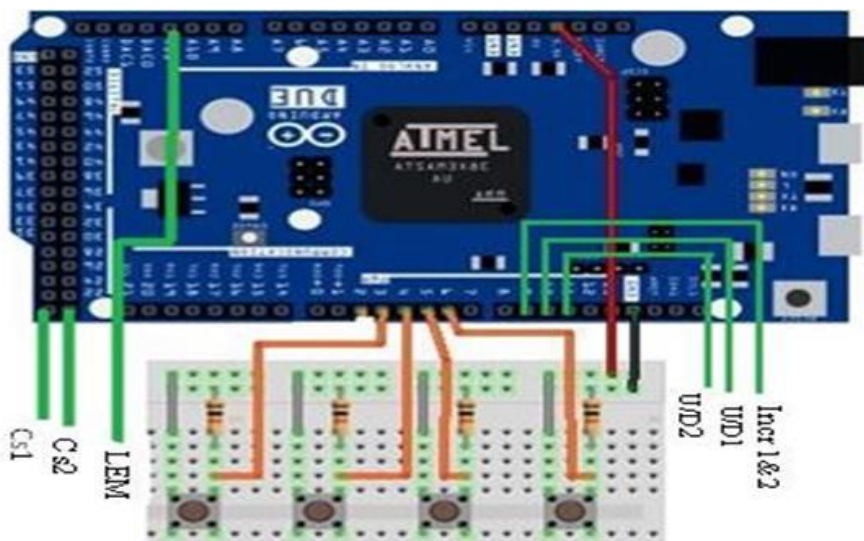
Figure 4-17: The push button circuit diagram and DS1804-50K pin out.

The DS1084 potentiometer has a total of 100 steps and a resistance of 500 Ω per step. A resistor and capacitor combination was calculated to provide the most linear sweeping movement through the frequency range from 25 kHz to 33 kHz. In order to distribute the resistance evenly across all the 100 steps, it was necessary to add resistance in series and in parallel to the digital pot to reduce the step size. Adding a resistance of 10 kΩ in parallel to the potentiometer controlling the frequency, narrow's the range down and makes admittance locking easier.

In order to change the wiper position of the digital potentiometers, the up/down, chipselect and increment pins have to be manipulated. The pins can only be altered when the correct sequence of instructions is followed, managed by the microcontroller. Changes in resistance can therefore be done in micro seconds, allowing for an accurate and timeous PWM output signal response.
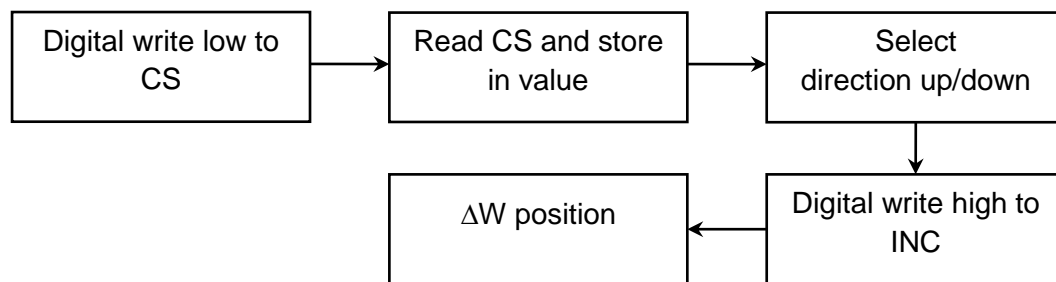
Figure 4-18: The steps required to change the wiper position.

Any high to low state on the INC pin will cause a position movement of the wiper towards the H terminal, during a low state and CS is low, any high to low transitions on INC will cause the position of the wiper to move towards the L terminal. if the wiper pin is required to move more than one position in the either direction, a clock signal is required to continuously change the state of the INC pin. The block diagram in Figure 4-18 details the sequence of steps required to change the wiper position, also refer to Appendix A code line 68 to 85.

4.2.7. Frequency control

The oscillator output frequency is altered when the microcontroller instructs the digital potentiometer to change its resistance. The step count (1 - 100) is then manipulated, which alters the frequency accordingly. Each step corresponds to a certain value of frequency as shown in Figure 4-19.
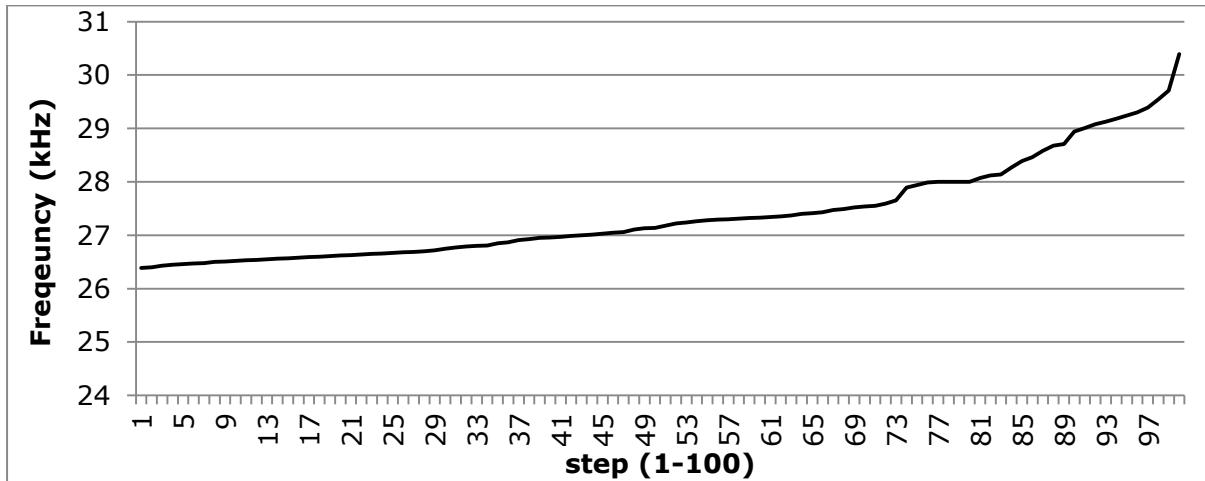
Figure 4-50: How the frequency changes as the steps are incremented.

It was noted that the steps were linear from 0 to 75 and after that the linearity was lost. This means that one cannot predict with 100% certainty the value of the frequency when you reach step 76 and above. The error margin was calculated to be approximately 5.77 %.

The variation was divided into an interval from 1 to 100 because the digital potentiometer has 100 steps. The 100 steps were used to perform the frequency sweep up and down. After each step, a current sample with its corresponding step count is stored in the memory of the microcontroller. After completing the 100 steps of variation, the highest current sample and corresponding step count is displayed. The highest value obtained indicates to where the resonant frequency can be found. The microcontroller instructs to the digital potentiometer to return to the position where the maximum current sample was taken.
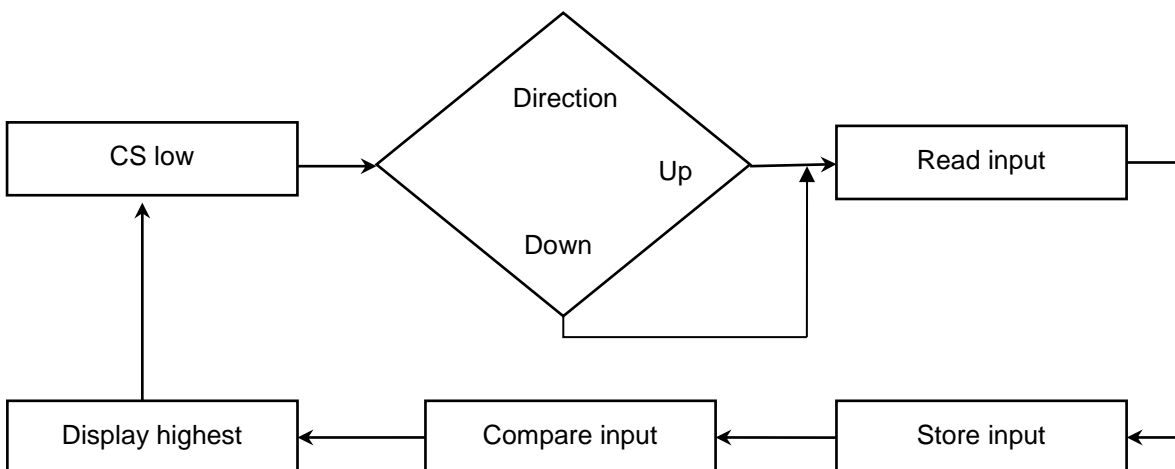
Figure 4-20: The frequency manipulating flow chart.

The block diagram in Figure 4-20 explains how the output frequency is manipulated, it is in the same manner that the power is adjusted. Once the frequency vs step data was logged, a cleaning algorithm was investigated. The block diagram in Figure 4-21 documents the sequence of events which provide the soluton to controlling the ultrasonic generator.
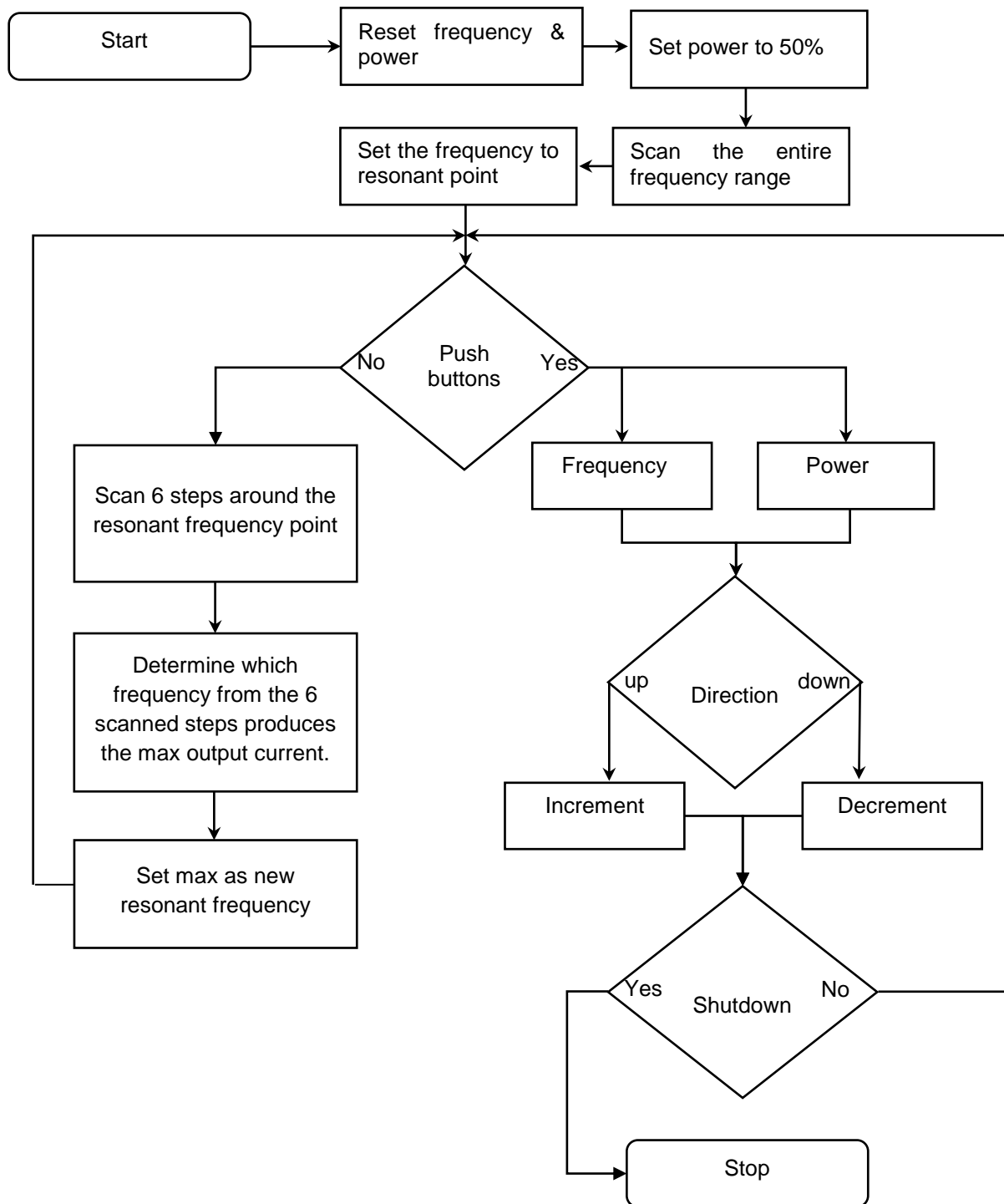
Figure 4-21: The generator cleaning process.

The graphs in Figure 4-22 depict the results of the desighned algorithem, showing the four phases which the generator autonomously executes when cleaning is initiated.
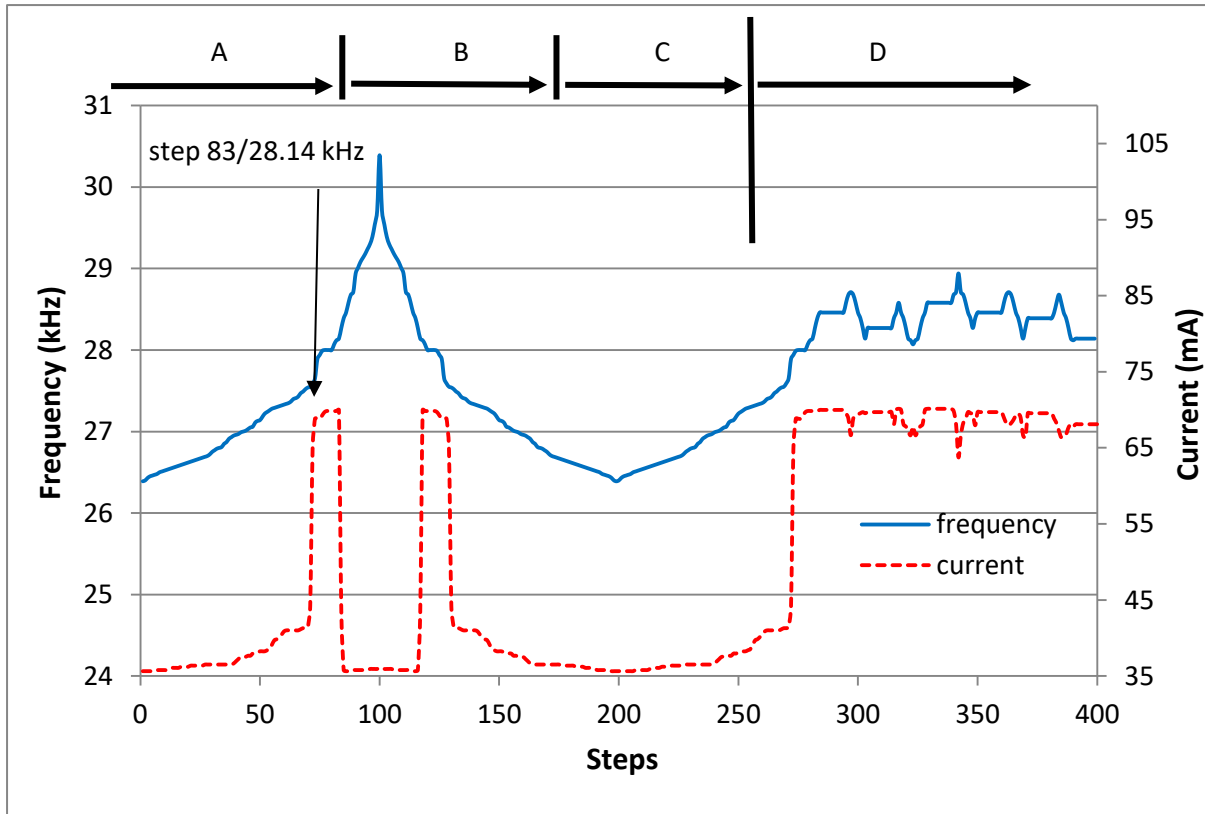
Figure 4-22: The generator frequency and current response curves amid the four phases.

During phase A, the steps are incremented from 0 to 100 and the current gets sampled and stored at each step. After 100 steps being completed, the highest value stored in memory along with the step count is noted. In the course of phase B, the digital potentiometer is decremented back to step 0 so that the step count can be monitored with greater accuracy. This inturn reduces the frequency down to zero and consequently mirrors the shape of the graph (steps 101 - 201).

Phase C then ramps the frequency up as the potentiometer is incremented to the step which produced the highest current sample (step 83). During phase D, The microcontroller samples three steps above and three steps below the resonant point. Each step is compared to the previous to determine if a new resonant point is to be selected. The upper and lower limits (six steps around the resonant point) of the automatic frequency scan are then changed to ensure that the selected resonant frequency remains at the centre of the scan.

4.3 Line walker robot

Once it was confirmed that the peculiar cleaning technique was possible, the task of designing a line walker that would transport the cleaning unit was undertaken.

A four legged concept which interlocks from either side of the transmission line was favoured to maximize stability.The design is based on a rectangular chassis that will be suspended bellow the line. A 12 V lithium ion battery pack and an Arduino Atmega 2560 powers and controls the robot. The four legs are connected to servo motors which are mounted onto the chassis and reach up towards the line. At the end of each leg a DC motor is attached to a wheel for propulsion.
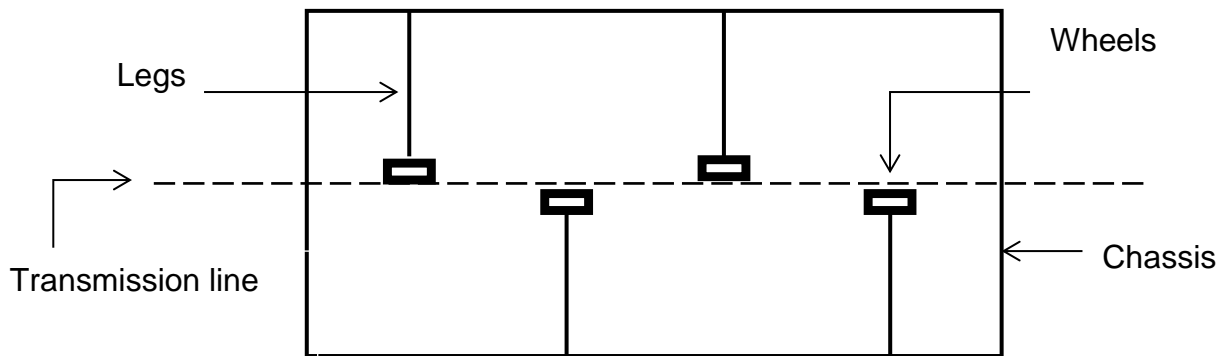
Figure 4-23: A top view illustrating the concept of the line walker

The robot has to overcome suspension clamps that are 245 mm in length, tension/ strain clamps that are 200 mm in length and dampers that are 230 mm in length. The line walker was developed to have enough space between each wheel to overcome these obstacles.

The chassis is 1 meter in length and each wheel is positioned 250 mm apart, allowing it to horizontally pass all the obstacles. A 100 mm clearance gap is required to avoid the obstacles vertically; this design caters for a 126 mm space between the line and the line walker when the wheel is moved out of the way. Figure 4-24 shows the rectangular chassis built with a sheet of 3 mm PCB (2) and an 3 mm aluminium support beam (1) positioned underneath the sheet to minimize flexing.
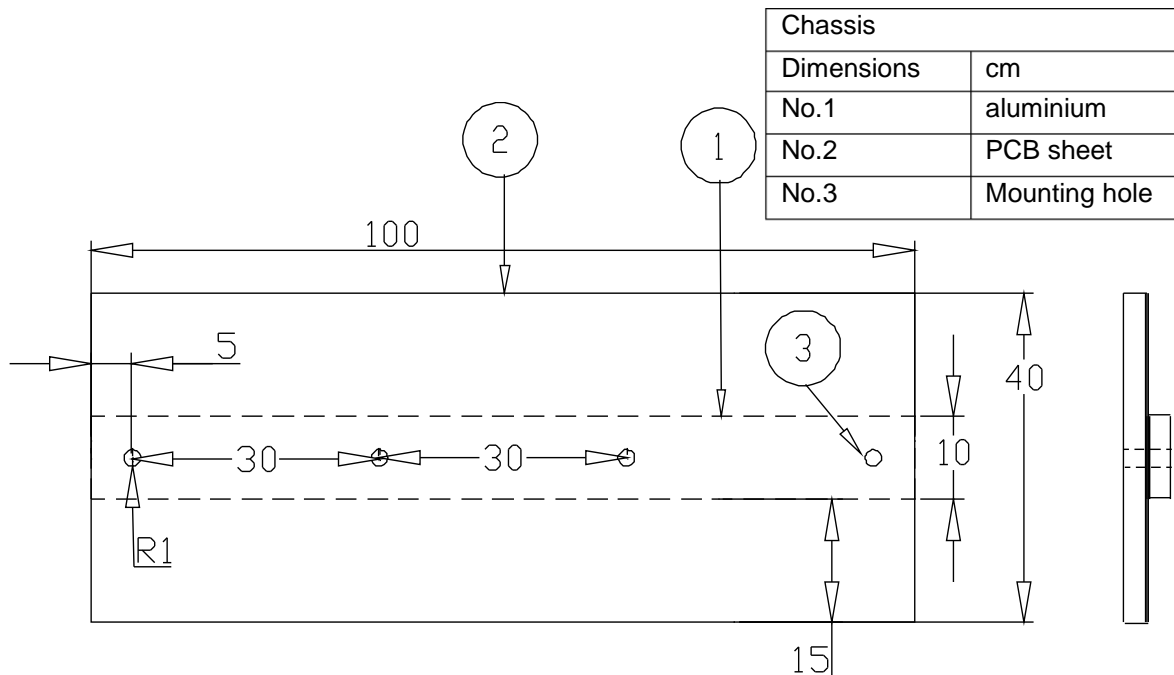
Figure 4-24: The line walker's chassis design.

A leg mechanism was then built to determine if servo motors would be competent actuators for the drone. The design included a DC propulsion motor mounted on the inside of an aluminium wheel, two supporting brackets and a 90 degree bend in the leg structure which was also made using PCB. The wheel assembly height was 10 cm and weighed 600 g shown in Figure 4-25.

Energy calculations:

$Force = Acceleration \times Mass$ $Work = Force \ \times Distance$

$Force = 9.81 \ \times 0.6$ $Work = 5.886 \ \times 0.10$

$Force = 5.886 \ N$ $Work = \ 0,5886 \ N. m$
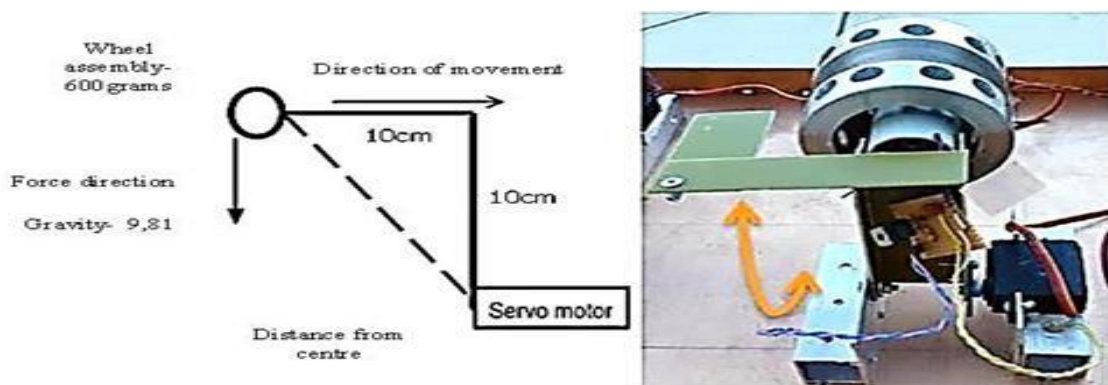
Figure 4-25: The first leg mechanism designed for the line walker.

A servo motor with a rotational torque of 9.3 kg/cm (0,91 N.m) was installed as it would supply enough torque required to raise the wheel and motor. The design worked but the actuators were strained when the 4 kg weight of the line walker chassis combined with the 3 kg cleaning unit was added. A much stronger design was required and was achieved through a pivot mechanism.

Revised energy calculations:

$Force = Acceleration \times Mass$ $\qquad$ $Work = Force \times Distance$

$Force = 9.81 \times 7$ $\qquad$ $Work = 68.67 \times 0,120$

$Force = 68.67\,N$ $\qquad$ $Work = 8.24\,\text{N.m}$

$Force\ per\ wheel = Total\ force\ /\ amount\ of\ wheels$

$Force\ per\ wheel = \ 8.24\,N.m\ /\ 4$

$Force\ per\ wheel = \ 2.6\,N.m$

4.3.1. Line walker design

The force required overcoming the weight of the chassis, wheel assembly and ultrasonic cleaning unit is 2.6 N.m per wheel. The new mechanism's mechanical advantage lies in the 3 pivot points which carry most of the structure's weight. The design has nine main parts depicted and explained below.

The wheel is upgraded to be lighter and is constructed with 3 mm cylindrical Perspex laminations. Two larger outer laminations are glued between 9 smaller ones to form the wheel. It hooks onto the line at a 60 degree angle, reducing the pressure on the DC motor shaft. The design includes a threaded key hole which runs through the laminations to meet perpendicularly to the centre hole. The key allows the wheel to be fixed to the shaft using a 6mm bolt and caters for a flush fit to avoid contact between the bolt head and the transmission line. Figure 4-26 shows the key hole, wheel dimensions and laminations used.
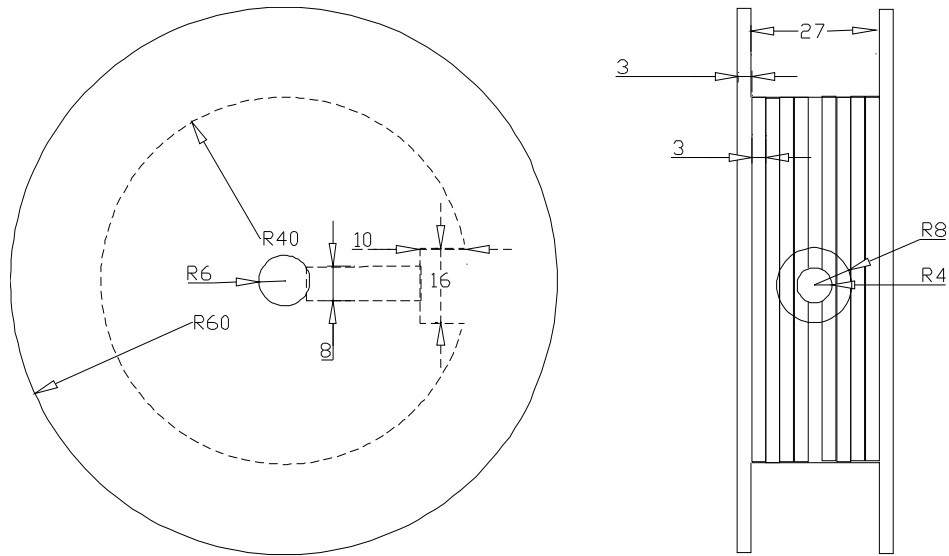
Figure 4-26: The Perspex wheel with a 6mm keyhole.

The DC motor in Figure 4-27 rotates the wheels through the motor's ball bearing shaft. The motor selected has a maximum rotating speed of 15 RPM when powered by 12 V and is positioned on top of the leg. An off-centred shaft hole is surrounded by three smaller mounting holes which allow the motor to be fixed to a base plate.
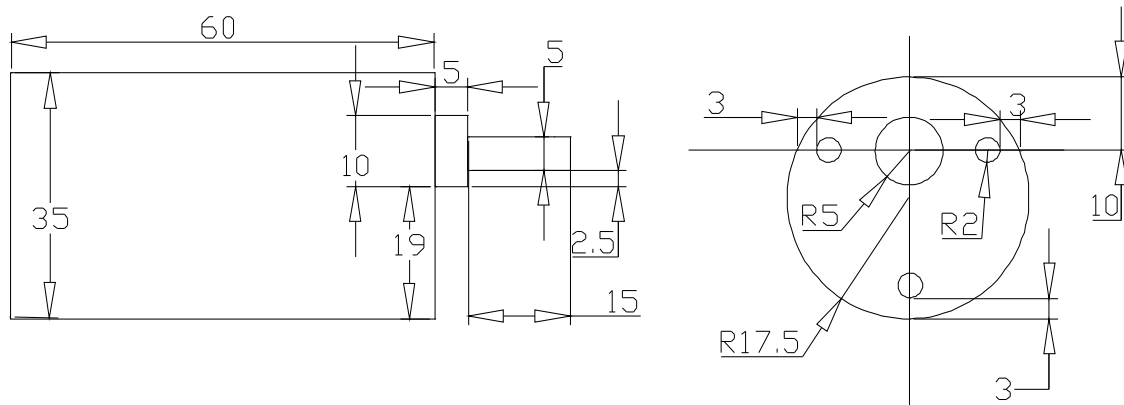
Figure 4-27: The DC propulsion motor.

The motor mounting base plate in Figure 4-28 is fixed to the top of the leg to house the DC motor. A single segment of PCB is shaped for the face of the motor and aligns the 3 mounting holes. The plate firmly connects the dc motor to the leg structure using 3 mm bolts. The notch on the right hand side of the plate is to position the limit switch assembly and the 20 mm slot at the bottom connects to the leg.
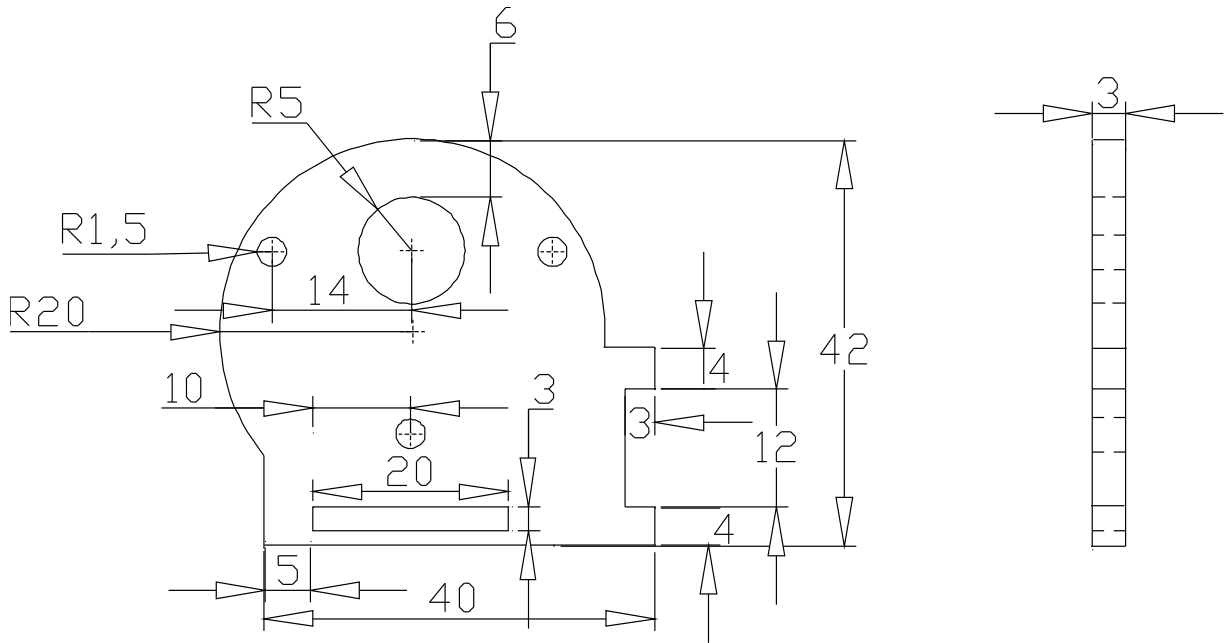
Figure 4-28: The mounting base plate

The leg is now a four dimensional PCB structure that has a 60 degree bend shown in Figure 4-29. The rigid structure is soldered together and pivots on a 6 mm bolt at the lower end of the leg. This main pivot point reduces the forces on the servo motor shaft as it supports most of the weight. A second pivot point situated close to the centre of the leg is linked to a lever.
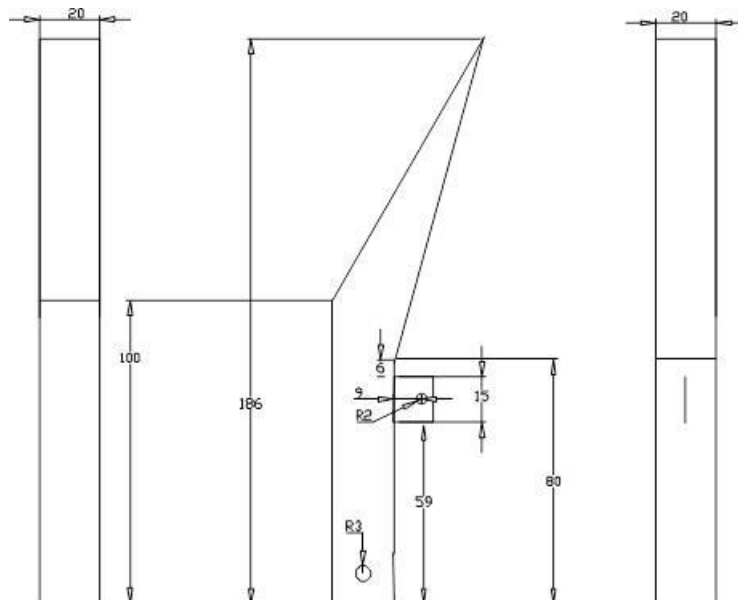
Figure 4-29: The leg structure made with PCB.

The leg is pivoted in between two lightweight 90 degree aluminium brackets. Mounted on to the chassis, each leg bracket in Figure 4-30 is held in position by two

6 mm bolts. The aluminium does not warp, which contributes to the accuracy and precision of the leg movement.
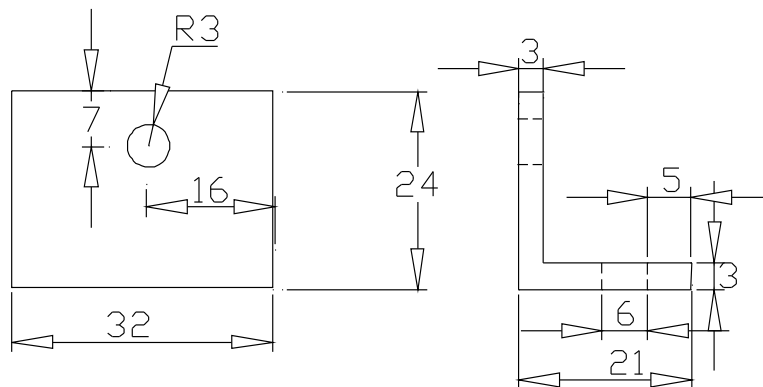
Figure 4-30: The leg's pivoting bracket.

A single segment of 3 mm PCB is used for the lever which connects the leg to the servo motor arm in Figure 4-31. The lever has two pivot points on either side of its length, a 3 mm x 12 mm bolt is used at the rounded end and a 3 mm x 20 mm bolt used on the other. These points change the rotational force of the servo motor into a horizontal pushing and pulling action.
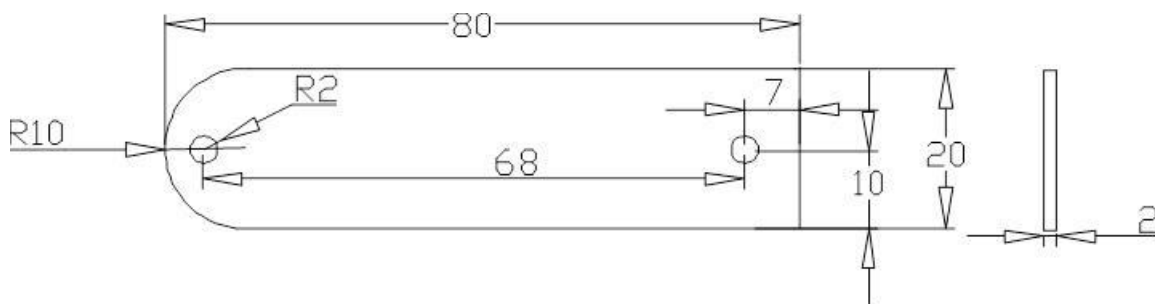
Figure 4-31: The lever, which connects the motors to the legs.

A stronger servo motor capable of delivering 30 kg/cm (2.94 N.m) was sourced. Stability is significantly increased by the upgraded servo motor in Figure 4-32. The servo arm is fixed to its shaft on one end and pivots the lever on the other. The device receives over 300 short signal pulses per second, allowing the motor to speed up quickly and provides constant torque. The servo motor has four mounting holes which fix the motor to another 90 degree aluminium bracket.
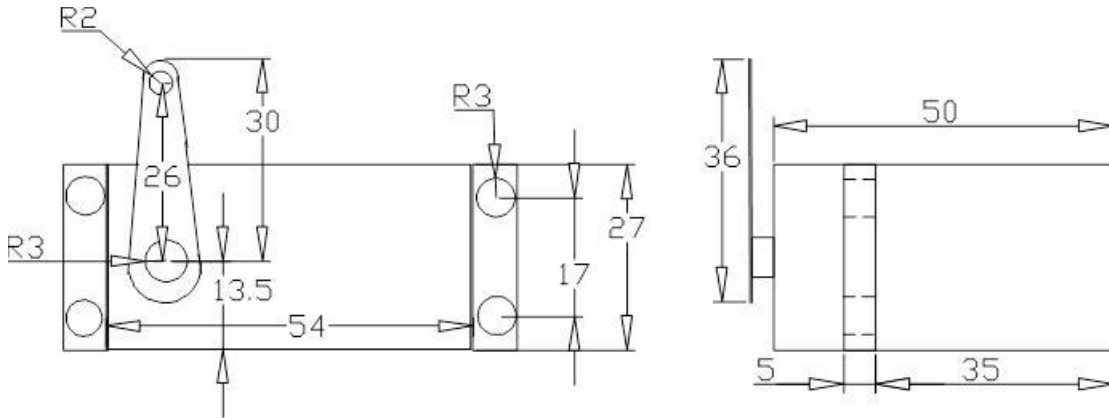
Figure 4-32: The servo motor.

An aluminium 90 degree servo motor bracket is then coupled to the chassis via two 6 mm bolts. The bracket withstands all the energy released by the servo's rotating shaft. They are lightweight, robust and have four 3 mm mounting holes to fix the motor in position shown in Figure 4-33.
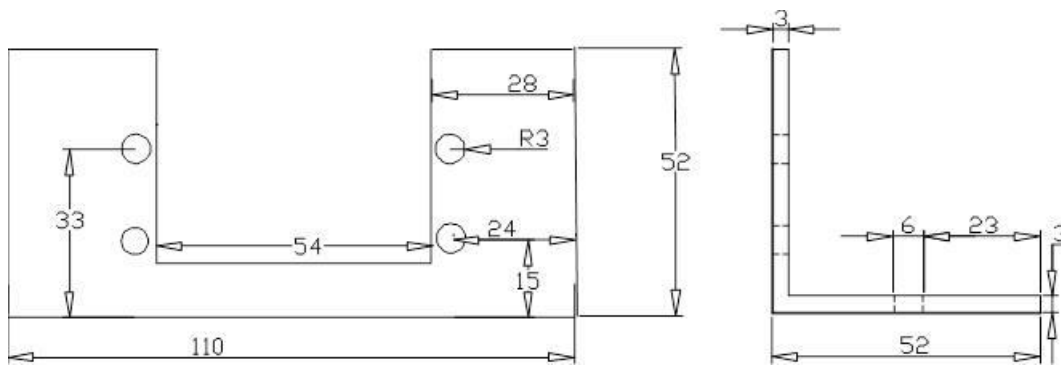
Figure 4-33: The aluminium bracket that mounts the servo motors.

The limit switch is mounted on a PCB platform just above the wheel, facing the front end of the line walker. The platform is fixed into the notch found in the motor mounting baseplate. 8 mm fish tank tubing is placed around the limit switch lever to extend its reach shown in Figure 4-34. Any object encountered in front of the wheels while moving forward will trigger the limit switch before making contact with the wheel. The microcontroller then removes the respective wheel out of the way.
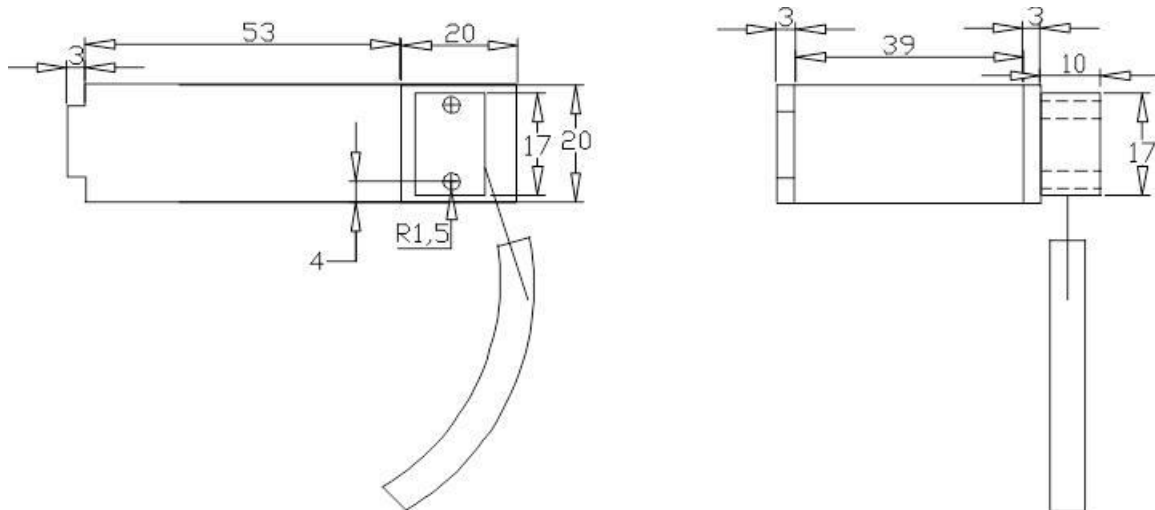
Figure 4-34: The limit switch assembly.

The ultrasonic distance measurement assembly in Figure 4-35 is only found on the third wheel of the walker. The assembly is also mounted on the DC motor base plate, but the sensor faces the rear of walker. The reason for this is to determine when the last wheel of the line walker has cleared the obstacle. When the 4th wheel is removed from the line to avoid an obstacle, the sensor starts to measure the distance between the third wheel and the obstacle while moving forward. Once a safe clearing distance is established, the controller instructs the 4th wheel to return to its position on the line.
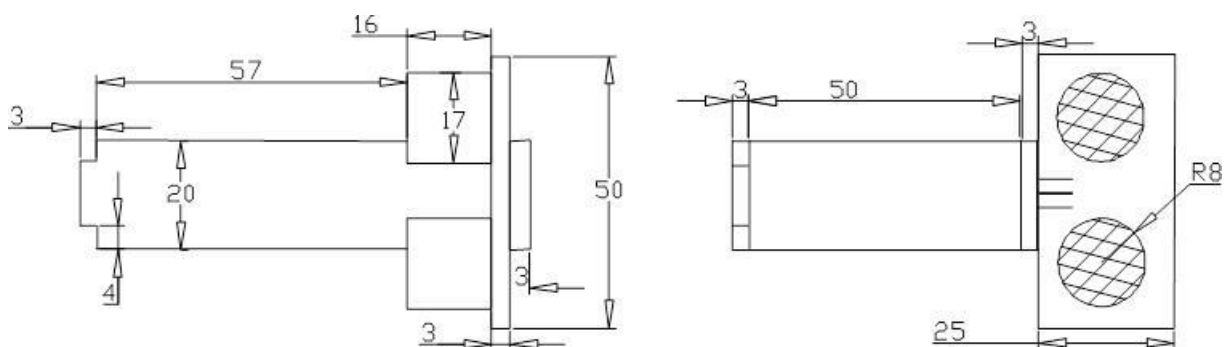
Figure 4-35: Ultrasonic distance measurement assembly.

The individual parts are then assembled to form a single leg structure shown in Figure 4-36. The constructed leg mechanism is then duplicated three times, allowing the weight of the line walker to be distributed evenly across the four leg assemblies.
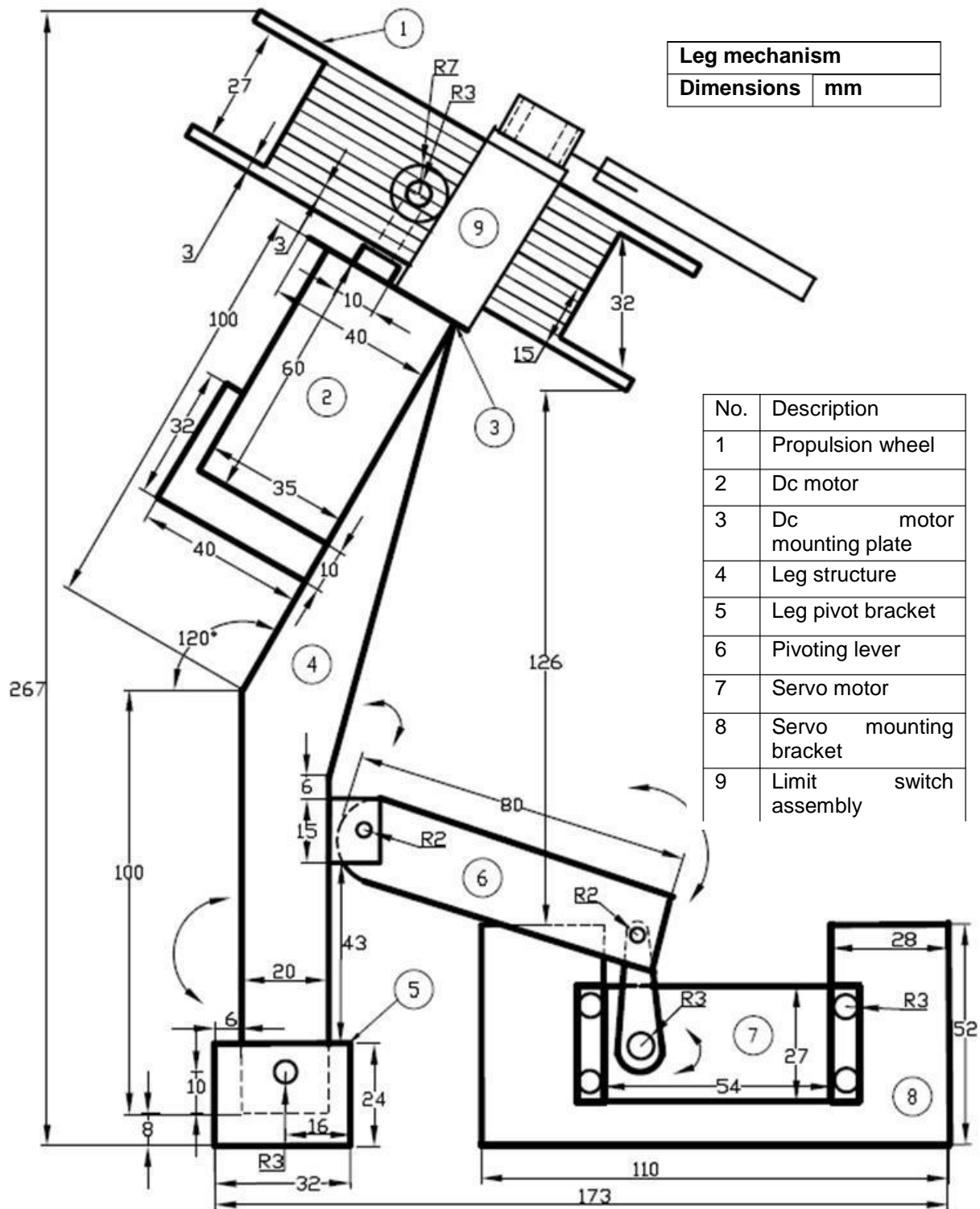
Figure 4-36: The new leg mechanism.

The accelerometer is placed close to the centre of the robot to determine if the chassis is correctly positioned on its axis. The fully assembled ultrasonic cleaning line walker is shown in Figure 4-37 with the Arduino, battery pack and cleaning unit placed in water tight containers.
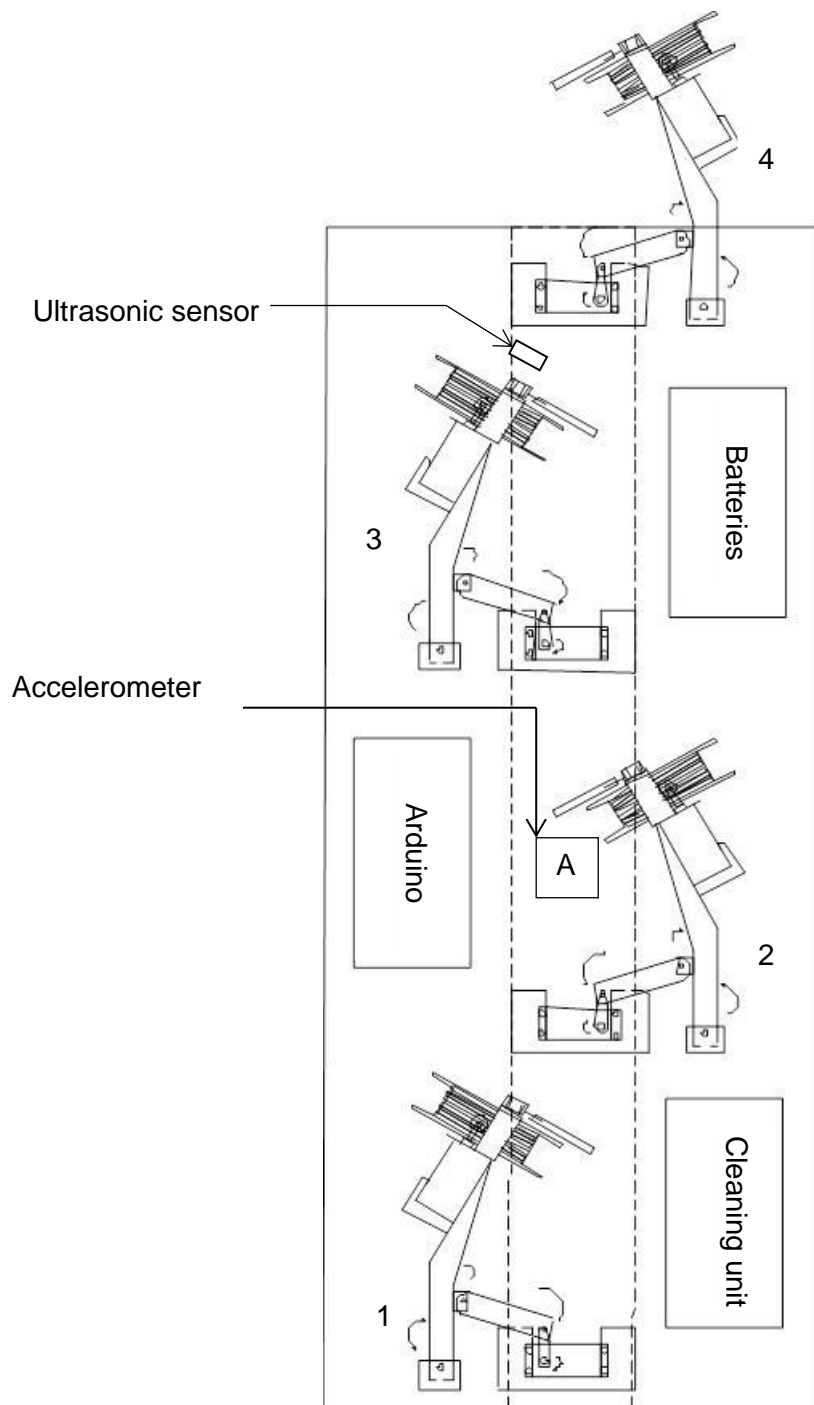
Figure 4-37: The fully assembled design of the ultrasonic cleaning line walker.

This concludes the various mechanical parts found on the line walker. The electronic components such as the motors and sensors need some external control circuitry in order to be interfaced with the microcontroller. The following section details the various control circuit requirements.

4.3.2. Control Circuitry

The 12 V DC battery contains sufficient voltage and current for all the motors and Arduino. Each leg has a individual control circuit for the motors. The Arduino cannot supply enough power to the motors as they require large amounts of current to operate and even more to start up. The propulsion motors is therefore connected to the battery via four IRF520 mosfets shown in Figure 4-38. The Arduino then applies a PWM signal to the gate of the mosfet to turn the motors on or off.
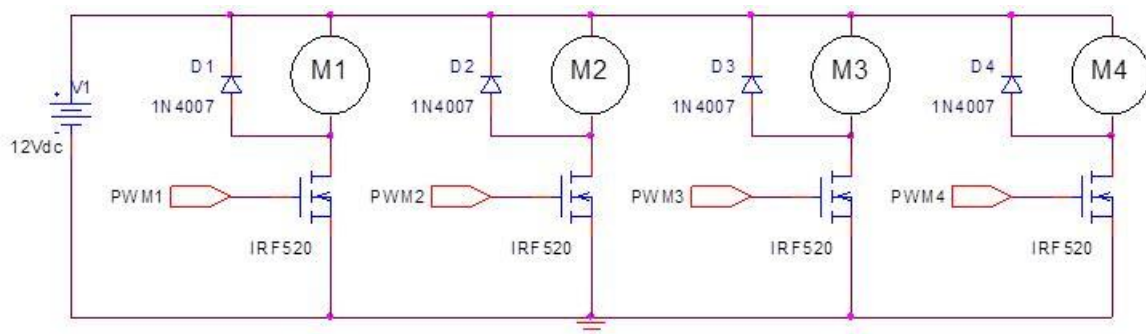
Figure 4-38: The DC motor control circuit.

AL7806 IC was used to step down the 12 V battery voltage for the 6 V servo motors, but this device failed to supply enough current to operate the servos comfortably. The three L7806 regulators in Figure 4-39 are therefore connected in parallel to supply sufficient current and avoid overheating.
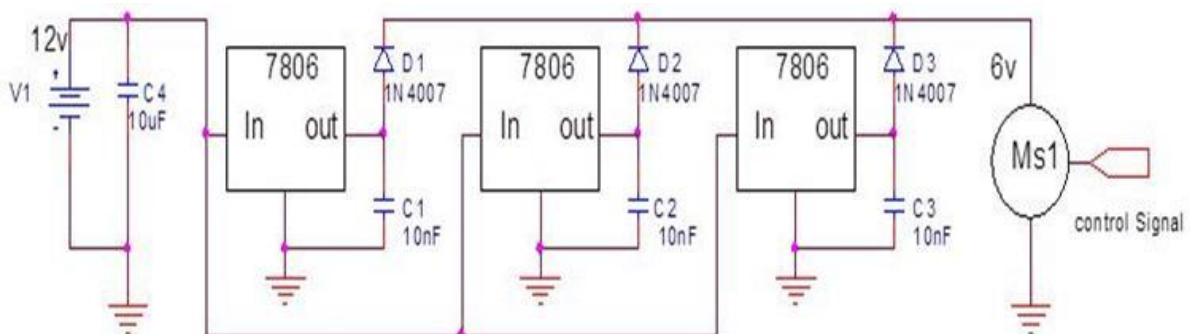
Figure 4-39: The servo motor control circuit.

The proximity sensors in Figure 4-40 are low voltage devices and therefore receive power directly from the Arduino 5 V rail. The limit switches only require one pull up

resistor to indicate their status and the HC-SR03 ultrasonic transducer module is directly compatible with the Arduino ADK board. This distance sensor does however require some code to set the device up for communicating on a 40 kHz frequency. The accelerometer is positioned with its x axis parallel to the chassis and requires one pull up resistor to communicate using the i2c protocol. The sensors transform real world information into electronic signals which the controller understands. Interacting with these signals is made simple when utilising the serial communication window provided by the Arduino software platform. The board rate for communication is set to 9600 through which all the sensory data is communicated.
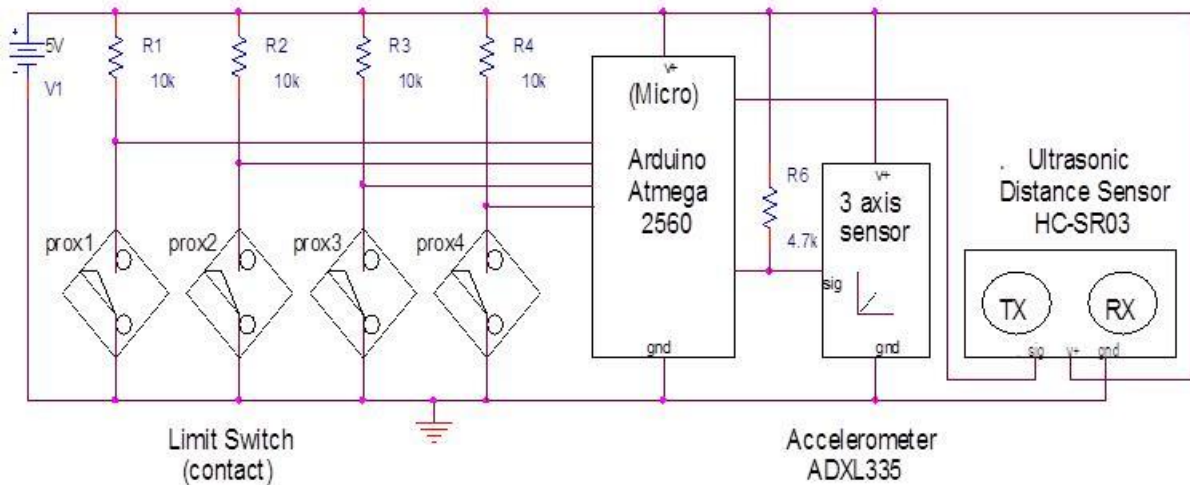
Figure 4- 40: The control circuitry for the proximity sensors.

Once all the sub components in of the line walker was designed and installed, an algorithm was written to link them together. The Arduino ADK is the device responsible for the activation and timing of all the individual components. The algorithm to walk and overcome the obstacles found on the high voltage transmission lines is as follows:

4.3.3. Code algorithm

While suspended on the line, the robot is required to propel forward and overcome an obstacle in its path. In order to do this, the robot is required to remove its wheels from the line in the correct sequence. It is therefore mandatory that the robot recognises the distance between each wheel and the obstacle. The following algorithm was designed to achieve obstacle navigation.

1. Robot moves forward.
2. If 1st limit switch is triggered, stop the robot.
3. Activate servo motor 1 to lift the first wheel.
4. Robot moves forward.
5. If 2nd limit switch is triggered, stop the robot.
6. Activate servo motor 1 to lower the 1st wheel then activate servo motor 2 to raise the 2nd wheel.
7. Robot moves forward.
8. If 3rd limit switch is triggered, stop the robot.
9. Lower the 2nd wheel with servo motor 2 then activate servo motor 3 to raise the 3rd wheel.
10. Robot moves forward.
11. If 4th limit switch is triggered, stop the robot.
12. Activate servo motor 3 to lower the 3rd wheel then activate the next servo to raise the 4th wheel.
13. If the distance between the 3rd wheel and the insulator is greater than 40cm raise the 4th wheel back onto the line.
14. Check if the robot is balanced.
15. Start at 1 again.

4.4 Project Budget

The project budget has been presented using three tables, Table 4-3 for the ultrasonic cleaning materials, Table 4-4 for the line walker materials, and Table 4-5 concludes with the total expenses of the system. The items in the far left column are accompanied by their price and brief description on the right. The project results are thereafter examined in the following Chapter.

Table 4-3: Ultrasonic cleaning expenses

Item	Price	Description
Battery	R1300	12 v 33 AH Lead acid
28 kHz transducer	R1500	Cleaning instrument
Mosfet driver ic	R50	Driver circuit
Mosfet irf520	R100	Power amplifier
Lem current transducer	R300	Current sensor
DS18B20 digital pot	R150	Interface between controller and generator
Micro controller	R1200	Arduino atmega 2560
Micro controller casing	R125	Waterproof housing for electronics
Sg3524 PWM IC	R50	Pulse width modulator for power and frequency
Analogue components	R250	Miscellaneous electronic components (resistors, capacitors and inductors)
Amplifier	R1000	N27 material, push pull transformer
SUBTOTAL 1	R8 225	

Table 4-4: Line walker expenses

Item	Price	Description
Batteries	R4000	Lithium-ion polymer 12 V / 2200 AH
DC motors	R1200	6 V / 200 RPM - propulsion
Wheels	R500	Perspex sheet (1 m x 1 m)
Micro controller	R1200	Arduino atmega 2560 development board
Proximity sensors	R400	Limit switches and distance sensor
Metal work	R500	Aluminium brackets and chassis support
Chassis	R2000	Copper pcb sheet (2 m x 1 m)
Nuts and bolts	R200	Miscellaneous M6 to M12
Accelerometer	R300	Sensor which balances the chassis
Servo motors	R3500	Actuators which manoeuvre the robotic legs
Analogue components	R1000	Miscellaneous electronic components (resistors, capacitors and inductors)
Battery & controller casings	R250	Waterproof housing for electronics
SUBTOTAL 2	R15 050	

Table 4-5: Ultrasonic cleaning line walker's total expenses

Item	Price	Description
Ultrasonic cleaning subtotal	R8 225	Ultrasonic cleaning expenses
Line walker subtotal	R15 050	Line walker expenses
TOTAL :	**R23 275**	

Chapter 5
Evaluation and Results

This Chapter discusses the experiment setup and results obtained predominantly for the ultrasonic cleaning system. The line walker results are also assessed, but in less detail as it is a secondary focus of this study. The success of the cleaning prototype can be assessed by the graphs depicting essential attributes such as admittance, frequency, power and time. Pictures taken before and after the cleaning process can be seen after which the system efficiency is evaluated. The final section of this Chapter will assess the line walker's navigational abilities.

In Chapter 4 it is proven that the transducer is being driven at resonance, so it is now only necessary to test if the assembly is capable of tracking changes in the resonant frequency and furthermore, its ability to clean.

Firstly, it was noted during the testing procedure that the resonant frequency of the transducer did not stay the same when the duty cycle was altered. Figure 5-1 indicates how the total power dissipated by the transducer affects its resonant frequency.
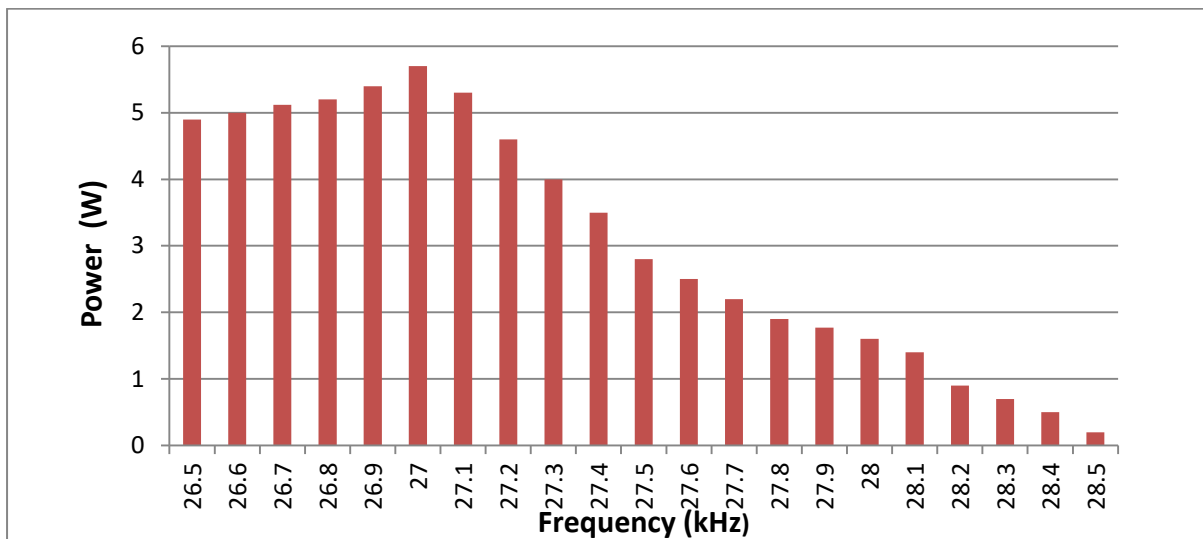
Figure 5-1: How the output power affects the resonant frequency.

When applying the delivery technique explained in Chapter 4, changes in the resonant frequency was observed when the input power; distance between transducer face and insulator; and the flow of water were altered. The input power

affects the electrical component of the insulator while the distance and water affect the mechanical component. The latter is due to changes in the load experienced by the face of the transducer.

5.1. Resonant frequency tracing results

The impedance analyser is used to drive the transducer and log the response to four different load conditions. The prototype generator is then used under the same conditions and the results compared. If the results are similar, it would prove that the system has the ability to track the resonant frequency. The experiment was set up using the delivery technique described in Chapter 4 and changes in the load were simulated using these four conditions:

- Suspending the transducer in air (no load, no water),
- placing the transducer face flat onto the insulator (no air gap) ,
- setting a 1 mm gap of water between the transducer face and insulator, and
- setting a 3 mm gap of water between the transducer face and insulator.

The impedance analyser results were recorded with the national instruments software package. The serial communications window in the Arduino software package was used to log the results produced by the prototype cleaner (current samples from LEM).The impedance analyser was used to perform two experiments to simulate the four conditions above. These experiments serve as control tests to provide an ideal reference with which the cleaning prototype results can be compared to. While the experiments are only true using this specific transducer, they help draw an analogy between an Ideal ultrasonic generator and the cleaning prototype designed.

5.1.1. Control Test 1:Resonant frequency tracking

The Impedance analyser was set up to read the admittance across the frequency range from 26 kHz to 30 kHz. The transducer was then suspended in the air (no load) whilst the analyser swept across the frequency range. The data was logged and the experiment repeated, only this time the proposed delivery method was introduced by placing the transducer face flat down onto the glass insulator. A tiny continuous flow of water was pumped in through the hole drilled into the transducer

(Chapter 4) and no air gap between the insulator and transducer could be observed. The leaking water dripped into the basin below whilst the analyser recorded the following results:
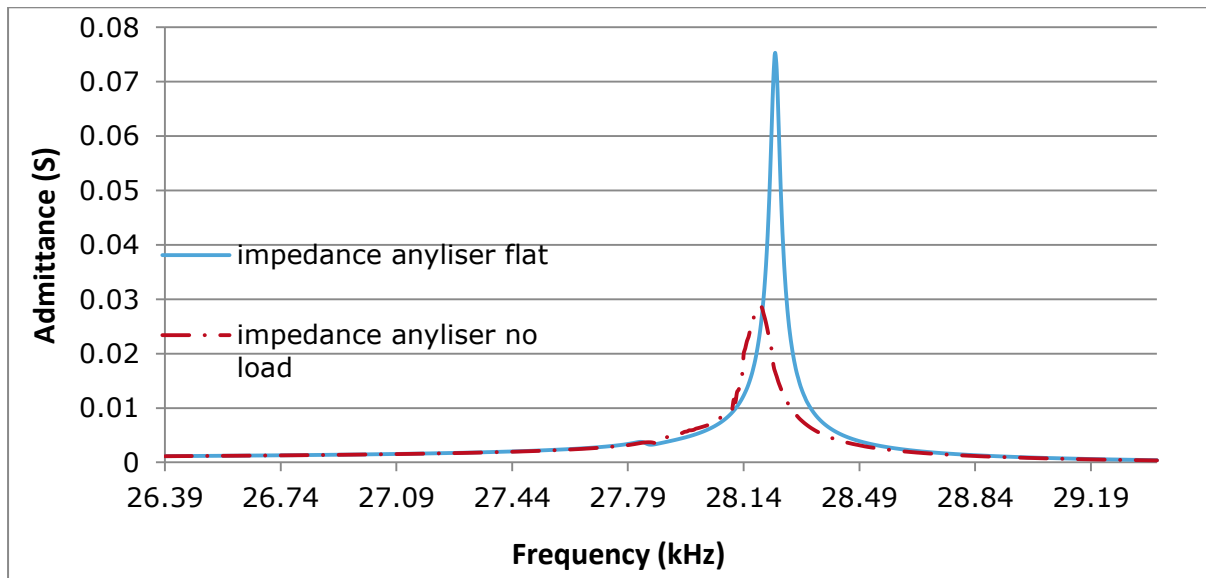
Figure 5-2: Control test1- resonant frequency shift due to load.

The first observation noted from Figure 5-2 is the large admittance spike produced when applying the delivery method. The admittance has increased from 287 mS to 753 mS. Secondly, the resonant frequency peak has shifted slighty up from a frequency of 28.19 kHz to 28.235 kHz. This explains why the tall graph is slightly shifted to the right, and furthermore, the narrow bandwidth seems unchanged on both accounts.

5.1.2. Prototype generator test1

Tracking the resonant frequency with the prototype generator will be proven if the generator output resembles the graphs shown In Figure 5-2. The generator output graphs are super imposed with the analyser graph in Figure 5-3 to provide clarity when examining the accuracy and precision of the prototype. The duty cyle of the generator was then set to 30% and the following results recorded:
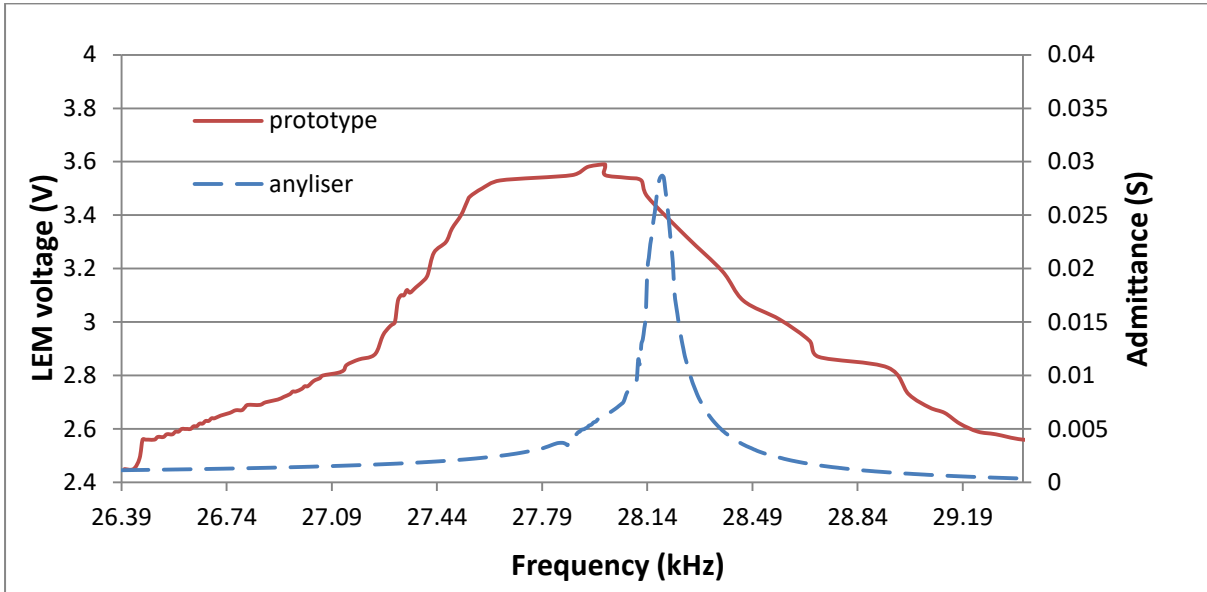
Figure 5-3: No load condition- prototype vs analyser.

5.1.3. Observations: No load

The generator performed well under the no load condition in Figure 5-3. It is pertinent to note that the bandwidth increases to 2.5 kHz and the shape of the graphs is similar. The resonant peak occurs at a slightly lower frequency when using the prototype but the wide bandwidth still covers 95% of the analyser's graph area.
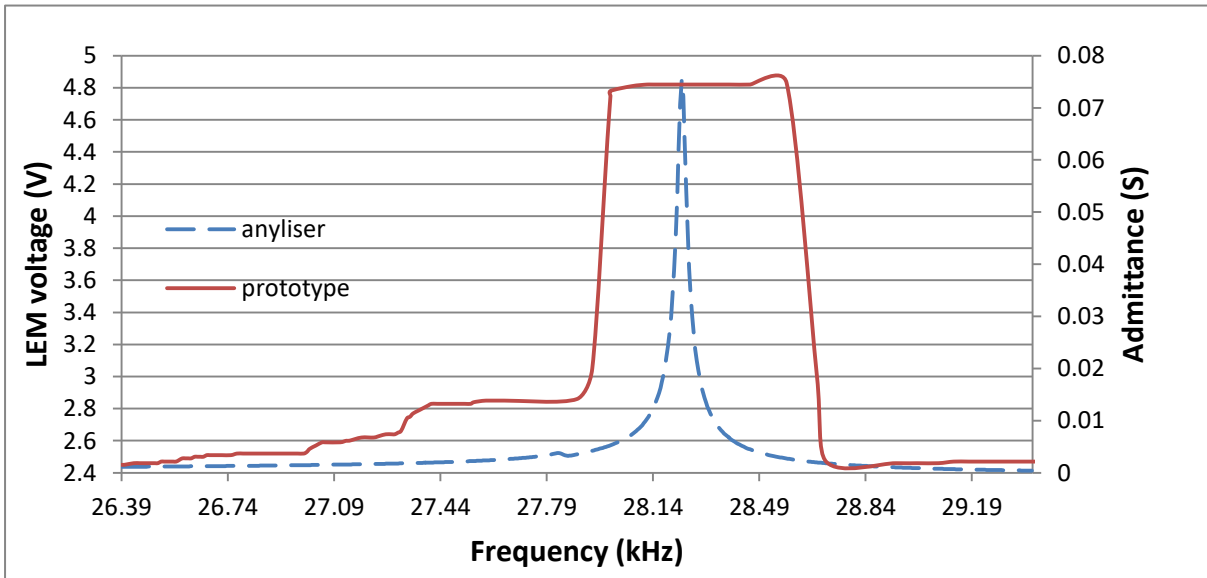
Figure 5-4: Flat faced condition- prototype vs analyser.

5.1.4. Observations: Flat faced

The generator has once again produced good results depicted in Figure 5-4. The most promising of which is the admittance spike which is tracked by the current

sensor and displayed as 4.9 V. The bandwidth has also been increased to 1 kHz and the generator output mimics the shape of the analyser's graph. The generator enters the resonant frequency rapidly and exits in a similar fashion, deduced from the sharp rise and fall angles displayed. The graphs are almost centrally aligned and the prototypes widened bandwidth is sufficient to operate over the entire frequency range that the analyser's graph covers.

5.1.5. Control Test 2: favourable transducer distance for delivery method

Another control test was done using the Impedance analyser to read the admittance across the frequency range from 26 kHz to 30 kHz. The transducer was suspended 1 mm above the insulator, and a tiny continuous flow of water was pumped through the hole drilled into the transducer. The water tension could be observed on the circumference of the transducer face, while the analyser swept across the frequency range and logged the data. The experiment was repeated with a 3 mm gap between the two sufaces and the analyser recorded the following results:
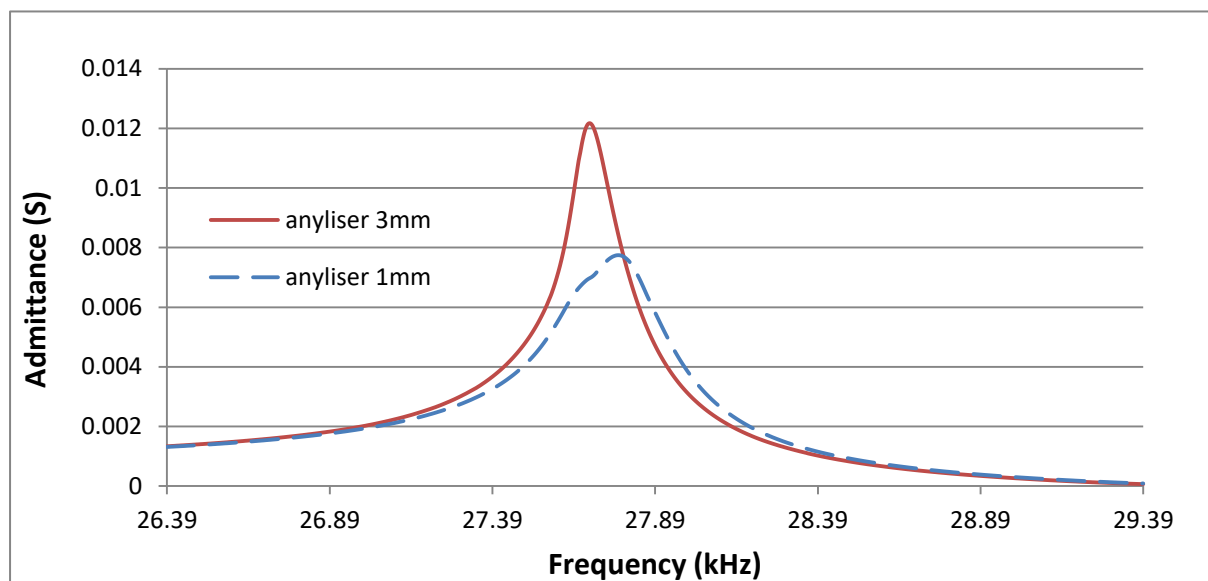
Figure 5-5: Control test 2- admittance greater using 3 mm gap.

The larger admittance peak is produced when the 3 mm gap is used in conjunction with the delivery method. The admittance has increased from 8 mS when using a 1 mm gap to 12 mS using the 3 mm gap. The resonant frequency peak has now reduced slightly from a frequency of 27.89 kHz to 27.75 kHz, shifting the graph slightly to the left this time. The bandwidth of both graphs is approximately 1 kHz and the two graphs are also similar in shape, and magnitude.

5.1.6. Prototype generator test 2:

A wide bandwidth and large admittance are favourable conditions when cleaning with ultrasound. Therefore the preferred distance between generator and insulator would be the distance with greater output power capabilities over a larger frequency range. The generator output graphs are superimposed with the analyser graph from Figure 5-5 to provide clarity when examining the accuracy of the prototype. The duty cycle of the generator was then set to 30% and the following results recorded:
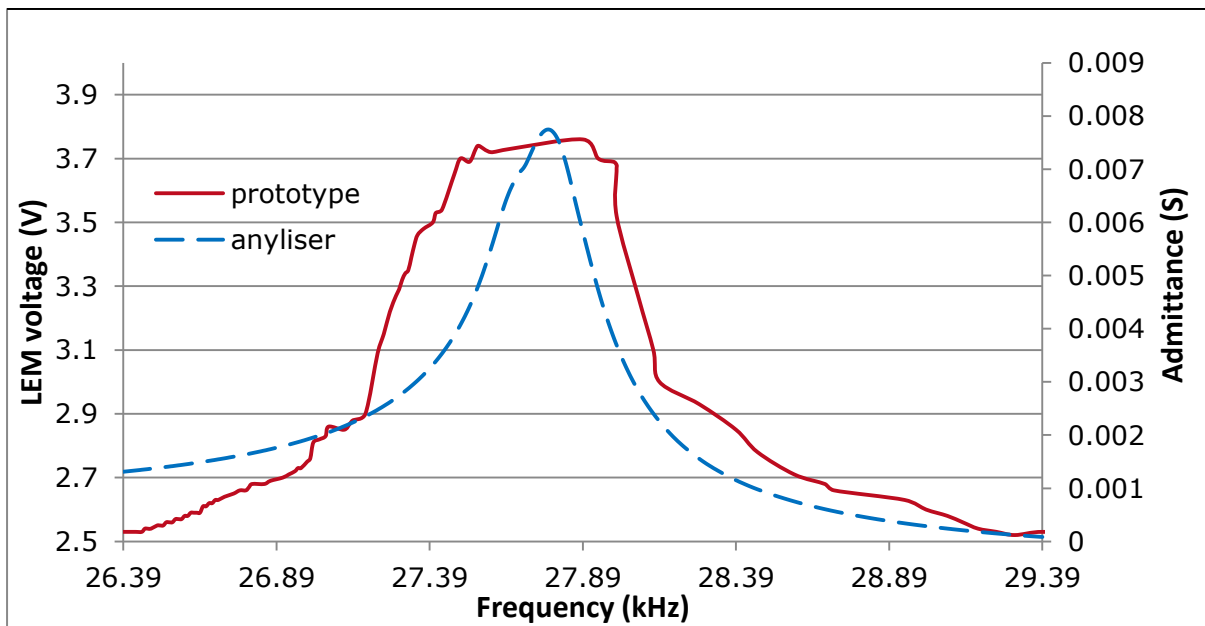
Figure 5-6: Prototype generator vs impedance analyser using 1 mm gap.

5.1.7. Observations: 1mm gap

The generator performed outstandingly well when implementing the 1 mm gap between transducer and insulator. Similar to the previous results, Figure 5-6 shows that the bandwidth has been increased to 2 kHz and that the shapes of the graphs are similar in appearance. The 8 mS resonant peak of the analyser occurs at 27.79 kHz situated right at the centre of the broader prototype peak represented by 3.79 V LEM output. Although the analyser response is slightly earlier at 26.39 kHz, it is balanced by a later prototype response at 28.39 kHz
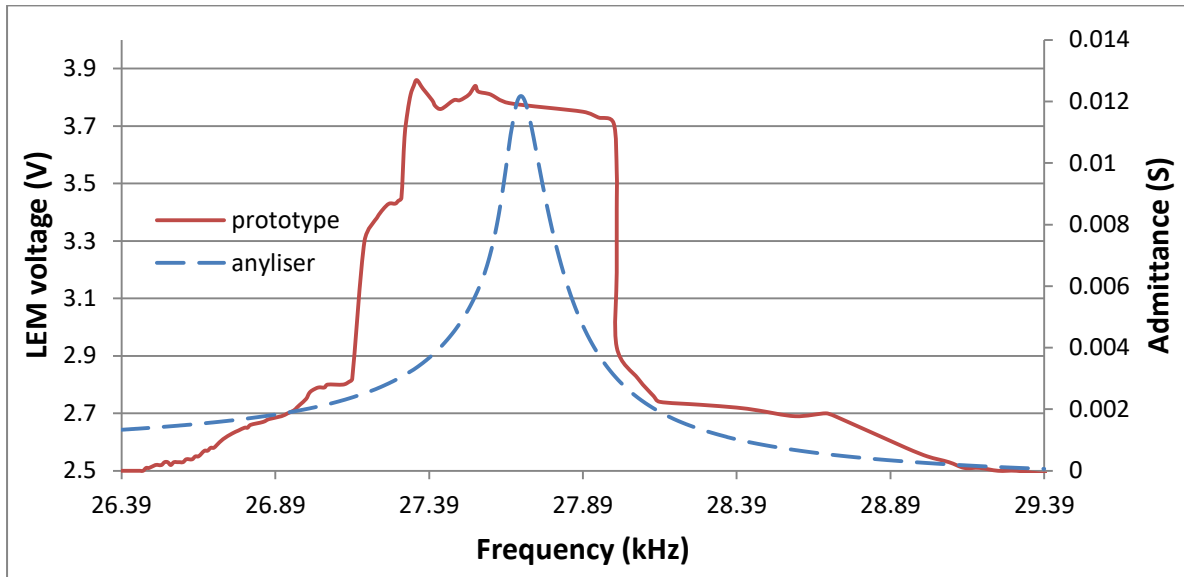
Figure 5-7: Prototype generator vs impedance analyser using 3mm gap.

5.1.8. Observations: 3 mm gap

The most pertinant observation from Figure 5-7 is the admittance spike tracked by the analyser as 12 mS, and represented by the current sensor as 3.85 V. The spike could be due to weak coupling between the transducer face and the insulator as the surface tension is redused when the gap is increased. The bandwidth has been increased to 1.5 kHz, and the peak of the generator output remains high over a longer frequency range. The graphs are almost centrally aligned, and similar in appearance.

5.1.9. Discussion: Resonant frequency tracing

From the graphs in Figure 5-2 one can see that the resonant frequency shifts once a load (water) is applied. The generator has successfully proven that it is capable of tracking the resonant frequency under several load conditions. The prototype reacts swiftly to any changes before stabilising when required to. All results show that the bandwidth of the transducer is increased when using the generator and all the peaks are also sustained over a greater frequency range when compared to the analyser outputs. This indicates that the results obtain in this set of experiments are acceptably accurate and yields good precision .

The current is directly proportional to the admittance; therefore the output power is greatest when the admittance is at maximum. In order to propagate the acoustic waves into the flowing water with enough pressure to clean the insulator, the power

will have to be set to a moderate level. The admittance of the transducer was found to be only 3.5 mS greater when applying the 3 mm gap and therefore only a slight power difference is present between the 1 mm and 3 mm conditions. The electrical data acquired seems to indicate that 3 mm gap condition is better suited for cleaning using the delivery method but this will be tested in the following section.

5.2. Ultrasonic cleaning results

After a few test runs it was determined that the 1 mm gap produces better cleaning results than the 3 mm gap. This is owed to better water surface retention using the smaller gap. Therefore the delivery method using a 1 mm gap was used in the following experiment.

5.2.1. Experiment setup: cleaning the insulator.

The experiment was set up inside a steel basin filled with enough water to submerge the 12 V pump. The insulator was then placed above the water inside the basin so that the dripping water would be collected and recycled. A 10 mm hose pipe (fish tank tubing) connected the pump to the transducer which was suspended by a stand and clamp 1 mm above the insulator.
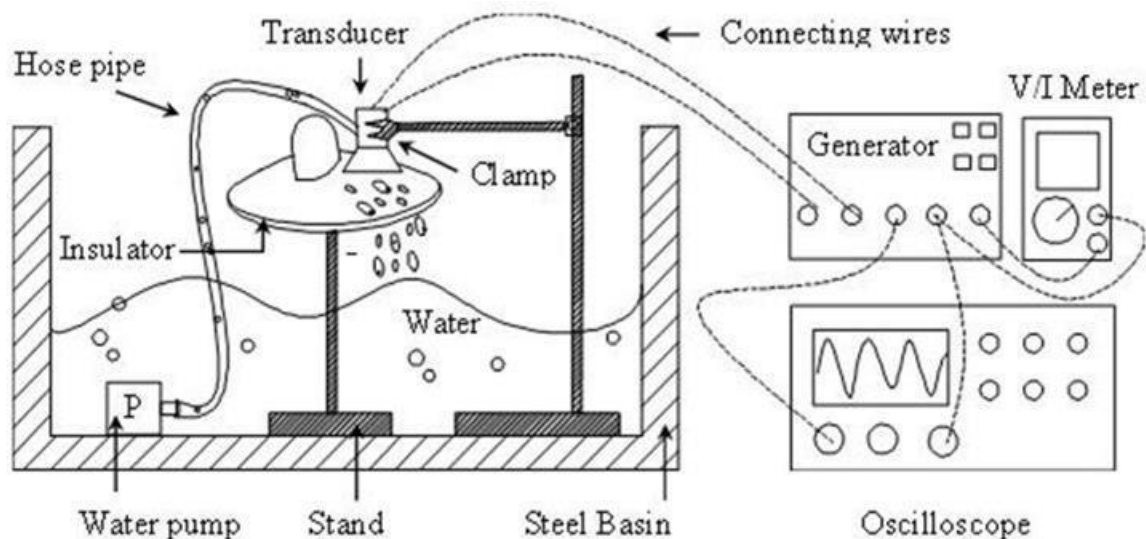
Figure 5-8: The cleaning experiment setup.

An image of the contaminated insulator was taken before the cleaning process, this was used as the reference image. The time was then monitored after the generator was turned on, and images were taken at regular intervals. The contaminant applied

to an area on the insulator was a 1 mm layer of engine grease, and 20 mℓ of sunlight liquid was added into the water.

The duty cycle of the generator was set to 40 % which produced around 5 W of output power and the experiment run at 45 second intervals. The insulator was then removed and placed in a controlled light box where the following images were taken. The Figures on the right focus on the contaminated area :

Figure 5-9: The 1 mm layer of grease applied to the surface of the insulator.

The experiment starts by applying a layer of grease to a predetermined area on the insulator. The contaminated circle measures 40 mm in diameter and 1 mm thick shown in Figure 5-9. The transducer face has a radius of 17 mm and will be positioned squarely above the contaminated circle.

Figure 5-10: The contaminated area after 45 seconds of cleaning.

The generator was turned on, water began to flow and the transducer was excited. An audible noise could be heard, suspected to be harmonics deflecting off the glass insulator. The system was on for 45 seconds after which a portion of the contaminated area was cleaned, depicted in Figure 5-10.

Figure 5-11: Cleaning starts from the centre of the contaminated area, 90 seconds run time.

From Figure 5-11 it can be seen that the transducer cleans the contaminated area starting from the center toward the circumference of the grease patch. This image was taken after 90 seconds whilst the pump maintained a slow but steady flow of solution (sunlight liquid and water).

Figure 5-12: More than 70% of the contaminated area is now visibly clean after 135 seconds.

After 135 seconds, bubbles could be seen forming in between the transducer and the insulator, on the outer lip of the transducer. From the bubbles observed it is concluded that cavitation is present, this is proven by a visibly reduced contaminated area shown in Figure 5-12.

The water, which provides the coupling between insulator and transducer, is continuously being flushed away. This causes the resonant frequency to shift, and the generator to adapt. Cavitation vacuoles are only developed if the generator is performing correctly, therefore it is proven that the admittance locking technique is functioning well.

Figure 5-13: The grease under the transducer face is removed, after 180 seconds.

As stated previously, the contaminated area on the insulator is slightly larger than the area of the transducer face. This is the reason, along with weaker coupling on the edges of the transducer, why some contaminant can still be seen left behind in Figure 5-13. The areas which were cleaned however, showed absolutely no trace of the grease left behind.

5.2.2. Efficacy of the cleaner

The transducer face has a radius of 30 mm, and the contaminated area was allowed to bleed 10 mm greater than the transducer face. The total area greased up amounted to a radius of 40 mm. Figure 5-9 and Figure 5-13 , representing the start condition and the end condition respectively were exported into the Photoshop software package. Here the images were subtracted from each other to assess how effectively the prototype can clean. The circumference of an evenly spaced grid is shaped like the face of the transducer and placed over the exact area where the experiment was conducted.
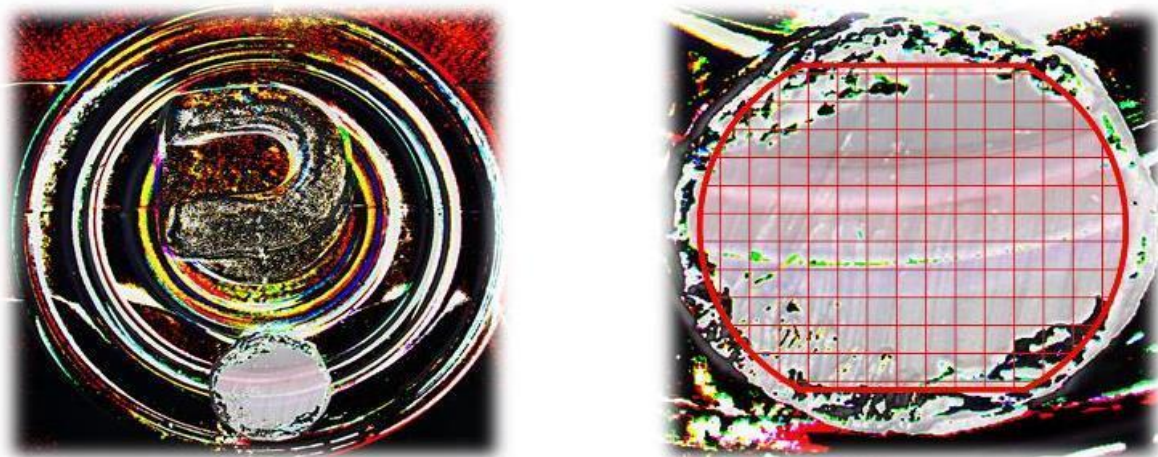
Figure 5-14: The subtracted images and the transducer shaped grid over the cleaned area.

From Figure 5-14 it is deduced that after 180 seconds of cleaning over the same area, a total amount of contaminant left behind accumulates to 10 of the grid blocks above. The total area under the face of the transducer was calculated to be 140 blocks. Therefore the total efficacy can calculate by:

$$140\ blocks - 10\ blocks = 130\ blocks$$

$$\therefore efficacy = \frac{130}{140} \times 100\ \%$$

$$efficacy = 93\%$$

5.2.3. Efficiency

One of the most prominent results is the cleaning time with respect to power, the graph indicates that no cleaning occurs with lower power levels. Too little acoustic energy is produced and therefore no cavitation bubbles are formed.

As the power increases however, some cavitation bubbles are formed and cleaning occurs. If the higher end of the scale is examined one can see that effective, fast cleaning occurs which shows how the energy contained in the bubbles has increased. The graph in Figure 5-15 indicates how fast an area of 2 cm² can be cleaned using the prototype designed.
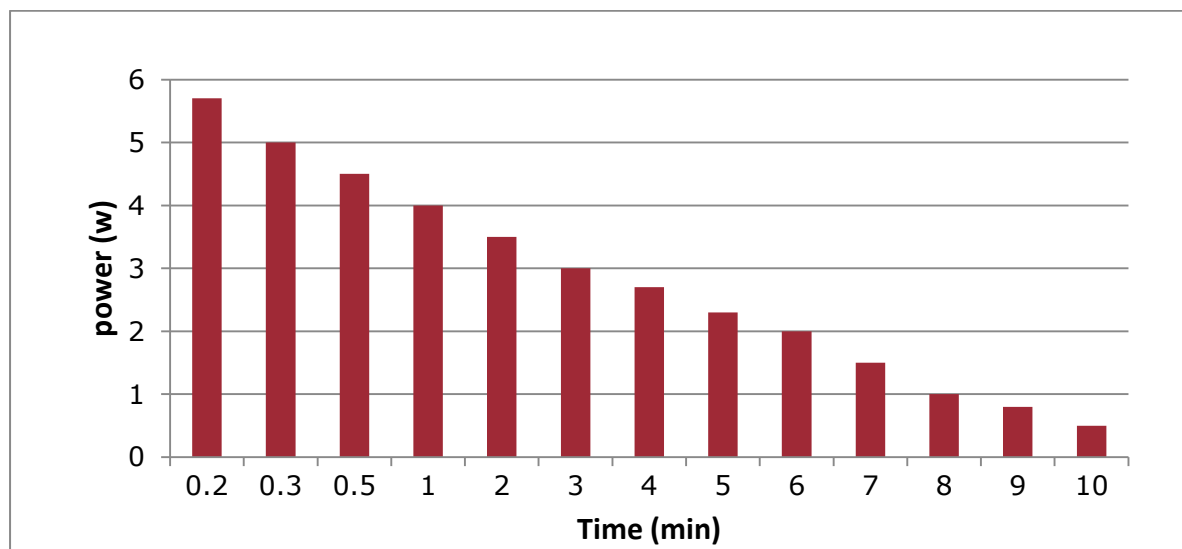
Figure 5-15: Cleaning time vs power.

The best efficiency result whilst still maintaining efficacy was recorded at a duty cycle of 40 %. An input power of 5.23 W and an output power of 3.92 W produce a system efficiency of 75 %. This proves that the system is not only an effective cleaner but

power conserving as well. In table 5-1 the system efficiency is evaluated as the duty cycle is altered

Table 5-1: system efficiency as duty cycle is increased

Duty cycle	Input power	Output power	efficiency
30 %	4.05 W	2.81 W	69 %
35 %	4.64 W	3.34 W	72 %
40 %	5.23 W	3.92 W	75 %
45 %	5.71 W	4.22 W	74 %

5.2.4. Discussion: ultrasonic cleaning results

The results in this experiment was undeniably positive, grease was successfully removed from the glass insulator in a very short period of time. The ultrasonic cleaner is effective in its ability to remove dirt from the target area. It was however observed that the areas close to the circumference of the transducer was least affected by the ultrasound. These areas are predominantly responsible for the reduced efficacy of 93 %.

The transducer cleans the target area from its centre, and works its way toward the circumference of the area whilst the water rinses the contaminant away. The harmonic frequencies can be heard searching, and locking onto the resonant frequency as the flowing water in the 1 mm gap continuously changes the load condition. The peculiar cleaning technique produces confident and conclusive results using only 5 W of power. With many avenues still to be improved, the concept now seems to have a great amount of potential, in a vast number of industries.

It does however become apparent that an automatic resonant frequency tracing technique is mandatory to compensate for changes such as the load input voltage, distance between the transducer and insulator as well as the flow of water. If these conditions vary without an ARFT, the transducer will fall out of resonance. The result will be less or no cleaning with a drastically reduced efficiency.

Once the peculiar cleaning technique was proven to be competent and efficient, the final task ahead was to test the device which would transport the cleaning prototype to the contaminated insulators.

5.3. Line walker results

The final experiment would require the line walker to navigate past an obstacle on the line. A live line was not used for this test, but the dimensions of the line and obstacle however are scaled 1:1.

5.3.1. Experiment 4: navigate an obstacle on the line.

The environment of a HVTL was simulated by installing a hollow steel rod 20mm in diameter across the 10 m long laboratory, at a height of 6 m. The line was supported on either side as well as in the centre where an obstacle was placed in order to simulate an insulator shown in Figure 5-16.
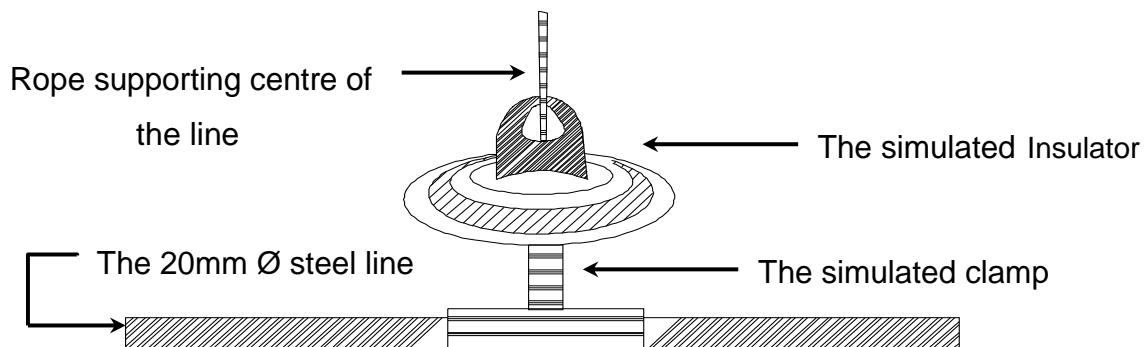
Figure 5-16: The simulated insulator and line setup.

The following observations show how the robot propels completely autonomously past the obstacle on the line. The process is thoroughly explained and each step undertaken to overcome the obstacle is documented.

The experiment is started by positioning the robot on the line facing the direction of the obstacle. The robot is then powered up after which it autonomously balances itself. This balancing action is achieved by either incrementing or decrementing the servo motor positions until each of the four leg mechanisms are in their desired locations. The accelerometer governs the amount of adjustment required, and each leg is independently manoeuvred.

The propulsion motors which are controlled by a PWM signal, are then activated and the robot moves forward until it approaches the obstacle on the line shown in Figure 5-17.

Figure 5-17: The robot approaches an obstacle on the line.

The first limit switch is triggered, indicating that the first wheel be removed from the line. This causes the centre of gravity to shift, as there are now only three legs supporting the weight of the robot. The data from the accelerometer is once again updated so that the necessary adjustments can be executed to the three remaining legs. After the robot has been balanced, it continues to propel forward, shown in Figure 5-18.

Figure 5-18: The first wheel is removed from the line.

When the limit switch of the second wheel reaches the obstacle, the first wheel is instructed to move back onto the line, the second wheel then manoeuvers off. The distance between the legs was chosen to ensure that the wheel returning to the line will have moved past the obstacle by the time the next limit switch is triggered.
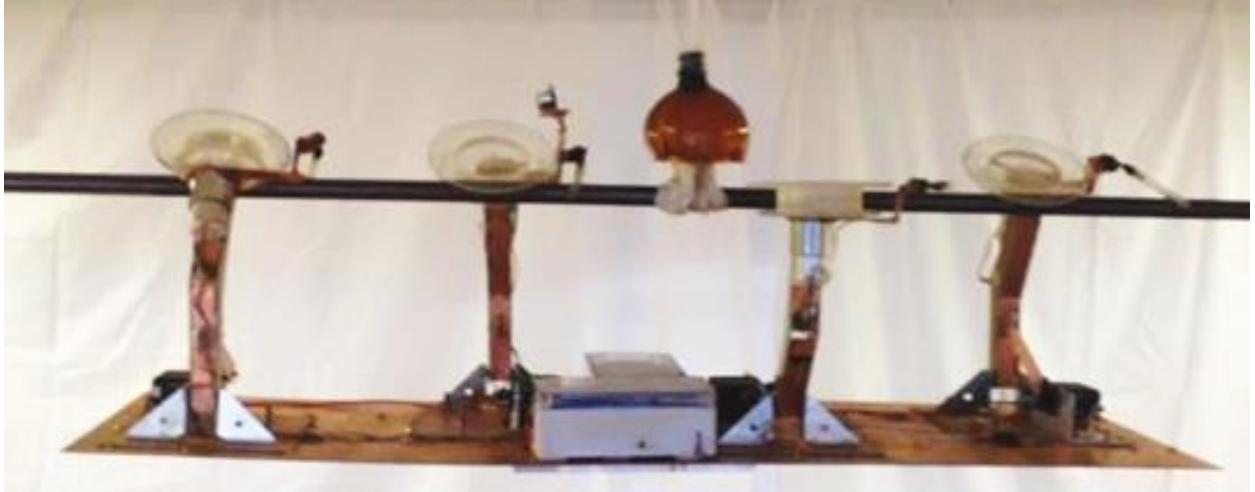
Figure 5-19: The second wheel is removed from the line.

The robot then continues moving forward and repeats the process for the third wheel, shown in Figure 5-20. The central proccessing unit (CPU) housing and the batteries are positioned in the centre of the chassis, more strain is therefore encountered on the two centre wheels, while the two outer wheels provide much needed stability.

Figure 5-20: The third wheel is removed.

The third wheel is returned in Figure 5-21 and the robot rectifies its balance before removing the fourth wheel. The ultrasonic distance sensor is positioned above the third wheel and measures the distance between the obstacle and the sensor. The measurement routine is initiated once the fourth wheel is removed.

Figure 5-21: The last wheel is taken off the line and the distance meter started.

The last wheel is brought back onto the line when a safe clearing distance has been established via the ultrasonic distance meter. The robot then corrects its balance and propels forward in search of the next obstacle shown in Figure 5-22.

Figure 5-22: The last wheel is returned.

Manufacturing the robot along with the experiments executed was very informative and a factastic opportunity to aquire insight into the field of robotics. The endeavour was enjoyed and complacence was achieved once the results were recorded.

5.3.2. Discussion: line walker results

After many hours of building and reprogramming, the line walker has finally produced a definitive result. The autonomous robot has successfully navigated an obstacle on the simulated high voltage transmission line. With only three wheels on the line, the

dexterous drone effortlessly propels forward. The robot's balance is continually being monitored and rectified before any wheels are removed. This task proved to be the most tedious due to the large size and weight of the complete assembly. The upgraded actuators produce powerful and accurate leg movements, capable of competently handling the weight.

The PCB chassis of the line walker is flexible, which assists the balancing act of the drone. The proximity sensors are perfectly positioned and operate unhindered. Many improvements can be made to this device but the core function, which is to navigate the HVTL has been achieved,

The total time taken to manoeuvre the entire chassis past the obstacle was recorded to be only 65 seconds. This can be considered fast, as the drone requires no human assistance, has a 1 m long chassis and a 20 kg payload to support. With no obstacle in front of the drone, it is capable of traversing along vast amounts of cable at a speed of 0.1 m/s.

The Line walker proved to be proficient in its ability to navigate the line autonomously. The drone detects obstacles, corrects its balance and is also fast in doing so. The line walker is a smart device, with much room for future upgrades.

With all the research questions answered, it is time to finally conclude this study with a few recommendations.

Chapter 6
Conclusion and future work

6.1. Conclusion

Various alternative solutions to the problem statement mentioned in Chapter 1 were investigated before an innovative cleaning method with a four wheeled line walker concept was developed as a possible solution.

As seen from the results obtained by using this peculiar delivery technique, it is possible to clean insulators using ultrasound directly. The direct method of applying the ultrasound proved to be an effective and efficient method of cleaning glass with grease as a contaminant. The novel method will require the transducer placement to be precise in order to yield the best results. The results suggest that a automatic resonant frequency tracing technique is actually mandatory for this application. This is due to the coupling issues experienced with the random act of n the water surface tension, combined by incorrect transducer placement. The solution offers great potential as it only requires a small quantity of water, no buckets or basins, and does not require the line to be de-energized while cleaning. The complete delivery solution will require more development if one is to clean the whole surface of the insulator accurately. The novel delivery technique makes use of the small generator circuit, a 12 V source and a transducer connected to an articulated arm. These few components cater for a compact and portable solution.

. The generator operates within the bandwidth of the transducer, and produces enough power to remove grease as a contaminant from the glass insulators. The generator's PWM controller circuit produces a stable oscillating driving signal while the push pull transformer provides the necessary power to achieve cavitation. The system operates manually via four push buttons or autonomously via the selected microcontroller, but the manual operation will produce a reduced reaction time and consequently slower cleaning times. The generator tracks the resonant frequency effectively, and mimics the output frequency response curves taken by the impedance analyzer. Tracking is achieved by manipulating the frequency using two digital potentiometers .initially, a complete scan of the frequency range is logged and paired with the corresponding current sample taken by a current sensor. The

frequency is then adjusted to the position/step, which produces the highest current sample. The portable unit delivers 5.7 mW of power, and yields short cleaning times, making it an ideal solution for this specific application.

The line walker robot is capable of travelling forward on the line at a speed of 0.1 m/s. Many challenges were overcome by upgrading, redesigning and reprogramming problematic areas within the system. The four leg structures are independently controlled and are responsible for removing the wheels from the line. The robot effortlessly navigates around obstacles and is capable of carrying the 10 kg ultrasonic payload. The main concerns while developing the robot was trying to maintain a level chassis when only three legs are coupled to the HVTL. The robot has to lift its weight up to replace the previously removed wheel from the line. This concern is addressed by implementing the pivoted leg mechanism to reduce the strain on the motors while increasing the mechanical torque of the system. The robot continuously monitors its balance on the line to ensure a stable movement, allowing for a safe and controlled motion when navigating the HVTL. the continuous growth in the field of robotics and the technological advancements available today has contributed greatly to the success of this   line walker design. This transportation device still has some development required but holds lots of future potential.

With cleaning times as little as 30 seconds / 2 cm² recorded and a line walker that navigates obstacles with ease, the project can be deemed successful. All the experiments were repeated to confirm the results obtained are authentic and can be reproduced.

 This ambitious project has a broad scope and will require a skillful team to fully develop in the future. The potential of this novel cleaning technique is intriguing and offers the possibility to clean using ultrasound where it previously was not possible, opening the doors to a new and wide range of applications.

6.2. Future work

The system is well designed and achieves the goals required to prove this study successful. Improvements to the entire project can however be made by:

- Improving efficacy by shaping the transducer face to mimic the shape of the insulator. This will improve the coupling which in turn would increase the system efficiency,
- I drip tray can be desighned to recycle the water used when cleaning,
- a camera module can assist with obstacle detection, data collection, and trancducer placement,
- the line walker design can be modified to overcome tension type line configurations.
- The mechanism which will controll the placement of the transduser could detach from the walker when cleaning is required.

Bibliography

Alonso, F. & Greenwell, C., 2013. *Underground vs. overhead: power line installation-cost comparison and mitigation.* [Online]
Available at: https://www.elp.com/articles/powergrid_international/print/volume-18/issue-2/features/underground-vs-overhead-power-line-installation-cost-comparison-.html
[Accessed 3 June 2014].

Beaty, H. 1998. *Electric power distribution systems: a nontechnical guide.* Oklahoma: PenWell.

Berglund, B., Johansson, J. & Lejon, T. 2006. High efficiency power amplifiers. *Ericsson Review,* 83(3):92-96, March.

Bialek, J., 2005. *Blackouts in the US/Canada and continental Europe in 2003: Is liberalisation to blame?.* St. Petersburg, IEEE.

Branson Ultrasonics Corp., 2000. *Branson 1510 Ultrasonic Cleaner.* [Online]
Available at: https://www.nist.gov/laboratories/tools-instruments/branson-1510-ultrasonic-cleaner
[Accessed 15 May 2014].

Buhringer, M. et al. 2010. Cable-crawler – robot for the inspection of high-voltage power lines that can passively roll over mast tops. *Industrial Robot: An International Journal,* 37(3):256-262, May.

Calkins, F., Smith, R. & Flatau, A. 2000. Energy-based hysteresis model for magnetostrictive transducers. *IEEE Transactions on Magnetics,* 36(2):429-439, March.

Capelo-Martínez, J.L. 2009. The power of ultrasound. In Capelo-Martínez, J.L.(eds). *Ultrasound in chemistry: analytical applications.* Weinheim: Wiley: 1-15.

Chiou, D. & Chen, M. 2009. Electromechanical modeling, characterization, and optimization design of the postcomplementary metal-oxide-semiconductor capacitive microarrayed ultrasonic transducer. *Journal of Micro/Nanolithography, MEMS, and MOEMS,* 8(2):8-9, April.

Claassen, B., 2005. *Digital control techniques for a multiple transduser array,* Cape Town: CPUT.

Cleaning Technologies Group, 2003. *Magnetostrictive versus piezoelectric transducers for power ultrasonic applications.* [Online]
Available at: https://www.ctgclean.com/magnetostrictive-versus-piezoelectric-transducers-for-power-ultrasonic-applications
[Accessed 20 November 2014].

Collins, F., 2009. *Toothbrush technology,dentifrices and dental biofilm removal.* Ohio, PennWell Corp..

Csanyi, E., 2012. *Electrical engeneering portal.* [Online]
Available at: http://electrical-engineering-portal.com/ceramic-porcelain-and-glass-insulators
[Accessed 7 August 2014].

Day, J. & Martin, M. 1998. Efficacy of a sonic toothbrush for plaque removal by caregivers in a special needs population. *Special Care in Dentistry,* 18(5):202-206, September.

Debenest, P. & Guarnieri, M. 2010. Expliner- From prototype towards a practical robot for inspection of high-voltage lines*. In 2010 1st International Conference on Applied Robotics for the Power Industry, Montreal, 5-7 October 2010.* Pasadena: IEEE: 1-6.

Design World, 2008. *Linear actuators bring flexibility to packaging.* [Online]
Available at: https://www.designworldonline.com/linear-actuators-bring-flexibility-to-packaging/
[Accessed 23 August 2014].

Dong, H., Wu, J., Zhang, G. & Wu, H. 2012. An improved phase-locked loop method for automatic resonance frequency tracing based on static capacitance broadband compensation for a high-power ultrasonic transducer. *IEEE Transactions on Ultrasonics, Ferroelectrics, and Frequency Control,* 59(2):205-210, February.

Engdahl, G. & Mayergoyz, I.D. 2000. *Handbook of giant magnetostrictive materials.* San Diego: Academic Press.

Eskom, 2009. *Annual report 2009,* Johannesberg: Eskom .

Eskom, 2011. *Tariffs and charges.* [Online]
Available at:
http://www.eskom.co.za/CustomerCare/TariffsAndCharges/Documents/Eskom%20Booklet.pdf
[Accessed 8 May 2015].

Fabijanski, P. & Lagoda, R. 2011. Modeling and identification of parameters the piezoelectric transducers in ultrasonic systems.In Sikalidis, C (eds). *Advances in Ceramics - Electric and Magnetic Ceramics, Bioceramics, Ceramics and Environment:* Rijeka: INTECH: 155-174.

Fairchild Semiconductor Corporation, 2002. *LM555: Single Timer.* [Online]
Available at: http://www.onsemi.com/PowerSolutions/product.do?id=LM555
[Accessed 15 January 2016].

Floyd, T., 2012. *Electronic devices.* 9th ed. Upper Saddle River: Pearson.

Foldyna, J., Sitek, L., Svehla, B. & Svehla, S. 2004. Utilization of ultrasound to enhance high-speed water jet effects. *Ultrasonics Sonochemistry,* 11(3-4):131-137, May.

Fuchs, J. 1995. Ultrasonic cleaning: Fundamental theory and application*. In Marshall Space Flight Center, Aerospace Environmental Technology Conference,* Alabama, *10-11 August 1994.* Huntsville, NASA: 369-378.

Fuchs, J. 2012. *Cleaning Technologies Group.* [Online]
Available at: http://www.ctgclean.com/tech-blog/2012/01/ultrasonics-transducers-

magnetostrictive-hardware/
[Accessed 25 April 2014].

Fuchs, j., 2012. *Ultrasonics - transducers - piezoelectric hardware.* [Online]
Available at: https://techblog.ctgclean.com/2012/01/ultrasonics-transducers-piezoelectric-hardware/
[Accessed 3 May 2014].

Garcia-Rodriguez, M., Garcia-Alvarez, J., Yañez, Y., Garcia-Hernandez, M.J., Salazar, J., Turo, A. & Chavez, J.A. 2010. Low cost matching network for ultrasonic transducers. *Physics Procedia,* 3(1):1025-1031, January.

Gonçalves, R. & Carvalho, J. 2013. Review and latest trends in mobile robots used on power transmission lines. *International Journal of Advanced Robotic Systems,* 10(408):1-14, December.

Gonen, T. 2013. *Modern power system analysis.* 2nd ed. Boca Raton: CRC Press.

Gurun, G., Hochman, M., Hasler, P. & Degertekin, F. 2012. Thermal-mechanical noise based CMUT characterization and sensing. *IEEE Transactions on Ultrasonics, Ferroelectrics, and Frequency Control,* 59(6):1267-1275, June.

Hernanz, R., Jose, A., Martin, C., Jose, J., Gogeascoechea, M. & Belver, Z. 2006. Insulator pollution in transmission lines. Renewable Energy & Power Quality, 1(4):124-130, April.

Heywang, W., Lubitz, K. & Wersing, W. 2008. *Piezoelectricity: evolution and future of a technology.* 114th ed. Berlin: Springer.

Hoeribiger, 2015. *Direct industry.* [Online]
Available at: http://www.directindustry.com/prod/hoerbiger-automatisierungstechnik-gmbh/product-5764-1315565.html
[Accessed 26 January 2015].

Hongguang, W., Yong, J., Aihua, L., Lijin, F. & Lie, L. 2010. Research of power transmission line maintenance robots in SIACAS*. In 2010 1st International Conference on Applied Robotics for the Power Industry (CARPI),* Montreal, 5-7 October 2010: IEEE: 1-7.

Huang, H. 2013. *The Atmel AVR microcontroller: Mega and Xmega in assembly and C.* Delmar: Cengage Learning.

Huang, Y., Haeggstrom, E.O, Zhuang, X., Ergun, A.S & Khuri-Yakub, B.T. 2005. A solution to the charging problems in capacitive micromachined ultrasonic transducers. *IEEE Transactions on Ultrasonics, Ferroelectrics, and Frequency Control,* 52(4):578-580, April.

Hughes, A. 2005. *Electric motors and drives: fundamentals, types and applications.* 3rd ed. Oxford: Elsevier.

Industrial Sonomechanics, 2015. *Introduction to ISM.* [Online]
Available at: http://sonomechanics.com/about_ism/introduction_to_ism/
[Accessed 23 January 2015].

Janocha, H., 2004. *Actuators: basics and applications.* Berlin: Springer.

Kanegsberg, B. & Kanegsberg, E. 2011. *Handbook for critical cleaning: cleaning agents and systems.* 2nd ed. Boca Raton: CRC Press .

Khuri-Yakub, B.T. & Oralkan, O. 2011. Capacitive micromachined ultrasonic transducers for medical imaging and therapy. *Journal of Micromechanics and Microengineering,* 21(5):54004–54014, April.

Kiessling, F., Nefzger, P., Nolasco, J. F. & Kaintzyk, U. 2014. *Overhead power lines: planning, design, construction.* Berlin: Springer.

Kim, J.O., Choi, S. & Kim, J.H. 1999. Vibroacoustic characteristics of ultrasonic cleaners. *Applied acoustics,* 58(2):211-288, October.

Kolumban, G., 2012. *Department of Measurement and Information Systems.* [Online]
Available at: http://www.mit.bme.hu/eng/oktatas/targyak/vimia305/M09
[Accessed 18 July 2014].

Kumar, P. & Kumar, R., 2013. Refurbishment of transmission lines resulting in improvement in pollution performance in northern region in India*. Power Engineer Journal,* 15(1):22-26, May.

Kumosa, M., Armentrout, D., Burks, B., Hoffman, J., Kumosa, L., Middleton, J. & Predecki, P. 2011. Polymer matrix composites in high voltage transmission line apllications*. In Proceedings of 18th International Conference on composite Materials ,* Jeju, 21-26 August 2011. Denver: University of Denver.

Lamm, E., 2003. *Controlled enviroments.* [Online]
Available at: http://www.cemag.us/articles/2003/10/development-ultrasonic-cleaning
[Accessed 7 August 2014].

Lancaster, R., 2012. *Electrical4u.* [Online]
Available at: http://www.electrical4u.com/electrical-insulator-insulating-material-porcelain-glass-polymer-insulator/
[Accessed 16 May 2014].

Langro, F., 2011. *Pneumatics vs electrics: A niche for each.* [Online]
Available at: http://www.designworldonline.com/pneumatics-vs-electrics-a-niche-for-each/
[Accessed 27 August 2014].

Lefrak, F., 2015. *Mini-circuits.* [Online]
Available at: http://www.minicircuits.com/app/AN20-001.pdf
[Accessed 20 June 2015].

LEM, 2011. *LEM.* [Online]
Available at: http://www.lem.com/docs/marketing/LDK%20leaflet%20complete%20web.pdf
[Accessed 23 December 2014].

Lou, F., 2012. *Electronic desighn- Back to Basics: Impedance Matching (Part 2).* [Online]
Available at: http://electronicdesign.com/communications/back-basics-impedance-matching-

part-2
[Accessed 10 July 2014].

Mantech Electronics, 2015. *Mantech Electronics.* [Online]
Available at: http://www.mantech.co.za/Stock.aspx?Query=sensorand
[Accessed 05 01 2015].

Mantech Electronics, 2015. *Mantech Electronics.* [Online]
Available at: http://www.mantech.co.za/Stock.aspx?Query=Gyroscopeand
[Accessed 05 01 2015].

Mantech Electronics, 2015. *Mantech Electronics.* [Online]
Available at: http://www.mantech.co.za/Stock.aspx?Query=batteryand
[Accessed 15 February 2015].

Mantech Electronics, 2015. *Mantech Electronics.* [Online]
Available at: http://www.mantech.co.za/Stock.aspx?Query=motorsand
[Accessed 8 February 2015].

McGrath, M. & Scanaill, C. 2013. *Sensor technologies: healthcare, wellness and environmental.* Dublin: Apress.

Min, B. 2015. *Power and the vote: elections and electricity in the developing world.* New York: Cambridge University.

Minnaar, U.J., Gaunt, C.T. & Nicolls, F. 2012. Characterisation of power system events on South African transmission power lines. *Electric Power Systems Research,* 88(1):25-32, July.

Mittal, K. & Jaiswal, R. 2015. *Particle adhesion and removal.* Beverly: Scrivener.

Mohan, N., Undeland, T. & Robbins, W. 2003. *Power Electronics: Converters, Applications, and Design.* 3rd ed. New York: John Wiley.

Mortimer, B., Du Bruyn, T., Davies, J. & Tapson, J. 2001. High power resonant tracking amplifier using admittance locking. *Ultrasonics,* 39(4):257-261, June.

Moses, A., Anderson, P., Phophongviwat, T. & Tabrizi, S., 2010. *Contribution of magnetostriction to transformer noise.* Cardiff, IEEE.

mplgmg, 2017. *High voltage transmission tower types in power industry.* [Online]
Available at: http://www.electricalpowerenergy.com/2014/02/high-voltage-transmission-tower-types-in-power-industry/
[Accessed 7 March 2017].

National Grid, 2015. *Technical issues of undergrounding high voltage electricity transmission lines.* [Online]
Available at: https://electrical-engineering-portal.com/download-center/books-and-guides/electricity-generation-t-d/undergrounding-hv-lines
[Accessed 9 10 2015].

Nexperia, 2016. *HEF4046B.* [Online]
Available at: https://www.nexperia.com/products/logic/synchronous-interface-logic/phase-locked-loops/series/HEF4046B.html
[Accessed 27 1 2017].

Olabi, A.G. & Grunwald, A. 2008. Design and application of magnetostrictive materials. *Materials & Design- Mater Design,* 29(2):469-483, January.

Olympus NDT, 2011. *Ultrasonic transducer technical notes.* [Online]
Available at: https://www.olympus-ims.com/en/resources/white-papers/ultrasonic-transducer-technical-notes/
[Accessed 23 April 2015].

Oralkan, O., Ergun, A.S., Johnson, J.A., Demirci, U., Kaviani, K., Lee, T.H. & Khuri-Yakub, B.T. 2002. Capacitive micromachined ultrasonic transducers: next-generation arrays for acoustic imaging. *IEEE transactions on ultrasonics, ferroelectrics, and frequency control,* 49(11):1596-1610, November.

Payne, G., 2005. *Digital locking techniques for a singal ultrasonic transduser,* Cape Town: Cape Peninsula University of Technology.

Pedeflous, F., 2014. *Omegasonics.* [Online]
Available at: http://blog.omegasonics.com/archives/will-ultrasonic-cleaning-damage-electrical-components
[Accessed 16 january 2015].

Pinson, M.B. & Bazant, M.Z. 2013. Theory of SEI formation in rechargeable batteries: capacity fade, accelerated aging and lifetime prediction. *Journal of the Electrochemical Society,* 160(2):A243-A250, January.

Pouliot, N. & Montambault, S., 2008. *Geometric design of the LineScout, a teleoperated robot for power line inspection and maintenance.* Pasadena, IEEE.

Pouliot, N. & Montambault, S., 2008. *Geometric design of the LineScout, a teleoperated robot for powerline inspection and maintenance.* Pasadena, IEEE.

Pouliot, N. & Montambault, S., 2009. *LineScout technology: from inspection to robotic maintenance on live transmission power lines..* Kobe, IEEE.

Precision Acoustics, 2015. *Shear wave transducers.* [Online]
Available at: http://www.acoustics.co.uk/product/shear-wave-transducers/
[Accessed 20 March 2015].

Pressure washers pro, 2013. *Insulator pressure washers.* [Online]
Available at: https://pressurewasherspro.com/pressure-washer-operations/insulator-pressure-washers/#.W9cRweJoSUn
[Accessed 26 May 2014].

Queiros, R., Girao, P.S. & Serra, A.C. 2005. Single-mode piezoelectric ultrasonic transducer equivalent circuit parameter calculations and optimization using experimental data. *IMEKO*

TC4 International Symposium on New Technologies in Measurement and Instrumentation, 2(1):468-471, April.

Red Eléctrica de España, 2008. *Red Eléctrica line and substation maintenance works.* [Online]
Available at: https://www.ree.es/en/press-office/monographs/red-electrica-line-and-substation-maintenance-works
[Accessed 22 September 2014].

Sherman, C. & Butler, J. 2007. *Transducers and arrays for underwater sound.* New York: Springer.

Shoh, A.. 1975. Industrial applications of ultrasound-A review I. High-power ultrasound. *IEEE Transactions on Sonics and Ultrasonics,* 22(2):60-70, March.

Sinclair, I. 2001. *Sensors and Transducers.* 3rd ed. Oxford: Butterworth-Heinemann.

Singh, A. 2008. *Microcontroller and embedded system.* Lucknow: New Age International.

Sivakumar, V., Chandrasekaran, F., Swaminathan, G. & Rao, P. 2009. Towards cleaner degreasing method in industries: ultrasound-assisted aqueous degreasing process in leather making. *Journal of Cleaner Production,* 17(1):101-104, January.

Stix, G. 1988. Working hot: life at 765 kV. *IEEE Spectrum,* 25(9):54-56, September.

Svilainis, L. & Motiejûnas, G., 2006. Power amplifier for ultrasonic transducer excitation. *Ultragarsas,* 58(1), pp. 30-36.

Terlemez, B., 2004. *Oscillation control in CMOS phase-locked loops.* Doctoral dissertation: Georgia Institute of Technology.

Texas Instruments, 2003. SG3524. [Online]
Available at: http://www.ti.com/lit/ds/symlink/sg3524.pdf
[Accessed 9 April 2015].

Toussaint, k., Pouliot, N. & Montambault, S., 2009. Transmission line maintenance robots capable of crossing obstacles: state-of-the-art review and challenges ahead. *Field Robotics,* 26(5), pp. 447-499.

Tri-State Generation and Transmission Association, 2009. *Overhead vs. underground.* [Online]
Available at: https://www.tristate.coop/sites/ts/files/PDF/TransmissionProjects-FAQ/TransprojFAQ-Understanding%20Undergrounding.pdf
[Accessed 16 June 2014].

Uchino, K., 2003. *Introduction to piezoelectric actuators and transducers,* Pennsylvania: PENNSYLVANIA STATE UNIV UNIVERSITY PARK.

Wang, L., Liu, F., Xu, S., Wang, Z., Cheng, S. & Zhang, J. 2010. Design, modeling and control of a biped line-walking robot. *International Journal of Advanced Robotic Systems,* 7(4):33-33, December.

Wang, L., Wang, H.G., Song, Y.F. & Pan, X.A. 2016. Development of a bio-inspired live line cleaning robot for suspension insulator strings. *International Journal of Simulation Systems, Science & Technology,* 17(48):24.1-24.9, January.

Weiss, M., 2011. *Public service commission of Wistconsin.* [Online]
Available at: https://psc.wi.gov/thelibrary/publications/electric/electric11.pdf
[Accessed 6 April 2015].

Wei, W., Yu-cheng, B., Gong-ping, W., Shui-xia, L. and Qian, C. 2013. The mechanism of a snake-like robot's clamping obstacle navigation on high voltage transmission lines. *International journal of advance robotic systems,* 10(9):330, September.

Yaku, M., Tangel, A. & Tangel, C. 2009. A microcontroller based generator design for ultrasonic cleaning machines. *Istanbul University-Journal of Electrical & Electronics Engineering,* 9(1):853-860, January.

Zenith Mfg & Chemical Corp., 2010. *Choosing the best ultrasonic frequency.* [Online]
Available at: http://www.zenith-ultrasonics.com/ultrasonic_frequency_selection.htm
[Accessed 10 September 2014].

Zhu, X. et al., 2006. *Single Arm Running Control Method of Inspection Robot Based on Obliquitous Sensor.* Kunming, IEEE, pp. 187-192.

Appendix A- The Code

```
****************************************************************

              The ultrasonic cleaning program
**************************************************************************************
 2 // Toriq Ramos 207022917
 3
 4 // declaration........................................
 5
 6 constint UD = 2; // Up & down of the frequency
 7 constint clock = 3 ; // clock pulse for the frequency pot and the duty
 8 cycle
 9 constintPushBfrequency = 5 ; //push button pinfor frequency pot
10 constint PushBfrequency1 =4;  //push button pinfor frequency pot
11 constintChipselectF = 22;// master command pinfor frequency pot
12 constint led = 12;           // led indicator for the push button
13 constintPushBDuty = 11 ;   // push button pin for Duty cycle pot
14 constint PushBDuty1 =10;   // push button pin for Duty cycle pot
15 constint UD2 = 7; // Up & down of the duty cycle
16 constintChipselectD = 30;//master command pinfor Duty cycle pot
17 // variables of the frequency pot
18 int PushBF1=0; // push button frequency 1
19 int PushBF2=0; // push button frequency 2
20 int POS=0;
21 intPos=0;
22 intreadingSteps = 0;
23 intreadingMaxValueStep = 0;
24 floatreadingMaxValue = 0;
25 // variables of the Duty cycle pot
26 int PushBD1=0; // push button duty cycle 1
27 int PushBD2=0; // push button duty cycle 2
28 //------------------------------------------------------------------
29 //------------------------------------------------------------------
30 void setup() {
31 // declaration of inputs
32 Serial.begin (9600);
33 pinMode(PushBfrequency,INPUT);
34 pinMode(PushBfrequency1,INPUT);
35 pinMode(PushBDuty,INPUT);
36 pinMode(PushBDuty1,INPUT);
37
38 // declaration of outputs
39 pinMode(led,OUTPUT);
40 pinMode(UD,OUTPUT);
41 pinMode(ChipselectF,OUTPUT);
42 pinMode(clock,OUTPUT);
43 pinMode(ChipselectD,OUTPUT);
44 pinMode(UD2,OUTPUT);// PWM pin for pulsing the duty cycle
45
46 digitalWrite(ChipselectF,HIGH);
47 digitalWrite(ChipselectD,HIGH);
48 Serial.println("Digital Controlled Ultrasonic Generator");
49 Serial.println("\nRESETTING THE FREQANCY FOR SCAN :   ");
50 Reset(); // call reset function to set the frequency to 0
51 Serial.print("FREQUANCY IS RESET");
52 Serial.print("\nRESETING DUTY CYCLE NOW");
```

```
53 ResetDutyCycle(); // reset the duty cycle to 0
54 Serial.print(":     DONE");
55 Serial.print("\nSETTING POWER TO HALF @ 50%");
56 DutyCycleHalf(); // set the duty cycle to 25%
57 Serial.print(":      DONE");
58 Serial.print("\nSTARTING SCAN:");
59 Scan();   //call scan function to sweep through the frequency range
60 }
61 //------------------------------------------------
62 void loop()
63 {
64 FrequencyPushButton();
65 DutyCyclePushButton();
66 }
67 //------------------------------------------------
68 voidDowndirectionD()// this function decrements the duty cycle pot
69 {
70 digitalWrite(ChipselectD,HIGH);
71 digitalWrite(clock,HIGH);
72 digitalWrite(UD2,HIGH);
73 digitalWrite(ChipselectD,LOW);
74 digitalWrite(clock,LOW);
75 digitalWrite(ChipselectD,HIGH);
76 }
77 voidUPDirectionD()// this functionincrements the duty cycle pot
78 {
79 digitalWrite(ChipselectD,HIGH);
80 digitalWrite(clock,HIGH);
81 digitalWrite(UD2,LOW);
82 digitalWrite(ChipselectD,LOW);
83 digitalWrite(clock,LOW);
84 digitalWrite(ChipselectD,HIGH);
85 }
86 voidDowndirection()// this function decrements the frequency pot
87 {
88 digitalWrite (ChipselectF, HIGH);
89 digitalWrite(clock,HIGH);
90 digitalWrite(UD,HIGH);
91 digitalWrite (ChipselectF, LOW);   //
92 delay (20);                //EEPROM STORE ON DS1804
93 digitalWrite(clock,LOW);
94 digitalWrite (ChipselectF, LOW);
95 }
96 voidUPDirection()// this function increments the frequency pot
97 {
98 digitalWrite (ChipselectF, HIGH);
99 digitalWrite(clock,HIGH);
100 digitalWrite(UD,LOW);
101 digitalWrite (ChipselectF, LOW );   //
102 delay (20);                //EEPROM STORE ON DS1804
103 digitalWrite(clock,LOW);
104 digitalWrite (ChipselectF, HIGH);
105 }
106 //-----------------------------------------------------------------
107 //-----------------------------------------------------------------
108 void Reset()// reset function sets the frequancy pot to zero
109
```

```
110 {
111 for(int a = 1; a <=100; a++)
112 {
113 digitalWrite(ChipselectF,LOW);  //activate ChipselectF
114 Downdirection();                // 100 steps down
115 delay(50);
116 }
117 digitalWrite(ChipselectF,LOW); // activate ChipselectF
118 UPDirection();                 // one step above zero
119 delay(50);
120 }
121 //------------------------------------------------------------------------
122 //-----------------------------------------------------------------------
123 voidResetDutyCycle()    // reset the duty cycle pot to zero
124 {
125 for(int c = 1; c <=100; c++)
126    {
127 digitalWrite(ChipselectD,LOW);//activate ChipselectD
128 DowndirectionD();
129 delay(50);
130 }
131 digitalWrite(ChipselectD,LOW); //activate ChipselectD
132 UPDirectionD();                // one step above zero
133 delay(50);
134 }
135 //------------------------------------------------------------------------
136 //-----------------------------------------------------------------------
137 voidDutyCycleHalf()// set the duty cycle to 50%
138 {
139 for(int d = 0; d < 35 ;d++)
140 {
141 digitalWrite(ChipselectD,LOW);
142 UPDirectionD();
143 delay(100);
144 }
145 }
146 //------------------------------------------------------------------------
147 //-----------------------------------------------------------------------
148 void Scan() // this function scans through the frequencies available
149 //          and stores the address of the frequancy that producers
150 //          the highest current value.
151 {
152 readingMaxValueStep = 0;
153 readingMaxValue = 0;
154 for(intreadingStep = 1; readingStep<=100 ; readingStep++ )
155    {
156 digitalWrite(ChipselectF,LOW);
157 UPDirection();
158 delay(100);
159 floatinputValue = analogRead(A15); // read current value
160 delay(100);
161 Serial.print("\nINPUT voltage ,");
162 Serial.print((inputValue*5)/1020);//convert LEM voltage to current
163 Serial.print("\t, Step ,");
164 Serial.print(readingStep);
165
166 if (inputValue>readingMaxValue)
```

```
167     {
168 readingMaxValue = inputValue;              // store max value
169 readingMaxValueStep = readingStep ; // store max value step
170     }
171 digitalWrite(ChipselectF,HIGH); // deactivatechipselectF
172 delay(30);
173     }
174 // displaying where the maximum values has occured
175 Serial.print("\nMax: ");
176 Serial.print(readingMaxValue*5/1023);
177 Serial.print("\tStep: ");
178 Serial.print(readingMaxValueStep);
179 Serial.print("\n");
180 Serial.print("");
181 // resetting to the frequency in order to set to his optimum point
182 digitalWrite(ChipselectF,LOW);
183 for(int a = 1; a <=100; a++)
184     {
185 Downdirection();
186 delay(30);
187     }
188 digitalWrite(ChipselectF,LOW); //
189 UPDirection(); // one step above zero
190 delay(30);
191 //-------------------------------------------------------------------
192 // set to the resonant frequency position- 4
193
194 for(int b = 1; b <readingMaxValueStep ; b++)
195     {
196 UPDirection();
197 delay(30);
198     }
199
200 digitalWrite(ChipselectF,HIGH);
201 }
202 //---------------------------------------------------------------------
203 //-------------------------------------------------------------------
204 voidFrequencyPushButton()
205 {
206  // read the state of the push buttons
207  PushBF1 = digitalRead(PushBfrequency);
208  PushBF2 = digitalRead(PushBfrequency1);
209 //-----------------------------------------------------------
210 //check if there are pressed
211 if (PushBF1 == HIGH) // check if push button 1 is pressed
212     {
213 digitalWrite(led,HIGH); // switch the led on if pressed
214 digitalWrite(ChipselectF,LOW);
215 UPDirection();
216 Serial.print("frequencypos");
217 Pos++;                               // increment frequency
218 Serial.println(Pos);
219 delay(1000);
220     }
221 else
222     {
223
```

```
224 digitalWrite(led,LOW);
225   }
226     // checking the state of the second push button
227 if (PushBF2 == HIGH) // check if push button 2 is pressed
228   {
229 digitalWrite(led,HIGH); // switch the led on if pressed
230 digitalWrite(ChipselectF,LOW);
231 Downdirection();
232 Serial.print("frequencypos");
233 Pos--;                              // decrement frequency
234 Serial.println(Pos);
235 delay(1000);
236   }
237 else
238  {
239     // turn the led off to indicate no action on the push button
240 digitalWrite(led,LOW);
241 }
242  }
243 //-----------------------------------------------------------------
244 //-----------------------------------------------------------------
245 voidDutyCyclePushButton()
246 {
247 // read the state of the push buttons controlling the duty cycle
248 PushBD1 = digitalRead(PushBDuty);
249 PushBD2 = digitalRead(PushBDuty1);
250 //check if they are pressed
251 // checking the state of the second push button
252 if (PushBD2 == HIGH) // check if push button 2 is pressed
253   {
254
255 digitalWrite(led,HIGH); // switch the led on
256 digitalWrite(ChipselectD,LOW);
257 DowndirectionD();
258 Serial.print("Duty cycle pos");
259     POS--;                    // decrement duty cycle
260 Serial.println(POS);
261 delay(100);
262   }
263 else
264   {
265 digitalWrite(led,LOW);       // turn the led off
266 }
267 //------------------------------------------------------------------
268 if (PushBD1 == HIGH) // check if push button 1 is pressed
269   {
270 digitalWrite(led,HIGH); // switch the led on
271 digitalWrite(ChipselectD,LOW);
272 UPDirectionD();
273 Serial.print("Duty cycle pos");
274     POS++;
275 Serial.println(POS);
276 delay(100);
277 if(POS>10)
278     {
279 admittancelocking();  // call admittance locking routine
280     }
```

```
281   }
282 else
283   {
284 digitalWrite(led,LOW);// turn the led off
285   }
286 }
287 //----------------------------------------------------------------
288 //----------------------------------------------------------------
289 voidadmittancelocking()  // this function ensures that the transducer
290 //               is always operated close to the resonantfrequancy
291 {
292 int LOOPY= 0;
293 while (LOOPY < 7)
294  {
295 int e = 0;
296 intScanlimmit =0 ;
297 int km = 0;
298 float inputValue1 = 0;
299 float inputValue2 =0;
300 float inputValue3 = 0;
301 Serial.print("Starting Admittance locking");
302 digitalWrite(ChipselectF,LOW);
303
304 int  MaxStep1 = readingMaxValueStep;
305 for( e = MaxStep1 ; e <= (MaxStep1 +3) ; e++)
306    {
307 digitalWrite(ChipselectF,LOW);
308 UPDirection();
309 delay(30);
310    inputValue1 = analogRead(A15);
311 delay(100);
312 Serial.print("\nINPUT voltage");
313 Serial.print((inputValue1*5)/1020);
314 Serial.print("\tStep Up 3:  ");
315 Serial.print(e);
316 if (inputValue1 >readingMaxValue)
317    {
318 readingMaxValue = inputValue1;
319 readingMaxValueStep = e;
320 delay(30);
321    }
322    }
323 int readingMaxValue1= 0;
324 int MaxStep2 = (e - 6);
325 for(Scanlimmit = e ; Scanlimmit> MaxStep2  ; Scanlimmit--)
326    {
327 digitalWrite(ChipselectF,LOW);
328 Downdirection();
329 delay(50);
330 inputValue2 = analogRead(A15);
331 delay(100);
332 Serial.print("\nINPUT voltage");
333 Serial.print((inputValue2*5)/1020); // covert LEM voltage
334 Serial.print("\tStep Down 12: ");
335 Serial.print(Scanlimmit);
336 if (inputValue2 > readingMaxValue1)
337    {
```

```
338     readingMaxValue1= inputValue2;
339 readingMaxValue = inputValue2;
340 readingMaxValueStep = Scanlimmit;
341 delay(30);
342     }
343  }
344 for( km = Scanlimmit ; km <readingMaxValueStep ; km++)
345    {
346 digitalWrite(ChipselectF,LOW);
347 UPDirection();
348 delay(50);
349     inputValue3 = analogRead(A15);
350 delay(100);
351 Serial.print("\nINPUT voltage");
352 Serial.print((inputValue3*5)/102);
353 Serial.print("\tStep Up to resonant point :");
354 Serial.print(km);
355 }
356 Serial.print("\nMax: ");
357 Serial.print(readingMaxValue*5/1023); // print max value
358 Serial.print("\tStep: ");
359 Serial.print(readingMaxValueStep);    // print max value step
360 Serial.print("\n");
361 Serial.print("");
362 delay(10);
363    }
364 }
365 //----------------------------------------------------------------
```

The line walker program

```
367 ****************************************************************************************************

368 #include <Servo.h>
369 #include <Wire.h>
370 #include <ADXL345.h>
371 ADXL345 adxl; //variable adxl is an instance of the ADXL345 library
372 Servo myservo;  // create servo object to control a servo
373 Servo myservo1;
374 Servo myservo2;        // servo motor pin
375 Servo myservo3;
376 intpos = 120;        // variable to store the servo position
377 intPWM = 9;                    // assigns pin 12 to variable PWM
378 intPWM1 = 10;
379 intPWM2 = 11;                  // assigns pin 12 to variable PWM
380 intPWM3 = 12;
381 int limit = 41;                          // limit switche pins
382 int limit1 = 39;
383 int limit2 = 37;
384 int limit3 = 35;
385 constintpingPin = 22; //ultrasonic distance measurement pin
386 int counter= 0;
387 intval = 0;
388 int speed0 = 0;
389 int speed1 = 250;
390 intmyEraser = 7;    // this is 111 in binary and is used as an eraser
391 intmyPrescaler = 2; // this could be a number in [1 , 6]. 3.9khz
392 void setup()  // setup loop
393 {
```

```
394 TCCR1B &= ~myEraser;      // this operation (AND plus NOT),  set the
395 three bits in TCCR2B to 0
396                           //now that CS02, CS01, CS00   are clear, we
397 write on them a new value:
398 TCCR1B |= myPrescaler;  //this operation (OR), replaces the last three
399 bits in TCCR2B with our new value 011
400
401 TCCR2B &= ~myEraser;      // this operation (AND plus NOT),  set the
402 three bits in TCCR2B to 0
403                           //now that CS02, CS01, CS00   are clear, we
404 write on them a new value:
405 TCCR2B |= myPrescaler;  //this operation (OR), replaces the last three
406 bits in TCCR2B with our new value 011
407
408 // by dividing timers 1 & 2 with prescaler the PWMfreq is now changed
409 on pins 12,11,10,9 = 40 Khz
410
411 Serial.begin(9600);
412
413 myservo.attach(48);  // attaches the servo on pin
414 myservo1.attach(49);
415 myservo2.attach(46);  // attaches the servo on pin
416 myservo3.attach(47);
417
418 pinMode(PWM, OUTPUT); // declares pin 12 as output
419 pinMode(PWM1, OUTPUT);
420 pinMode(PWM2, OUTPUT); // declares pin 12 as output
421 pinMode(PWM3, OUTPUT);
422
423 pinMode(limit, INPUT);
424 pinMode(limit1, INPUT);
425 pinMode(limit2, INPUT);
426 pinMode(limit3, INPUT);
427
428   // set defualt position to 90 degrees
429 myservo.write(pos);
430 myservo1.write(pos);
431 pos=125;
432
433 myservo2.write(pos);
434 pos=130 ;
435 myservo3.write(pos);
436 delay(300);
437
438 Serial.begin(9600);
439 adxl.powerOn();
440
441   //set activity/ inactivity thresholds (0-255)
442 adxl.setActivityThreshold(75); //62.5mg per increment
443 adxl.setInactivityThreshold(75); //62.5mg per increment
444 adxl.setTimeInactivity(10); // how many seconds of no activity is
445 inactive?
446
447   //look of activity movement on this axes - 1 == on; 0 == off
448 adxl.setActivityX(1);
449 adxl.setActivityY(1);
450 adxl.setActivityZ(1);
```

```
451
452   //look of inactivity movement on this axes - 1 == on; 0 == off
453 adxl.setInactivityX(1);
454 adxl.setInactivityY(1);
455 adxl.setInactivityZ(1);
456
457   //look of tap movement on this axes - 1 == on; 0 == off
458 adxl.setTapDetectionOnX(0);
459 adxl.setTapDetectionOnY(0);
460 adxl.setTapDetectionOnZ(1);
461
462   //set values for what is a tap, and what is a double tap (0-255)
463 adxl.setTapThreshold(50); //62.5mg per increment
464 adxl.setTapDuration(15); //625Î¼s per increment
465 adxl.setDoubleTapLatency(80); //1.25ms per increment
466 adxl.setDoubleTapWindow(200); //1.25ms per increment
467
468   //set values for what is considered freefall (0-255)
469 adxl.setFreeFallThreshold(7);  //(5 - 9)  recommended - 62.5mg  per
470 increment
471 adxl.setFreeFallDuration(45);  //(20  -  70)  recommended  - 5ms  per
472 increment
473
474   //setting all interupts to take place on int pin 1
475   //I had issues with int pin 2, was unable to reset it
476 adxl.setInterruptMapping(                    ADXL345_INT_SINGLE_TAP_BIT,
477 ADXL345_INT1_PIN );
478 adxl.setInterruptMapping(                    ADXL345_INT_DOUBLE_TAP_BIT,
479 ADXL345_INT1_PIN );
480 adxl.setInterruptMapping(                     ADXL345_INT_FREE_FALL_BIT,
481 ADXL345_INT1_PIN );
482 adxl.setInterruptMapping(                      ADXL345_INT_ACTIVITY_BIT,
483 ADXL345_INT1_PIN );
484 adxl.setInterruptMapping(                    ADXL345_INT_INACTIVITY_BIT,
485 ADXL345_INT1_PIN );
486
487   //register interupt actions - 1 == on; 0 == off
488 adxl.setInterrupt( ADXL345_INT_SINGLE_TAP_BIT, 1);
489 adxl.setInterrupt( ADXL345_INT_DOUBLE_TAP_BIT, 1);
490 adxl.setInterrupt( ADXL345_INT_FREE_FALL_BIT,  1);
491 adxl.setInterrupt( ADXL345_INT_ACTIVITY_BIT,   1);
492 adxl.setInterrupt( ADXL345_INT_INACTIVITY_BIT, 1);
493 }
494 void loop()
495 {
496 intx,y,z;
497 adxl.readAccel(&x,  &y,  &z); //read the accelerometer values and store
498 them in variables  x,y,z
499  x= x/10;
500  y= y/10;
501  z= z/10;
502 Serial.print(x);   // display x, y and z values
503 Serial.print("  ");
504 Serial.print(y);
505 Serial.print("  ");
506 Serial.println(z);
507
```

```
508
509
510 val = digitalRead(limit);  // read input value
511 if (val == HIGH)
512 {         // check if the input is HIGH (button released)
513
514
515 analogWrite(PWM,  speed0); // stop movement
516 analogWrite(PWM1, speed0);
517 analogWrite(PWM2, speed0);
518 analogWrite(PWM3, speed0);
519
520 pos = 30;  // in steps of 1 degree
521 myservo.write(pos);  // servo to go to position invariable 'pos'
522 delay(1000);        // waits 1s for the servo to reach the position
523 }
524
525
526 val = digitalRead(limit1);  // read input value
527 if (val == HIGH) {     check if the input is HIGH (button released)
528
529 analogWrite(PWM,  speed0); // stop movement
530 analogWrite(PWM1, speed0);
531 analogWrite(PWM2, speed0);
532 analogWrite(PWM3, speed0);
533 pos = 60 ;
534 myservo.write(pos)// servo to go to position in variable 'pos'
535 delay(1000);      // waits 15ms for the servo to reach the position
536 pos = 120;
537 myservo3.write(pos);  //servo to go to position in variable 'pos'
538 delay(1000);
539
540 Acc1(); // ***********************balance1****************
541
542 // this block adjusts the position of the remaining legs to acquire
543 //good balance while the 1st leg is removed.
544
545 pos = 120 ;
546 myservo.write(pos);  //servo to go to position in variable 'pos'
547 delay(1300);   // waits 1.3s for the servo to reach the position
548 myservo1.write(pos);
549 delay(800);
550 pos = 125;
551 myservo2.write(pos);
552 delay(800);
553
554 pos = 130;
555 myservo3.write(pos);
556 delay(1000);
557 pos = 0  ;      // remove the first wheel from the line.
558 myservo1.write(pos);
559 delay(1000);   // waits 15ms for the servo to reach the position
560 }
561 val = digitalRead(limit2);  // read input value
562 if (val == HIGH) {   // check if the input is HIGH (button released)
563
564 analogWrite(PWM,  speed0); // stop movement
```

```
565 analogWrite(PWM1, speed0);
566 analogWrite(PWM2, speed0);
567 analogWrite(PWM3, speed0);
568 pos = 95 ;        // goes from 180 degrees to 0 degrees
569 myservo1.write(pos); //servo to go to position in variable 'pos'
570 delay(1000);
571
572 Acc2();//***********************balance2********************
573 // this block adjusts the position of the remaining legs to acquire
574 //good balance while the 2nd leg is removed
575
576 pos = 120 ;
577 myservo1.write(pos);  // servo to go to position in variable 'pos'
578 delay(1000);       // waits 15ms for the servo to reach the position
579 myservo.write(pos);  // servo to go to position in variable 'pos'
580 delay(800);
581 pos = 125;
582
583 myservo2.write(pos);
584 delay(1000);
585 pos = 130;
586 myservo3.write(pos
587 delay(800);
588 pos = 0  ;       // remove second wheel from the line
589 myservo2.write(pos);
590 delay(1000);
591    }
592
593 val = digitalRead(limit3);  // read input value
594 if (val == HIGH)
595   {          // check if the input is HIGH (button released)
596
597 analogWrite(PWM,  speed0); // stop movement
598 analogWrite(PWM1, speed0);
599 analogWrite(PWM2, speed0);
600 analogWrite(PWM3, speed0);
601 pos = 110  ;      // goes from 180 degrees to 0 degrees
602 myservo2.write(pos);
603 delay(1000);
604
605 Acc3(); //*************balance3*****************************
606
607 // this block adjusts the position of the remaining legs to acquire
608 //good balance while the 3rd leg is removed
609 pos = 120  ;
610 myservo2.write(pos);
611 delay(1000);
612
613 myservo1.write(pos);
614 delay(800);
615 pos = 125;
616 myservo.write(pos);
617 delay(800);
618
619 pos = 130;
620 myservo3.write(pos;
621 delay(1000);
```

```
622
623 pos = 70 ;                    // remove 3rd wheel from the line.
624 myservo3.write(pos);
625 delay(1000);       // waits 15ms for the servo to reach the position
626
627 ultrasonicDistance(); call the distance measurement routine
628 analogWrite(PWM,  speed0); // stop movement
629 analogWrite(PWM1, speed0);
630 analogWrite(PWM2, speed0);
631 analogWrite(PWM3, speed0);
632 pos = 90 ;      // goes from 180 degrees to 0 degrees
633 myservo3.write(pos);
634 delay(1000);
635
636 Acc4();//****************balance last*********************
637 // this block adjusts the position of the remaining legs to acquire
638 //good balance while the 4th leg is removed
639
640 pos = 130 ;
641 myservo3.write(pos);
642 delay(1000);
643 pos = 125;
644
645 myservo.write(pos);
646 delay(800);
647 pos = 120;
648 myservo1.write(pos);
649 delay(800);
650 myservo2.write(pos);
651 delay(1000);
652
653 }
654
655 analogWrite(PWM, speed1); // foward movement
656 analogWrite(PWM1, speed1);
657 analogWrite(PWM2, speed1);
658 analogWrite(PWM3, speed1);
659
660 }// close loop
661
662 //***********************************************************
663
664 void Acc1(){
665
666 intx,y,z;
667 adxl.readAccel(&x, &y, &z); //read the accelerometer values and store
668 them in variables  x,y,z
669   x= x/10;
670   y= y/10;
671   z= z/10;
672 Serial.print(x);
673 Serial.print("  ");
674 Serial.print(y);
675 Serial.print("  ");
676 Serial.print(z);
677
678   // Output x,y,z values - Commented out
```

```
679 pos= 120;
680 while ( x >=1 &pos<=148) {
681 pos= pos + 2 ;// in steps of 2 degrees
682
683 myservo1.write(pos);
684 delay(100);
685 myservo2.write(pos);
686 delay(100);
687   // myservo3.write(pos);
688 delay(500);   // waits 500ms for the servo to reach the position
689
690 adxl.readAccel(&x, &y, &z);
691
692   x= x/10;
693   y= y/10;
694   z= z/10;
695 Serial.print(x);       // print x y and z values from accelerometer
696 Serial.print("  ");
697 Serial.print(y);
698 Serial.print("  ");
699 Serial.print(z);
700 Serial.print("  ");
701 Serial.println(pos);
702 }
703
704 }
705   //return returntype;
706   //implied by closing curly bracked
707
708 //-----------------------------------------------------------------
709 void Acc2(){
710 pos= 120;
711
712 intx,y,z;
713 adxl.readAccel(&x, &y, &z); //read the accelerometer values and store
714 them in variables  x,y,z
715  x= x/10;
716  y= y/10;
717  z= z/10;
718 Serial.print(x);
719 Serial.print("  ");
720 Serial.print(y);
721 Serial.print("  ");
722 Serial.print(z);
723 Serial.println(pos);
724   // Output x,y,z values - Commented out
725
726 while ( y >= -5 &pos<=150){
727 pos= pos ++;
728                              // in steps of 1 degree
729 myservo.write(pos);
730 delay(2);
731 myservo2.write(pos);
732 delay(2);
733 myservo3.write(pos);
734 delay(2);
735
```

```
736 adxl.readAccel(&x, &y, &z);
737   x= x/10;
738   y= y/10;
739   z= z/10;
740 Serial.print(x);
741 Serial.print("  ");
742 Serial.print(y);
743 Serial.print("  ");            // Output x,y,z values
744 Serial.print(z);
745 Serial.print("  ");
746 Serial.println(pos);
747 }}//return returntype, implied by closing curly bracket
748 //-----------------------------------------------------------
749 void Acc3(){
750 pos= 120;
751 intx,y,z;
752 adxl.readAccel(&x, &y, &z); //read the accelerometer values and store
753 //them in variables  x,y,z
754   x= x/10;
755   y= y/10;
756   z= z/10;
757 Serial.print(x);
758 Serial.print("  ");
759 Serial.print(y);               // Output x,y,z values
760 Serial.print("  ");
761 Serial.print(z);
762 Serial.println(pos);
763 while ( y >= -1 &pos<=160 ) {
764 pos++;
765                                 // in steps of 1 degree
766 myservo1.write(pos);              // tell servo to go to position in
767 variable 'pos'
768 delay(2);
769 myservo.write(pos);
770 delay(2);
771 myservo3.write(pos);
772 delay(2);                        // waits 15ms for the servo to reach
773 the position
774
775 adxl.readAccel(&x, &y, &z);
776   x= x/10;
777   y= y/10;
778   z= z/10;
779 Serial.print(x);
780 Serial.print("  ");
781 Serial.print(y);
782 Serial.print("  ");
783 Serial.print(z);
784 Serial.print("  ");
785 Serial.println(pos);
786 }
787 }
788 //-----------------------------------------------------------
789 void Acc4(){
790 intx,y,z;
791 adxl.readAccel(&x, &y, &z); //read the accelerometer values and store
792 them in variables  x,y,z
```

```
793
794 pos= 115;
795 myservo.write(pos);                        // tell servo to go to position in
796 variable 'pos'
797 delay(2);
798
799  x= x/10;
800  y= y/10;
801  z= z/10;
802 Serial.print(x);
803 Serial.print("  ");
804 Serial.print(y);
805 Serial.print("  ");
806 Serial.print(z);
807 Serial.println(pos);
808   // Output x,y,z values - Commented out
809 pos=120;
810 while ( y >= -4 &pos<=170){
811 pos= pos++;
812                                        // in steps of 1 degree
813 myservo1.write(pos);
814 delay(2);
815 myservo2.write(pos);
816 delay(2);
817   //myservo.write(pos);
818 // delay(2);
819
820 adxl.readAccel(&x, &y, &z);
821
822  x= x/10;
823  y= y/10;
824  z= z/10;
825 Serial.print(x);
826 Serial.print("  ");
827 Serial.print(y);
828 Serial.print("  ");
829 Serial.print(z);
830 Serial.print("  ");
831 Serial.println(pos);
832 }
833 pos= 125;
834 myservo.write(pos);
835  //delay(500);
836
837 }
838   //return returntype;
839   //implied by closing curly bracked
840 //********************************************************************
841 voidultrasonicDistance(){
842 // read distance between 3rd wheel and the obstacle (insulator)
843
844 long duration, inches,cm;
845     cm =100;
846 while (cm <= 39  or cm >= 51 ) {
847 analogWrite(PWM, speed1); // foward movement speed1
848 analogWrite(PWM1, speed1);
849 analogWrite(PWM2, speed1);
```

```
850 analogWrite(PWM3, speed1);
851
852
853    // The PING))) is triggered by a HIGH pulse of 2 or more
854 microseconds.
855    // Give a short LOW pulse beforehand to ensure a clean HIGH pulse:
856 pinMode(pingPin, OUTPUT);
857 digitalWrite(pingPin, LOW);
858 delayMicroseconds(2);
859 digitalWrite(pingPin, HIGH);
860 delayMicroseconds(5);
861 digitalWrite(pingPin, LOW);
862
863    // The same pin is used to read the signal from the PING))): a HIGH
864    // pulse whose duration is the time (in microseconds) from the
865 sending
866    // of the ping to the reception of its echo off of an object.
867 pinMode(pingPin, INPUT);
868 duration = pulseIn(pingPin, HIGH);
869
870    // convert the time into a distance
871 inches = microsecondsToInches(duration);
872    cm = microsecondsToCentimeters(duration); // convert to cm
873
874 Serial.println("****************************************************");
875
876 Serial.print(cm);
877 Serial.print("cm");
878 Serial.println();
879
880 delay(1000);
881
882 } // while loop closed
883 delay (1000);
884
885 } // ultraonicdistance end - return
886
887 longmicrosecondsToInches(long microseconds)
888 {
889 return microseconds / 74 / 2;
890 }
891 longmicrosecondsToCentimeters(long microseconds)
892 {
893    // The speed of sound is 340 m/s or 29 microseconds per centimeter.
894    // The ping travels out and back, so to find the distance of the
895    // object we take half of the distance travelled.
896 return microseconds / 29 / 2;
897 }
```

THE END

Appendix B –Cleaning results

CLEANING TIME	RMS VOLTAGE	PEAK TO PEAK VOLTAGE	RMS CURRENT IN mA	PEAK TO PEAK CURRENT IN mA	MEAN POWER IN W	FREQUENCY IN kHz
N/A	2.06	6.08	2.18	9.2	0.049	28.11
N/A	4.19	13.2	2.4	10.8	0.076	27.94
N/A	8.13	24.4	3.93	16	0.024	28.01
N/A	12.2	36	5.34	17.6	0.062	27.96
N/A	16	48	7.23	24	0.106	27.94
N/A	19.9	59.2	9.03	29.6	0.175	27.93
N/A	23.8	69.6	8.74	30	0.201	27.98
	27.7	81.6	9	29.2	0.244	27.98
10minutes	31.7	92	9.13	30.8	0.28	27.95
	39.8	114	9.9	34	0.355	27.86
	44	128	10.7	36	0.447	27.881
	52	125	13.1	42.4	0.653	27.89
2minutes	60.5	176	15.4	50.4	0.858	27.802
30seconds	68.2	196	21.9	65.6	1.46	27.962
24seconds	71.9	210	26.6	79.2	0.995	27.842
15seconds	76	220	29.3	85.6	2.2	27.85
7seconds	81.9	230	45.6	138	3.734	27.782
5seconds	82.2	232	70.3	202	6.006	27.68

Appendix C - Inductor design specifications

Inputs

kcu	Ta (°C)	Ts (°C)	Freq. [kHz]	Material	Inductance [µH]	Idc [A]	Iac(b-p) [A]	Ipeak [A]	Irms [A]	LI_pI_{rms} [milliJoules]	δ [mm]
0.4	25	40	28	N41	42	5.000	1.000	6.000	5.033	1.27	0.44599211

Triangular Waveform Assumed for AC current

DESIGN OUTPUTS

Core Type	Core #	LI_pI_{rms} [milliJoules]	Jrms [A/mm²]	Bpeak [mT]	N [#]	Acu [mm²]	Airgap [mm]	Skin, Prox. Effects?	Vc+Vw [cm³]
E-core	#N/A	0.00	#N/A	#N/A	#N/A	#N/A	#N/A	#N/A	#N/A
EC-core	EC35	3.06	2.4	370	8	2.10	0.13	YES	12.0
EFD-core	#N/A	0.00	#N/A	#N/A	#N/A	#N/A	#N/A	#N/A	#N/A
EP-core	#N/A	0.00	#N/A	#N/A	#N/A	#N/A	#N/A	#N/A	#N/A
ER-core	ER28	1.74	1.6	370	8	3.23	0.15	YES	10.1
ETD-core	ETD29	2.40	2.2	370	9	2.24	0.17	YES	10.4
PM-core	PM 114/93	341.62	1.0	367	0	4.96	-68959.09	YES	898.8
Potcore	P30/19	2.15	1.8	370	5	2.76	0.10	YES	10.0
PQ-core	PQ26/20	1.32	2.4	370	6	2.12	0.10	YES	7.6
RMH-core	RM10/I	1.57	2.6	370	7	1.96	0.13	YES	6.5
U-core	U/10/8/3	0.12	3.5	370	81	1.44	#NUM!	YES	1.1

Appendix D - Transformer design specifications

Design Inputs

kcu	Ta (°C)	Ts (°C)	Freq. [kHz]	Material	Vpri,rms	Ipri,rms	Vsec,rms	Throughput Isec,rms	Power	δ[cm]
0.67	24	42	28	N27	15	0.7	150	0.07	21	0.04459921

Design Outputs

Core Type	Core #	V-A Rating [watts]	Jrms [A/mm²]	Bac [mT]	Npri [#]	Nsec [#]	Acu,pri [mm²]	Acu,sec [mm²]	Skin,Prox. Effects?	Vc+Vw [cm³]	Lleakage [nH]	Efficiency [%]
E-core	#N/A	0	#N/A	#N/A	#N/A	#N/A	#N/A	#N/A	#N/A	#N/A	#N/A	#N/A
EC-core	EC35	167	1.8	129	11	111	0.38	0.04	YES	12	74	94.44%
EFD-core	#N/A	0	#N/A	#N/A	#N/A	#N/A	#N/A	#N/A	#N/A	#N/A	#N/A	#N/A
EP-core	EP7	4	3.8	245	46	459	0.18	0.02	YES	0	594	99.51%
ER-core	ER9.5	0	2.0	142	100	996	0.34	0.03	YES	0	5135	99.91%
ETD-core	ETD29	125	1.7	123	13	130	0.41	0.04	YES	10	101	95.70%
PM-core	PM 50/39	875	1.3	96	3	34	0.54	0.05	YES	75	35	82.34%
Potcore	#N/A	0	#N/A	#N/A	#N/A	#N/A	#N/A	#N/A	#N/A	#N/A	#N/A	#N/A
PQ-core	PQ20/16	38	2.1	148	13	132	0.33	0.03	YES	3	143	97.86%
RM-I core	RM4/I	7	3.2	212	41	412	0.22	0.02	YES	0	407	99.29%
U-core	U/10/8/3	8	2.6	175	82	819	0.27	0.03	YES	1	3658	98.94%

Appendix E –Schematic diagrams
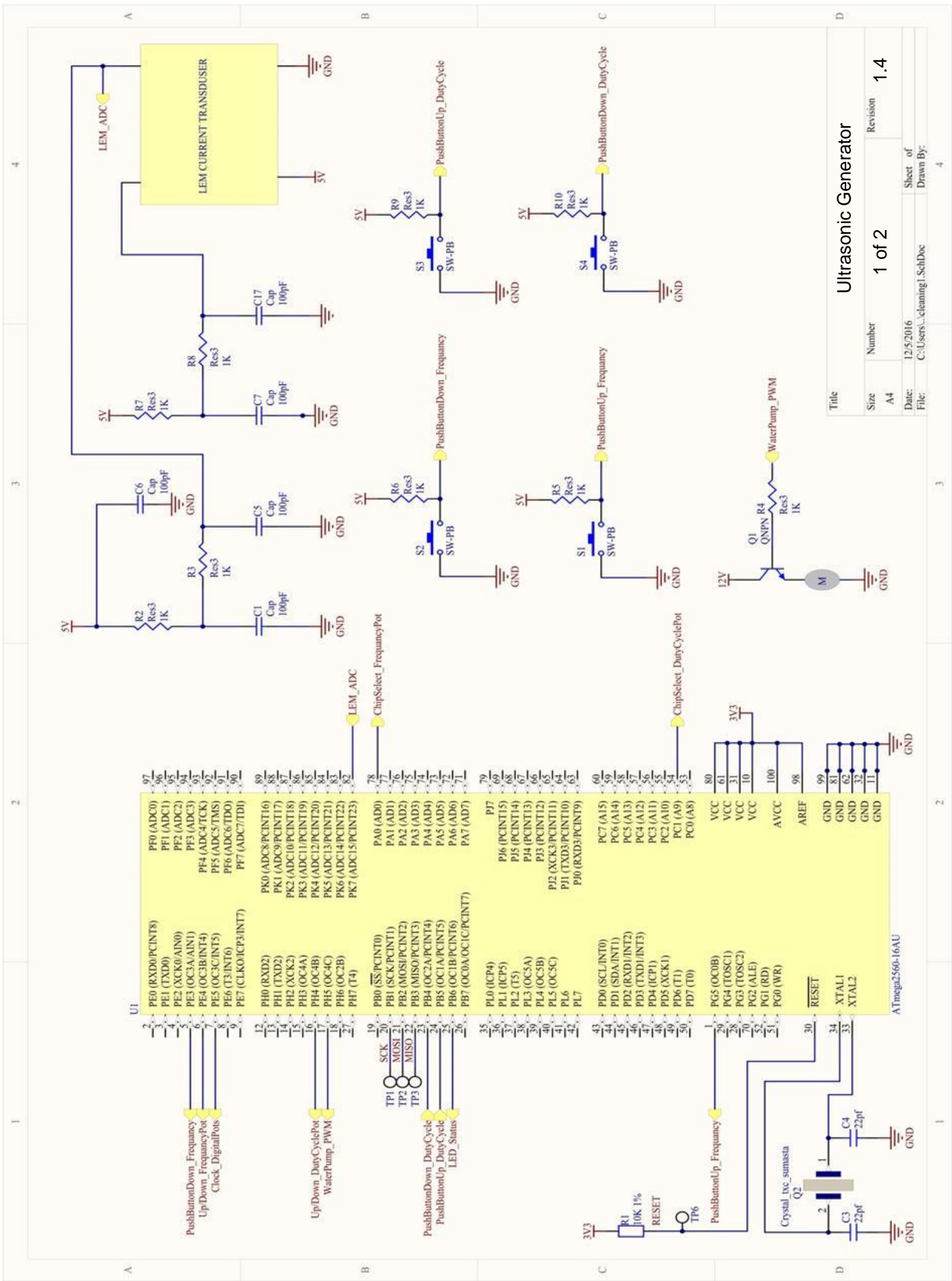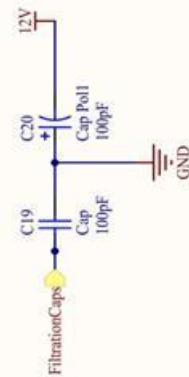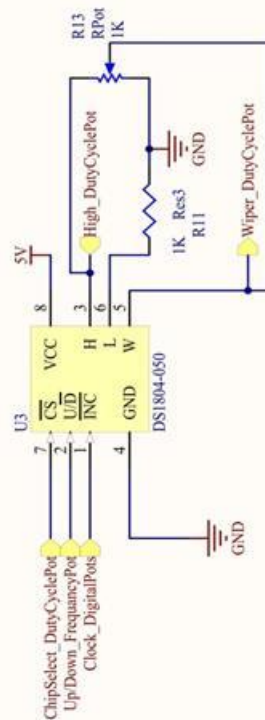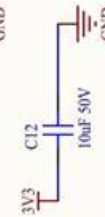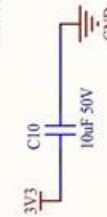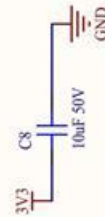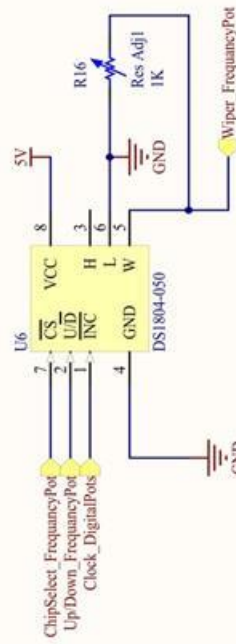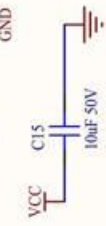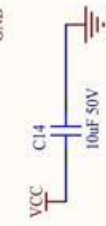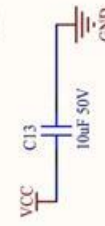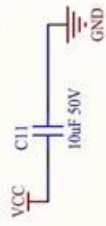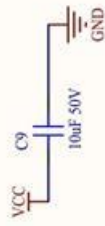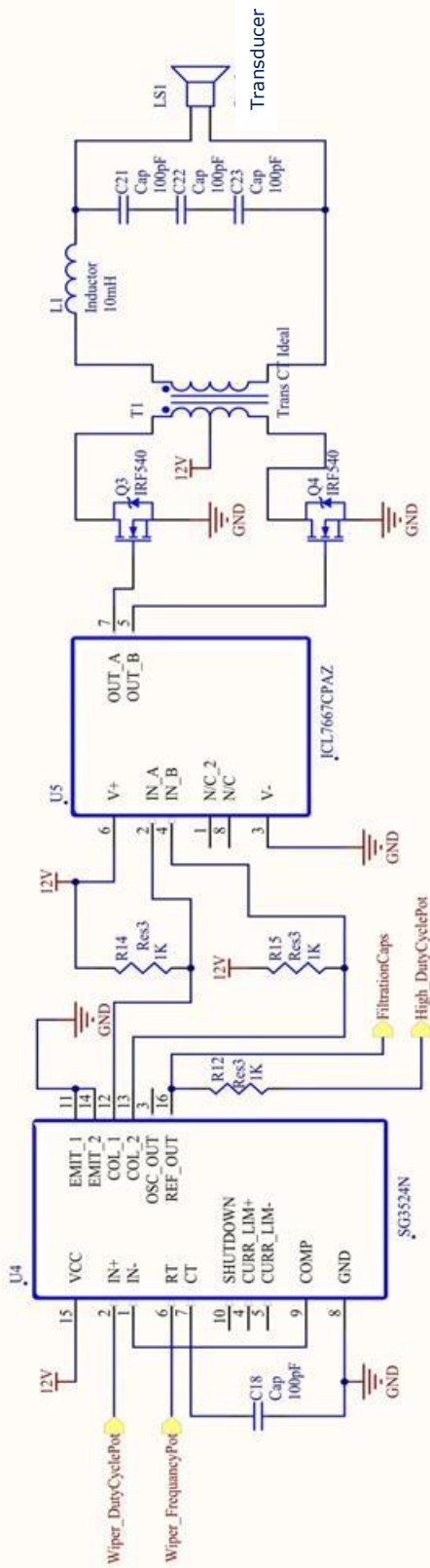
Ultrasonic Generator

Revision 1.4

Title

Size A4

Number

Date: 12/5/2016

File: C:\Users\...\generator.SchDoc

Sheet of

Drawn By:

2 of 2

Line Walker

Line Walker